NASA TECHNICAL NOTE

NASA TN D-4928

NASA TN D-4928

CASE FILE
COPY

WIND-TUNNEL INVESTIGATION OF A LARGE JET TRANSPORT MODEL EQUIPPED WITH AN EXTERNAL-FLOW JET FLAP

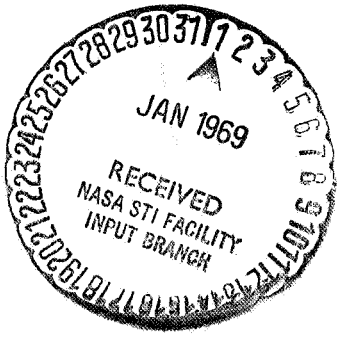

by Lysle P. Parlett, Marvin P. Fink, and Delma C. Freeman, Jr.

Langley Research Center
Langley Station, Hampton, Va.

NATIONAL AERONAUTICS AND SPACE ADMINISTRATION • WASHINGTON, D. C. • DECEMBER 1968

WIND-TUNNEL INVESTIGATION OF A LARGE JET TRANSPORT MODEL EQUIPPED WITH AN EXTERNAL-FLOW JET FLAP

By Lysle P. Parlett, Marvin P. Fink, and Delma C. Freeman, Jr.
Langley Research Center

SUMMARY

A wind-tunnel investigation has been carried out to determine the aerodynamic characteristics of a model of a large jet transport aircraft equipped with an external-flow jet-augmented flap. The tests were conducted in the Langley full-scale tunnel by using a model powered by scaled nitrogen-driven, fan-jet engines.

The results of the investigation have been analyzed for the case of an airplane having a thrust-weight ratio of 0.30 for both take-off and landing. These results indicated that the model with the external-flow jet flap could achieve a maximum trimmed lift coefficient of approximately 4.0 with this thrust-weight ratio. When this maximum lift coefficient was examined with consideration of reasonable operational safety margins based on flight experience with several powered-lift airplanes, it appeared that a safe operational approach lift coefficient was about 2.2. Based on this analysis, it appeared that the use of the jet flap would provide increases in operational lift coefficient of the airplane and would give substantial improvements in take-off and landing performance. Static longitudinal stability and trim could be achieved over the entire lift range by the use of a horizontal tail with an area of 22 percent of the wing area. The out-of-trim moments caused by operation with the critical engine out could be trimmed throughout the entire lift range by the use of conventional rudder, aileron, and spoiler controls.

INTRODUCTION

Early experimental investigations of external-flow jet flaps on general research models (for example, see refs. 1 to 5) have demonstrated that desirably high lift coefficients can be generated with this system. At first, interest in the idea dropped off mainly because of problems of high temperatures on the aircraft structure. Recently, however, interest in the jet-flap scheme has been renewed because of the development of high-bypass-ratio turbofan engines with relatively cool exhaust; these engines make the system more feasible from structural considerations.

The present investigation was conducted to obtain specific information on the external-flow jet-flap concept as applied to heavy logistic transport configurations. The model used in the investigation was powered by four high-bypass-ratio fan-jet engines and was equipped with double-slotted trailing-edge flaps. The flap was designed for use on the airplane without application of the jet-flap principle and was not optimized for use in a jet-flap application. The investigation was performed in the Langley full-scale tunnel and included studies not only of the longitudinal characteristics, but also of the lateral control characteristics under symmetrical and asymmetrical power conditions. The data obtained were used to make estimates of the reductions in take-off and landing speeds that might be achieved by the use of an external-flow jet flap on the configuration. Since there are no accepted operating requirements for such powered-lift aircraft, a set of requirements based on NASA flight experience with three large powered-lift airplanes was devised for use in the present analysis. These requirements are presented in an appendix by Marion O. McKinney and Joseph L. Johnson, Jr., of the Langley Research Center.

SYMBOLS

The data are referred to a system of axes originating at a center of gravity located at 0.25 mean aerodynamic chord and on the fuselage reference line. (See fig. 1.)

b	wing span, feet (meters)
C_D	drag coefficient, D/qS
C_L	lift coefficient, L/qS
$C_{L,t}$	tail lift coefficient, L_t/qS
$C_{L,\Gamma}$	jet-induced circulation lift coefficient, L_Γ/qS
C_l	rolling-moment coefficient, M_X/qSb
ΔC_l	incremental rolling-moment coefficient
C_m	pitching-moment coefficient, $M_Y/qS\bar{c}$
$C_{m,t}$	tail pitching-moment coefficient, $M_{Y,t}/qS\bar{c}$

$C_{m_\alpha} = \frac{\partial C_m}{\partial \alpha}$

C_n yawing-moment coefficient, M_Z/qSb

ΔC_n incremental yawing-moment coefficient

C_T thrust coefficient, T/qS

C_Y lateral-force coefficient, F_Y/qS

ΔC_Y incremental side-force coefficient

C_μ engine mass flow coefficient, mv/qS

c local chord, feet (meters)

$\bar{c}$ mean aerodynamic chord, feet (meters)

D drag, pounds (newtons)

F_A net axial force, pounds (newtons)

F_N normal force, pounds (newtons)

F_R resultant force, vectorial sum of A and N, pounds (newtons)

F_Y lateral force, pounds (newtons)

i_t tail incidence, degrees

L lift, pounds (newtons)

L/D lift-drag ratio

L_t tail lift force, pounds (newtons)

L_Γ	jet circulation lift, pounds (newtons)
M_X	rolling moment, foot-pound (newton-meter)
M_Y	pitching moment, foot-pound (newton-meter)
M_Z	yawing moment, foot-pound (newton-meter)
m	mass flow through engine, slugs/sec
q	dynamic pressure, $\rho V^2/2$, pounds/foot^2 (newtons/meter^2)
S	wing area, feet^2 (meters^2)
S_t	horizontal tail area, feet^2 (meters^2)
T	total installed engine thrust, pounds (newtons)
v	exit velocity of engine exhaust, feet/second (meters/second)
V	free-stream velocity, feet/second (meters/second)
W	weight of airplane, pounds (newtons)
X, Y, Z	body reference axes unless otherwise noted
x, y	distances along X-axis and Y-axis, respectively, inches (centimeters)
α	angle of attack, degrees
γ	flight-path angle, degrees
δ	control deflection, degrees
δ_a	aileron deflection, positive when trailing edge is down, degrees
δ_e	elevator deflection, positive when trailing edge is down, degrees

δ_f flap deflection, degrees

δ_j jet deflection angle, degrees

δ_r rudder deflection, positive when trailing edge is deflected to left, degrees

δ_s spoiler deflection, degrees

η flap-system turning efficiency, F_R/T

ρ air density, slugs/feet^3 (kilograms/meter^3)

Subscripts:

A approach condition

L left; also landing conditions

max maximum

R right

S stall conditions

T take-off condition

t tail

1,2 represents different power settings

MODEL AND APPARATUS

The investigation was conducted on the four-engine high-wing jet-transport model illustrated by the three-view drawing of figure 2. The principal dimensional characteristics of the model are given in tables I and II. The leading edge of the wing was swept an average of 28^o and incorporated leading-edge slats and double-slotted trailing-edge flaps. A detailed sketch of the flap assembly and engine pylon arrangement is shown in

figures 2(b) and 2(c). The positions of these slats and flaps were not optimized during the present tests but were set in accordance with results of previous power-off tests. These positions, therefore, may not necessarily have been the best for powered-lift operation.

The model engines represented high-bypass-ratio fan-jet engines, and were installed at 3° negative incidence to blow directly on the trailing-edge flap system. The engine turbines were driven by compressed nitrogen and turned fans which could produce the same pressure ratio (approximately 1.4) as their full-scale counterparts. Bell-mouth attachments having large radius inlet lips were provided for use during static calibration tests. Flow-through nacelles of the same external size and shape as the powered nacelles but without fans or turbines were installed in place of the powered nacelles for forward-speed thrust-calibration tests.

The model was mounted on a six-component strain-gage balance and was supported on a strut in the test section of the Langley full-scale tunnel, which is 30 by 60 feet (9.12 by 18.3 meters). Photographs of the model mounted in the tunnel test section are shown in figure 3.

TESTS AND PROCEDURES

Calibrations were made to determine the engine-installed thrust as a function of engine speed in revolutions per minute with the model at an angle of attack of 0°, flap deflection being zero. The tests were then made by setting the engine speed to give the desired thrust, or thrust coefficient, at an angle of attack of 0° and then maintaining constant engine speed as the model was tested through a range of angle of attack. The thrust calibrations were made at each of the two free-stream dynamic pressures used in the tests, 11 and 20 pounds per square foot. The thrusts used in computing the thrust coefficients for forward-flight tests are the difference between the longitudinal force with power on and the longitudinal force with flow-through nacelles, both for the same free-stream dynamic pressure. The longitudinal force with flow-through nacelles was not actually measured on this model but was computed by subtracting the increment of drag due to the windmilling rotating parts from the total drag of the model in the windmilling condition. The windmilling drag of the rotating parts was determined from data (unpublished) taken from a previous test program (using the same engines and wing) in which drag measurements were made in the windmilling and flow-through conditions. The thrust calibrations were made through a range of engine speeds up to 40 000 revolutions per minute, at which speed the fans developed, in the static case, their rated pressure ratio of approximately 1.4 and a thrust of approximately 100 pounds (445 N) each.

Flap turning angles and turning efficiencies were determined from measurements of the normal and axial forces made in the static thrust condition with flaps deflected and undeflected. For these tests, the engine inlets were adapted to static operation by the addition of the bell-mouth inlets.

During the wind-on tests, various changes were made to the flap gaps and deflections or to the control surface deflections, and each resulting model condition was tested through an angle-of-attack range from -4° to 16° at two or more thrust coefficients. All wind-on tests were made at free-stream dynamic pressures of either 11 or 20 psf (527 or 958 N/m^2), which correspond to airspeeds of 90 ft/sec and 135 ft/sec (29.5 and 44.3 m/sec), respectively. The Reynolds number range covered in the tests varied from about 1.0×10^6 to 1.5×10^6 based on the mean aerodynamic chord of the wing.

No wind-tunnel jet boundary corrections were applied to the data because such corrections were calculated for the most critical conditions and were found to be negligible.

RESULTS AND DISCUSSION

Lift Characteristics

It is obvious from inspection of figures 4 to 22 that the data from the present investigation were somewhat erratic. This characteristic is believed to result from poor flow over the flaps which is attributed to the fact that the flap locations were optimized for the power-off condition during previous tests at a different Reynolds number. This belief is substantiated by the fact that subsequent tests of the same model on the same test setup with a flap optimized for the particular test conditions gave very consistent data.

Basic longitudinal data for the model (tail-off, leading-edge flaps deflected) are presented in figure 4. This figure shows that the stall angle and the maximum lift coefficient increase with increasing thrust coefficient and that as flap deflection increases, the effects of power on the lift characteristics become more pronounced. The higher flap deflections produce lift coefficients up to about 4.3 at the maximum thrust coefficient and angle of attack. As expected, the high lift coefficients are accompanied by large diving moments because of the rearward location of the flap loads.

The effectiveness of a jet-flap system is usually analyzed in terms of $C_{L,\Gamma}$, the jet-induced circulation lift coefficient. The $C_{L,\Gamma}$ is significant because it represents a lift component not solely attributable either to the upward component of the deflected engine thrust or to the power-off lift of the wing and is therefore an indication of the ability of the integrated engine-wing-flap system to utilize engine power to produce additional large increments of lift coefficient. A typical resolution of total lift coefficient into

its three components is shown for a 70° flap setting in figure 5. The C_L at $C_T = 0$ represents the circulation lift normally developed by the wing and flap system in a moving airstream in the power-off condition. In the powered condition, the engine slipstream impinges on the flap system and is thereby deflected downward through the angle δ_j. The slipstream momentum is also identified as engine gross thrust and is expressed in coefficient form as C_μ; the term $C_\mu \sin \delta_j$ represents the lift contribution due to redirection of engine gross thrust (at zero angle of attack). The flow of the engine slipstream through the flap system and downward from the trailing edge as a jet sheet produces not only the $C_\mu \sin \delta_j$ force, but also induces a flow which augments the circulation over the wing. This increased circulation gives rise to the third lift component, the jet-induced added circulation lift $C_{L,\Gamma}$.

As mentioned previously, the data for the present paper were obtained at several values of engine net thrust coefficient C_T, whereas much of the earlier jet-flap work was done by using the slipstream momentum coefficient C_μ as the thrust parameter. To permit comparison of the present lift characteristics with those of earlier investigations, the relationship between C_T and C_μ for the present model has been computed and is presented as a function of C_T (per engine) in figure 6.

By using $C_{L,\Gamma}$ as the basis for comparison and converting C_T to C_μ by means of figure 6, the effectiveness of the flap system of the present model is compared with that of the model of reference 1 in figure 7. The model of reference 1 was designed specifically for jet-flap operation, and although the $C_{L,\Gamma}$ values which it produced do not necessarily represent the ideal, they have been considered generally representative of those to be expected from an efficient external-flow jet-flap system. Figure 7 shows that at the lower values of C_μ, the jet-induced circulation lift for the two models was in good agreement, but at the higher values of C_μ the present model was relatively ineffective.

Because the jet-induced lift is highly dependent on the direction and velocity of the engine slipstream as it leaves the flap system, it appears that for best jet-flap performance, the flap system should be capable of turning the slipstream through large angles efficiently. The slipstream turning angle δ_j and the static turning efficiency η for the present model are shown in figure 8, which is a plot of the ratio of the normal force to thrust F_N/T against the ratio of net axial force to thrust F_A/T. The turning efficiency, which varies from 0.85 to 0.60 for the range of flap angles studied, is low enough to account partially for the relatively poor jet-flap performance. A probable cause for these low static efficiencies is that the flap system was not designed specifically for a jet-flap application. The jet exhaust impinged directly on the main flap and caused most of the turning to take place below the flap system; the data of reference 1 indicate that better turning would probably have resulted if the jet exhaust had been spread out,

flattened, and directed toward the flap gaps so that the turning would have been more gradual and more of the turning could have been done by the upper surfaces of the flap system.

Effect of leading-edge flaps.- In its design configuration, the model was tested with the leading-edge flap having a 1-percent-chord gap. The data presented in figure 9(a) indicated that this leading-edge flap arrangement generally added a small increment of lift, but did not increase the stall angle of attack except at the higher thrust coefficients. The results of a few exploratory tests made with the gap sealed indicated that the sealing considerably increased the maximum C_L by increasing the stall angle of attack. (See fig. 9(b).) Unfortunately, most of the tests were made with the gap unsealed (design configuration); therefore, the lift characteristics are not as good as they would have been had the tests been made with this improved configuration.

Effect of thrust distribution.- A few tests were made to determine the jet-flap effect produced by operation of only the inboard engines. The results of these tests are presented in figure 10 and show that for a given total C_T, the inboard engines alone produced as much lift as all four engines. This result agrees with that of reference 1, where it was pointed out that locating the engines inboard to reduce pitching moments had no adverse effect on lift.

Static Longitudinal Stability and Trim

Basic longitudinal data for the model with the tail on for several flap deflections and various thrust conditions are presented in figures 11 to 14. The data of these figures show that the model had longitudinal stability for all flap deflections and thrust levels and that longitudinal trim could be achieved up to a lift coefficient of about 4.0.

Pitching-moment data presented in figure 10 for the tail-off condition show that for the jet-flap system, large lift coefficients are accompanied by large diving moments. In order to provide some fundamental information concerning the trim and stability requirements of the horizontal tail in a jet-flap system, the following analysis has been made. Presented in figure 15 is a plot of calculated tail pitching-moment coefficients available for trim about the $0.25\bar{c}$ station as a function of tail area for various tail lift coefficients. Also shown are the pitching-moment coefficients required of the tail to produce longitudinal trim about the $0.25\bar{c}$ station (very nearly the aerodynamic center of the wing-fuselage combination) as determined from tail-off tests at lift coefficients of 3.0 and, by extrapolation, 4.0. This plot shows that for a tail area of 0.22 S_t/S (the case for the present model), the tail must produce a tail lift coefficient of 1.0 for trim at a tail-off lift coefficient of 4.0.

Another point to be considered in selection of tail size is that there is a rearward shift of the neutral point as the tail size is increased and this relationship is a linear function of the tail size for any configuration, all other factors being equal. The variation of neutral point with tail size for the present model may be derived directly from figure 16, which presents plots of $C_{m_{\alpha,t}}$ and $\partial C_m/\partial C_L$ against S_t/S. The data show that adding tail area of 0.22 S_t/S changed $\partial C_m/\partial C_L$ from 0.08 to -0.23. One interesting point not brought out in the results of figures 15 and 16 is that an increase in tail size permits a rearward shift in the center of gravity to maintain a given static margin. Results of calculations (based on those outlined in ref. 4) of tail lift coefficient required as a function of tail size for constant 10-percent static margin are presented in figure 17. In preparing this figure, it was assumed that sufficient power was available to produce the indicated lift coefficients and that changes in lift coefficients would be made only by changes in power at constant angle of attack ($\alpha = 5^\circ$). These data show that at a tail area of 0.34 S_t/S, the center of gravity coincides with the flap center of pressure so that no tail force is required for trim.

Lateral and Directional Control and Trim

Control effectiveness.- Incremental force and moment coefficients showing lateral and directional control moments at flap deflections of 0°, 35°, and 55° are presented in figures 18 to 21.

Data of figure 18 show that rudder effectiveness was relatively unaffected by changes in angle of attack, thrust, or flap deflection.

Data from aileron effectiveness tests are shown in figure 19. These data show that the ailerons lost effectiveness at the higher angles of attack for the thrust-off condition. The application of thrust, however, significantly increased the aileron effectiveness near the stall angle of attack at the flap deflection of 35°, and generally through the angle-of-attack range at the 55° deflection. Yawing moments are small for all test conditions.

The results of tests to determine spoiler effectiveness are presented in figure 20. The spoilers produced considerably larger rolling moments than did the ailerons at any given condition of engine thrust, flap deflection, or angle of attack. At the 55° flap deflection, application of thrust greatly increases the rolling moment, but this increase did not occur at 35° flap deflection. In the jet-flap operation the jet exhaust acts powerfully to delay or prevent stall; it is possible that the increase in rolling moment for the $\delta_f = 55^\circ$ case is a result of the elimination of stall on the unspoiled wing or flap. The yawing moments produced by the spoilers are favorable and are generally increased by the application of thrust.

Ailerons and spoilers acting together (fig. 21) generate large rolling moments accompanied by favorable yawing moments through the angle-of-attack range up to the stall, power-off or power-on, at flap deflections of 35° and 55°; the moments are very nearly the same as the sum of the moment from individual aileron and spoiler tests, and thus indicate that interference effects between the ailerons and spoilers are small.

Asymmetric thrust conditions.- The results of tests to determine the effect of asymmetric thrust conditions are presented in figure 22. These data show that large lateral forces and moments would be produced in the event of the failure of one or both engines on the same side. It should be pointed out, however, that the data presented are limited in application because through mistake they were determined for very high thrust coefficients and are therefore representative of extreme engine-out conditions. Interpolation of these data in terms of the thrust-weight ratios representative of subsonic jet aircraft was performed in order to provide engine-out data directly applicable to this type of aircraft. Interpolations of rolling-moment data were made by constructing plots of rolling moment against thrust. It was assumed that rolling moment is due to asymmetric lift and that a plot of rolling moment against thrust would therefore have the same general shape as a plot of C_L against C_T (initially large slope, decreasing with increasing C_T). Yawing moments were considered to be due to asymmetric drag; thus, because drag is very nearly a linear function of thrust, yawing moments were reduced by simple straight-line interpolation to the desired thrust level. The coefficients thus determined for the lateral out-of-trim moments were plotted against lift coefficient and are presented in figures 23 and 24 for flap deflections of 35° and 55°. Coefficients for the control moments available are also presented in figures 23 and 24 for purposes of comparison. The lift coefficients of figures 23 and 24 have also been interpolated to correspond to the same conditions of thrust, angle of attack, and control deflection for which the lateral moments were computed.

Figure 23 shows that the ailerons provide more than enough rolling moment to offset the engine-out moments for 35° flap deflection but become inadequate for roll trim at the higher lift range for the 55° flap deflection. The spoilers alone provide more than enough rolling moment for trim; the combination of ailerons and spoilers produces moments greatly in excess of what would be required for trim and allows large margins for maneuver.

Figure 24 shows that the rudder alone is capable of providing yawing trim and maneuver moments throughout the test lift-coefficient range. If spoilers are used in conjunction with ailerons for roll trim in the engine-out condition, the favorable yawing moment caused by spoiler deflection may be considered as part of the available yaw control. Curves representing the sum of rudder yawing moment and the yawing moment due to spoiler deflection are presented in figure 24 and show that the spoiler contribution

appreciably increases the margin available for maneuvering in yaw at the high end of the lift-coefficient range. It should be pointed out that this discussion treats the effectiveness of the spoilers with regard to lift and roll only; the performance penalty which would result from spoiler drag is not considered. The yawing moments due to aileron deflection are small, as shown by figure 19, and have therefore been neglected in the present discussion.

APPLICATION OF DATA

This section of the paper examines the significance of the foregoing aerodynamic data in terms of the take-off and landing performance of the particular aircraft represented by the test model.

Rules Used in Analysis

In estimating the take-off and landing performance of an airplane, it is necessary to determine how much of the nominally available lift coefficient can be used and still allow adequate margins for safety. The present Federal Air Regulations (ref. 6) base their requirements on the power-off stall speed and therefore are not directly applicable for powered-lift aircraft. In order to evaluate the take-off and landing performance of the present jet-flap configuration, therefore, it was necessary to devise some corresponding rules for powered-lift aircraft. In the present analysis, two approaches were taken to devise such rules. One approach was to apply the applicable rules of the Federal Air Regulations on the basis of using the power-on stall speed where the regulations specify power-off stall speed. The second approach was to set up a special set of rules based on the NASA experience of references 7 to 9 on three different four-engine powered-lift aircraft. The specific rules used in the present analysis, based on these two approaches are given in the appendixes. Actually, the results of applying these two different sets of rules are not very different for an aircraft of the subject type, as will be shown by the subsequent analysis.

Aircraft Physical Characteristics

The take-off and landing analysis was performed for an aircraft having the configuration of the present model and having the following additional physical characteristics:

Initial take-off weight, lb (N)	710 000 (3 160 000)
Midpoint landing and take-off weight, lb (N)	533 000 (2 370 000)
Wing area, ft^2 (m^2)	6200 (659)
Number of engines	4
Installed thrust per engine, lb (N)	40 000 (178 000)

Aerodynamic Data Used in Analysis

In order that the analysis might be made for the best lifting configuration found in the tests, that with the gap of the leading-edge flap sealed, some extrapolation of the data is required for most conditions. This gap-sealed configuration was tested only for a 35° flap setting. The data for this condition, which are presented in figure 9(b), show that sealing the gap of the leading-edge flap markedly increased the lift at high angles of attack and delayed the stall to angles above the maximum test angle of 16°. Figure 9(b) also shows that sealing the gap did not have any significant effect on the lift at the lower angles of attack. Unfortunately, most of the tests were made with the gap open since that was the design condition of the airplane. Therefore, for the purpose of the present analysis, the increments in maximum lift due to sealing the gap of the leading-edge flap shown in figure 9(b) were applied to the test data for other conditions. The results of this extrapolation, in terms of $C_{L,max}$, are shown in figure 25. The test data for the lower angles of attack, angles below about 8°, were used directly since there was generally no significant effect of sealing the gap at these lower angles.

Lift Analysis

Figure 26 presents a comparison of the lift capability of the high-lift mechanical flap system of the model with the lift that could be achieved with this same flap system if it were used as a jet flap. The comparison is based on the maximum lift coefficients as estimated by the foregoing procedures. It has been pointed out previously in this paper that the present jet-flap system is not as efficient as others which have been tested; nevertheless, figure 26 shows that the present jet-flap system produces markedly higher lift than the mechanical flap system for nearly all power-on conditions. Maximum lift is not the whole story, however. The question is how much of this lift is usable when proper allowances are made for safe aircraft operation. The magnitude of the usable lift coefficient is indicated by the following analysis based on the operational rules of appendixes A and B.

Take-off condition.- For the operation based on present civil regulations, figure 27(a) shows the take-off operational envelope for a flap deflection of 20°. From this figure it can be seen that the required 1.7° sustained climb at $1.2\ V_{S,T}$ with one engine inoperative can just be achieved at a lift coefficient of 1.8 with this flap setting (point ① on this figure). As a matter of interest, it can also be seen from this figure that the climb angle at the same lift coefficient with all engines operating is 5.0° (point ② on the figure).

For the operation based on NASA powered-lift flight experience, figure 27(b) shows the take-off operational envelope for a flap deflection of 15°. From this figure it can be

seen that the required sustained climb angle of 2.3° at 1.2 $V_{S,T}$ with one engine inoperative can be achieved at a lift coefficient of 1.75 with this flap setting (point ① on the figure). It can also be seen from this figure that a climb angle of 6.1° at the same lift coefficient can be maintained with all engines operating (point ② on the figure).

Landing and approach conditions.- For the operation based on present civil regulations, figure 28(d) shows the landing operational envelope for a flap deflection of 55°. From this figure it can be seen that the requirement for a 1.8° sustained climb at a speed of 1.3 $V_{S,L}$ with all engines operating can just be met at this flap setting (point ① on the figure). For this flap setting the maximum lift coefficient at full thrust is 3.90. For the approach condition the requirement is for a sustained climb of at least 1.5° with one engine inoperative at a speed no greater than 1.5 $V_{S,A}$. Figure 28(b) shows that this requirement is met with a flap setting of 40° (point ① on the figure). The regulations further indicate that the approach speed should not be less than 1.3 $V_{S,A}$. The condition of this speed and a glide slope of 3° is indicated as point ② in figure 28(b). The approach lift coefficient in this case is 2.05.

For the operation based on NASA powered-lift flight experience, the rules for the landing condition are the same as those of the Federal Air Regulations (ref. 6) so the landing condition would be the same, flap deflection 55° and a maximum lift coefficient of 3.90. The data of figure 28(d) show that the angle of attack for this condition is 7°, which is 9° below the maximum test angle of 16°, and the wing had not stalled at 16°. For the approach condition the flap setting is determined by the requirement for being able to arrest the descent and maintain level flight with one engine inoperative at the approach speed. This requirement can be met with a flap setting of 45°, as shown by point ① in figure 28(c). The engine-out climb requirement also requires a sustained climb of 2° by reduction in flap setting and at the approach airspeed. This requirement is met by reducing the flap setting to 35° as shown in figure 28(a) by point ①. The approach lift coefficient was determined by the requirement that the angle of attack be at least 10° below the stall. The stall angle for this aircraft configuration is not known exactly, since figure 9(b) shows no indication of stall at the maximum test angle of attack of 16°. It was therefore assumed that operation at an angle of attack of 7° would be satisfactory. With the power setting for a 3° glide slope, this angle of attack corresponds to a lift coefficient of 2.20 as indicated by point ② in figure 28(c). The fact that the approach speed, determined by this lift coefficient, is consistent with the requirement for an approach speed of at least 1.2 $V_{S,A}$ is also indicated in figure 28(c). The last requirement is that a maneuver-acceleration capability of at least 1.2g be available at constant speed. The data of figure 29 show that angle-of-attack change at a constant thrust coefficient (which is the case at constant speed and constant power) would give a maximum lift coefficient of 2.95, or a maneuver factor of 1.35g which is well in excess of the requirement.

Comparison of lift results.- The following table illustrates the point made earlier that the results of the analysis made on the basis of the modified Federal Air Regulations and the NASA powered-lift experience are not very different.

Condition	Modified civil regulations	Powered-lift experience
Take-off flap setting, deg . . .	20	15
Take-off lift coefficient	1.80	1.75
Landing flap setting, deg . . .	55	55
Landing $C_{L,max}$	3.90	3.90
Approach flap setting, deg . .	40	45
Approach C_L	2.00	2.20

Estimated Take-Off and Landing Performance

In order to show what the maximum allowable lift coefficient of the jet-flap system means in terms of take-off and landing performance as compared with that of a conventional flap system, simplified take-off and landing computations (from refs. 10 and 11) in which velocities and distances are computed as functions of lift coefficient are presented in figures 30(a) and 30(b). The data of figure 30(a) show that the approach lift coefficient of the configuration with the mechanical flap was about 1.5 and the speed was about 128 knots (66 m/sec). With the jet flap, the approach lift coefficient was 2.2 and the speed was about 108 knots (55.7 m/sec). On the right-hand side of this figure, it is seen that this difference in lift coefficient resulted in a reduction in landing distance from 4500 feet (1370 m) to about 3300 feet (1000 m). These calculations were made for a weight of 533 000 pounds (2 370 000 N), which was the assumed landing weight of the aircraft at the midpoint of the design mission where good short-field performance is required. In order to show how the jet flap compares with the mechanical flap in terms of take-off performance, calculations were performed for this same weight on the basis that if superior short-field performance was required for delivery of equipment into a primitive military site at the turn-around point of the mission, similar short-field performance was needed for removal of similar material from that site. The results of these calculations (fig. 30(b)) show that the jet flap reduces the take-off speed from about 128 knots (66 m/sec) to about 108 knots (55.7 m/sec) and reduces the take-off distance from about 4000 feet (1220 m) to about 3400 feet (1040 m). These calculations were made by assuming that the aircraft was accelerated along the ground with the flaps retracted. The flaps were then deflected to the take-off setting and the climbout over a 50-foot (15.2 m) obstacle was made with the requirement that the aircraft be capable of a sustained climb angle of 2° with one engine inoperative and with the speed at 1.2 V_S.

CONCLUSIONS

The results of a wind-tunnel investigation to determine the effects of an external-flow jet flap on the aerodynamic characteristics of a model of a large jet aircraft may be summarized as follows:

1. The use of the jet flap provided increases in the operational lift coefficient which gave substantial improvement in take-off and landing performance compared with that of a mechanical flap system.

2. Static longitudinal stability and trim could be achieved at the maximum lift coefficient by the use of a horizontal tail having an area of 22 percent of the wing area.

3. The out-of-trim moments caused by one-engine-out operation could be adequately offset by conventional rudder, aileron, and spoiler controls up through the maximum allowable operational lift coefficient.

Langley Research Center,
National Aeronautics and Space Administration,
Langley Station, Hampton, Va., August 27, 1968,
737-01-00-05-23.

APPENDIX A

REQUIREMENTS BASED ON PRESENT CIVIL REGULATIONS

The following requirements used in the present analysis were based on the Federal Air Regulations of reference 6 with power-on stall speed substituted for the power-off stall speed of the regulations. The particular requirements given are the ones appropriate to the analysis of the present paper.

Take-Off

With the take-off flap setting, the aircraft shall be capable of a sustained 3.0 percent gradient (1.7°) climb with one engine inoperative at a speed of 1.2 $V_{S,T}$, where $V_{S,T}$ is the stalling speed at the take-off flap setting with full power.

Landing

With the landing flap setting, the aircraft shall be capable of a 3.2 percent gradient (1.8°) climb with all engines operating at full thrust and at an airspeed of not more than 1.3 $V_{S,L}$, where $V_{S,L}$ is the stalling speed with the landing flap setting and with full power.

Approach

With the approach flap setting, the aircraft shall be capable of a 2.7 percent gradient (1.5°) climb with one engine inoperative at an airspeed no greater than 1.5 $V_{S,A}$, where $V_{S,A,1}$ is the stalling speed with the approach flap setting and with full power.

The approach flap setting shall be such that the stalling speed $V_{S,A,1}$ with this flap setting shall be no more than 1.1 $V_{S,L}$.

Landing distance shall be determined on the basis of an approach speed of at least 1.3 $V_{S,A,1}$.

APPENDIX B

REQUIREMENTS BASED ON NASA POWERED-LIFT FLIGHT EXPERIENCE

By Marion O. McKinney and Joseph L. Johnson, Jr.
Langley Research Center

The following requirements devised for present analysis are based on NASA flight experience with the three powered-lift aircraft of references 7 to 9. Each of the requirements is followed by a statement of the NASA experience on which the requirement is based.

Take-Off

Take-off speed.- The take-off speed shall not be less than 1.2 $V_{S,T}$, where $V_{S,T}$ is the stall speed with the take-off flap setting and full power. On the two powered-lift aircraft for which take-offs were made (refs. 8 and 9), a take-off speed of 1.2 $V_{S,T}$ was chosen by the pilots as being a safe speed although take-offs were made at speeds as low as 1.1 $V_{S,T}$. These aircraft achieved speeds of 1.3 $V_{S,T}$ by the time they reached a height of 35 feet.

Climb.- The aircraft shall be capable of a sustained climb angle of 2.3° (4.0 percent gradient) with one engine inoperative with the flaps in the take-off position, and at a speed of 1.2 $V_{S,T}$. The powered-lift aircraft of references 8 and 9 were capable of climb angles of 5° to 6° for the foregoing conditions, but there was no evidence that such angles were marginal. Recourse was therefore made to other NASA take-off experience which indicates that this requirement might be considered appropriate.

Approach

Approach speed.- Approach speed should not be less than 1.2 $V_{S,A,2}$, where $V_{S,A,2}$ is the stalling speed with the approach flap setting and power for level flight. The speed thus defined was specifically indicated as the chosen approach speed in reference 7. The approach speeds for the aircraft of references 8 and 9 seemed to have been determined by the maintenance of an angle of attack or angle-of-attack margin, but were consistent with this requirement.

Angle of attack.- Angle of attack for the approach condition should be at least 10° below the stall. This angle-of-attack margin was specifically indicated as being appropriate in reference 8. The aircraft of reference 9 was apparently arbitrarily flown with a somewhat larger margin, and the aircraft of reference 7 was operated with a somewhat smaller margin of about 8°.

APPENDIX B

Maneuver margin.- An acceleration capability of at least 1.2g should be available at constant airspeed. Actually, a maneuver capability of about 1.4g was established for all three of the airplanes by the speed margin required, but in the case of reference 7, it was observed that a value of 1.2g was never exceeded. No maximum maneuver factor was reported in references 8 and 9.

Engine-out wave-off and climb.- In the event of failure of one engine on approach, it should be possible to arrest the descent and maintain level flight without change in flap setting or airspeed. It should also be possible after arresting the descent to establish a sustained climb angle of 2° (3.5 percent gradient) by retraction of the flap and without change in airspeed.

The aircraft of references 8 and 9 were operated at conditions that would meet these requirements and actual wave-offs with one engine out were simulated on the airplane of reference 8. Reference 7 suggests that the Federal Air Regulations engine-out climb requirement is probably adequate. This requirement, which is probably less critical than the preceding requirement, is for a 1.5° (2.7 percent gradient) climb at a speed of not more than 1.5 $V_{S,A,1}$.

Landing

For a wave-off with the landing-flap setting, the aircraft should be capable of a 1.8° (3.2 percent gradient) climb at a speed of not more than 1.3 $V_{S,L}$ where $V_{S,L}$ is the stalling speed with the landing flap setting and with full power on. The NASA flight tests did not include a separate landing condition, but if such a condition is used, the requirement based on the Federal Air Regulations of reference 6 might be used in lieu of any specific NASA experience.

REFERENCES

1. Campbell, John P.; and Johnson, Joseph L., Jr.: Wind-Tunnel Investigation of an External-Flow Jet-Augmented Slotted Flap Suitable for Application to Airplanes With Pod-Mounted Jet Engines. NACA TN 3898, 1956.

2. Lowry, John G.; Riebe, John M.; and Campbell, John P.: The Jet-Augmented Flap. Preprint No. 715, S.M.F. Fund Paper, Inst. Aeron. Sci., Jan. 1957.

3. Johnson, Joseph L., Jr.: Wind-Tunnel Investigation of a Small-Scale Sweptback-Wing Jet-Transport Model Equipped With an External-Flow Jet-Augmented Double Slotted Flap. NASA MEMO 3-8-59L, 1959.

4. Johnson, Joseph L., Jr.: Wind-Tunnel Investigation of the Static Longitudinal Stability and Trim Characteristics of a Sweptback-Wing Jet-Transport Model Equipped With an External-Flow Jet-Augmented Flap. NACA TN 4177, 1958.

5. Fink, Marvin P.: Aerodynamic Characteristics, Temperature, and Noise Measurements of a Large-Scale External-Flow Jet-Augmented Flap Model With Turbojet Engines Operating. NASA TN D-943, 1961.

6. Anon.: Airworthiness Standards: Transport Category Airplanes. Federal Aviation Regulation Part 25, Rules Service Co. (Washington, D.C.), Feb. 1, 1965.

7. Hall, Albert W.; Grunwald, Kalman J.; and Deal, Perry L.: Flight Investigation of Performance Characteristics During Landing Approach of a Large Powered-Lift Jet Transport. NASA TN D-4261, 1967.

8. Quigley, Hervey C.; and Innis, Robert C.: Handling Qualities and Operational Problems of a Large Four-Propeller STOL Transport Airplane. NASA TN D-1647, 1963.

9. Quigley, Hervey C.; Innis, Robert C.; and Holzhauser, Curt A.: A Flight Investigation of the Performance, Handling Qualities, and Operational Characteristics of a Deflected Slipstream STOL Transport Airplane Having Four Interconnected Propellers. NASA TN D-2231, 1964.

10. Wood, Karl D.: Technical Aerodynamics. Second ed., McGraw-Hill Book Co., Inc., 1947.

11. Perkins, Courtland D.; and Hage, Robert E.: Airplane Performance Stability and Control. John Wiley & Sons, Inc., c.1949.

TABLE I.- DIMENSIONS OF MODEL

Wing:		
Area, ft^2 (m^2)	20.14	(1.87)
Span (to theoretical tip), in. (cm)	149.9	(380.7)
Aspect ratio	7.75	
Length of mean aerodynamic chord, in. (cm)	21.16	(53.75)
Location of quarter chord of mean aerodynamic chord, referenced to nose of model, in. (cm)	64.87	(164.77)
Spanwise station of mean aerodynamic chord, in. (cm)	30.91	(78.51)
Root chord, in. (cm)	31.18	(79.20)
Tip chord (theoretical tip), in. (cm)	10.47	(26.59)
Break station chord, in. (cm)	19.32	(49.07)
Spanwise station of break station, in. (cm)	32.25	(81.92)
Sweep of quarter-chord line:		
Inboard panel, deg	24.08	
Outboard panel, deg	25.00	
Dihedral of quarter-chord line:		
Inboard panel, deg	-3.50	
Outboard panel, deg	-3.50	
Incidence of mean aerodynamic chord, deg	4.50	
Horizontal tail:		
Area, ft^2 (m^2)	4.43	(0.412)
Span, in. (cm)	57.40	(145.80)
Length of mean aerodynamic chord, in. (cm)	11.65	(29.59)
Location of quarter-chord mean aerodynamic chord, referenced to nose of model, in. (cm)	153.74	(390.50)
Incidence	Variable	
Engines:		
Spanwise location of inboard engines, in. (cm)	27.36	(69.49)
Spanwise location of outboard engines, in. (cm)	42.57	(108.13)
Incidence of all engine center lines, deg	-3.00	
Moment reference:		
Longitudinal location, referenced to nose of model, in. (cm)	64.87	(164.77)
Vertical location, referenced to top of fuselage at wing, in. (cm)	7.87	(19.99)

TABLE I.- DIMENSIONS OF MODEL – Concluded

Control surface dimensions:		
Rudder:		
Span, in. (cm)	16.84	(42.8)
Chord, upper end, parallel to water line, in. (cm)	4.27	(10.85)
Chord, lower end, perpendicular to hinge line, in. (cm)	4.35	(11.06)
Hinge-line location, percent chord	75	
Sweep of hinge line, deg	31.4	
Elevator:		
Span, in. (cm)	21.21	(53.9)
Chord, outboard end, in. (cm)	2.03	(5.16)
Chord, inboard, in. (cm)	4.05	(10.29)
Hinge-line location, percent chord	73	
Sweep of hinge line, deg	16.5	
Aileron:		
Span, in. (cm)	15.00	(38.1)
Chord, outboard end, in. (cm)	3.75	(9.52)
Chord, inboard end, in. (cm)	4.75	(12.07)
Buttock line of inboard end, in. (cm)	55.74	(141.7)
Hinge-line location, percent chord	70	
Sweep of hinge line, deg	20.2	
Spoiler (inboard panel):		
Span, in. (cm)	26.63	(67.8)
Chord, inboard end, in. (cm)	2.91	(7.39)
Chord, outboard, in. (cm)	1.93	(4.90)
Buttock line of inboard end, in. (cm)	5.62	(14.28)
Hinge-line location, percent chord	68	
Sweep of hinge line, deg	17	
Spoiler (outboard panel):		
Span, in. (cm)	24.38	(61.9)
Chord, inboard end, in. (cm)	1.93	(4.90)
Chord, outboard, in. (cm)	1.43	(3.63)
Buttock line of inboard end, in. (cm)	32.25	(81.9)
Hinge-line location, percent chord	68	
Sweep of hinge line, deg	20.7	

TABLE II.- AIRFOIL COORDINATES FOR WING, VANE, AND FLAP

(a) Wing coordinates at buttock line 7.98 in. (20.27 cm)

x_{upper}		y_{upper}		x_{lower}		y_{lower}	
in.	cm	in.	cm	in.	cm	in.	cm
-0.007	-0.018	0.160	0.406	0.077	0.196	-0.140	-0.356
.040	.102	.287	.729	.172	.437	-.229	-.582
.099	.281	.378	.960	.254	.645	-.286	-.726
.199	.505	.487	1.237	.366	.930	-.349	-.886
.454	1.153	.678	1.722	.605	1.537	-.458	-1.163
1.410	3.581	1.049	2.664	1.415	3.594	-.736	-1.869
2.827	7.181	1.351	3.432	2.822	7.168	-1.045	-2.654
5.649	14.348	1.703	4.326	5.649	14.348	-1.408	-3.576
8.470	21.514	1.892	4.806	8.477	21.532	-1.595	-4.051
11.288	28.672	1.963	4.986	11.308	28.722	-1.646	-4.181
14.106	35.829	1.925	4.890	14.139	35.913	-1.565	-4.206
16.926	42.992	1.787	4.539	16.968	43.099	-1.360	-3.454
19.759	50.188	1.556	3.952	19.784	50.251	-1.053	-2.675
22.601	57.407	1.213	3.081	22.590	57.379	-.688	-1.748
25.442	64.623	.725	1.842	25.398	64.511	-.319	-.810
28.248	71.750	.036	.091	28.241	71.732	-.036	-.091

TABLE II.- AIRFOIL COORDINATES FOR WING, VANE, AND FLAP – Continued

(b) Wing coordinates at buttock line 29.99 in. (76.17 cm)

x_{upper}		y_{upper}		x_{lower}		y_{lower}	
in.	cm	in.	cm	in.	cm	in.	cm
-0.005	-0.013	0.117	0.297	0.056	0.142	-0.102	-0.259
.028	.071	.208	.528	.123	.312	-.166	-.422
.070	.178	.272	.691	.182	.462	-.206	-.523
.140	.356	.349	.886	.263	.668	-.249	-.632
.318	.808	.482	1.224	.438	1.113	-.359	-.912
.981	2.492	.748	1.900	1.033	2.624	-.567	-1.440
1.990	5.055	.911	2.314	2.040	5.182	-.632	-1.605
4.007	10.178	1.230	3.124	4.052	10.292	-.782	-1.986
6.028	15.311	1.370	3.480	6.062	15.397	-.846	-2.149
8.049	20.444	1.429	3.630	8.031	20.399	-.853	-2.167
10.070	25.578	1.410	3.581	10.079	25.601	-.807	-2.050
12.090	30.709	1.317	3.345	12.089	30.706	-.707	-1.796
14.110	35.839	1.152	2.926	14.099	35.811	-.555	-1.410
16.141	40.998	.892	2.266	16.098	40.889	-.376	-.955
18.157	46.119	.517	1.313	18.112	46.004	-.196	-.498
20.151	51.184	.023	.058	20.147	51.173	-.014	-.036

TABLE II.- AIRFOIL COORDINATES FOR WING, VANE, AND FLAP – Continued

(c) Wing coordinates at buttock line 42.57 in. (108.13 cm)

x_{upper}		y_{upper}		x_{lower}		y_{lower}	
in.	cm	in.	cm	in.	cm	in.	cm
-0.0077	-0.0196	0.104	0.264	0.050	0.127	-0.091	-0.231
.024	.061	.184	.467	.109	.277	-.147	-.373
.055	.140	.241	.612	.160	.406	-.182	-.462
.114	.290	.307	.780	.230	.584	-.218	-.554
.265	.673	.423	1.074	.379	.963	-.277	-.704
.831	2.111	.652	1.656	.888	2.256	-.402	-1.021
1.691	4.295	.841	2.136	1.746	4.435	-.512	-1.300
3.414	8.672	1.060	2.692	3.459	8.786	-.615	-1.562
5.143	13.063	1.179	2.995	5.168	13.127	-.665	-1.689
6.866	17.440	1.223	3.106	6.879	17.473	-.677	-1.720
8.5919	21.8234	1.1994	3.0465	8.5925	21.8250	-.6427	-1.6325
10.3149	26.1998	1.1097	2.8186	10.3063	26.1780	-.5616	-1.4265
12.0374	30.5750	.9582	2.4338	12.0207	30.5326	-.4387	-1.1143
13.7659	34.9654	.7328	1.8613	13.7291	34.8719	-.2943	-.7475
15.4841	39.3296	.4201	1.0671	15.4478	39.2374	-.1507	-.3828
17.1862	43.6529	.0189	.0480	17.1826	43.6438	-.0189	-.0480

TABLE II.- AIRFOIL COORDINATES FOR WING, VANE, AND FLAP – Continued

(d) Wing coordinates at buttock line 52.48 in. (133.30 cm)

x_{upper}		y_{upper}		x_{lower}		y_{lower}	
in.	cm	in.	cm	in.	cm	in.	cm
-0.009	-0.023	0.096	0.244	0.046	0.117	-0.085	-0.216
.014	.036	.170	.432	.100	.254	-.136	-.345
.044	.112	.221	.561	.145	.368	-.167	-.424
.095	.241	.282	.716	.208	.528	-.199	-.505
.228	.579	.386	.980	.340	.864	-.249	-.632
.728	1.849	.589	1.496	.785	1.994	-.352	-.894
1.486	3.774	.753	1.913	1.541	3.914	-.438	-1.113
3.007	7.638	.944	2.398	3.048	7.742	-.516	-1.311
4.534	11.516	1.047	2.659	4.548	11.552	-.564	-1.433
6.054	15.377	1.079	2.741	6.055	15.380	-.587	-1.491
7.571	19.230	1.048	2.662	7.565	19.215	-.560	-1.422
9.088	23.084	.957	2.431	9.076	23.053	-.486	-1.234
10.605	26.937	.812	2.062	10.586	26.888	-.376	-.955
12.124	30.795	.611	1.552	12.095	30.721	-.247	-.627
13.637	34.638	.348	.884	13.609	34.567	-.120	-.305
15.138	38.451	.017	.043	15.135	38.443	-.017	-.043

TABLE II.- AIRFOIL COORDINATES FOR WING, VANE, AND FLAP – Continued

(e) Wing coordinates at buttock line 67.45 in. (171.13 cm)

x_{upper}		y_{upper}		x_{lower}		y_{lower}	
in.	cm	in.	cm	in.	cm	in.	cm
0.011	0.028	0.084	0.213	0.041	0.104	-0.075	-0.191
.004	.010	.148	.376	.086	.218	-.118	-.300
.027	.069	.191	.485	.124	.315	-.144	-.366
.066	.168	.243	.617	.174	.442	-.170	-.432
.172	.437	.330	.838	.279	.709	-.208	-.528
.573	1.455	.494	1.255	.630	1.600	-.277	-.704
1.176	2.987	.619	1.572	1.231	3.127	-.325	-.826
2.391	6.073	.767	1.948	2.424	6.157	-.367	-.932
3.612	9.174	.846	2.149	3.610	9.169	-.413	-1.049
4.822	12.248	.861	2.187	4.808	12.212	-.449	-1.140
6.026	15.306	.819	2.080	6.011	15.268	-.434	-1.102
7.230	18.364	.726	1.844	7.214	18.324	-.373	-.947
8.437	21.430	.592	1.504	8.414	21.372	-.281	-.714
9.637	24.478	.427	1.085	9.622	24.440	-.174	-.442
10.824	27.493	.238	.605	10.826	27.498	-.073	-.185
12.038	30.577	.013	.033	12.036	30.571	-.013	-.033

TABLE II.- AIRFOIL COORDINATES FOR WING, VANE, AND FLAP – Continued

(f) Vane coordinates, inboard vane

Inboard end						Outboard end					
x		y_{upper}		y_{lower}		x		y_{upper}		y_{lower}	
in.	cm	in.	cm	in.	cm	in.	cm	in.	cm	in.	cm
0	0	0	0	0	0	0	0	0	0	0	0
.115	.292	.30	.76	.20	.51	.080	.203	.22	.56	.15	.38
.231	.587	.38	.97	.22	.56	.160	.406	.27	.69	.15	.38
.346	.879	.43	1.09	.18	.46	.240	.610	.33	.84	.11	.28
.461	1.171	.46	1.17	.09	.23	.322	.818	.34	.86	.05	.13
.578	1.468	.46	1.17	.03	.08	.402	1.021	.35	.89	0	0
.693	1.760	.46	1.17	-.05	-.13	.482	1.224	.34	.86	-.04	-.10
.924	2.347	.43	1.09	-.09	-.23	.642	1.631	.33	.84	-.08	-.20
1.155	2.934	.37	.94	-.12	-.30	.803	2.040	.27	.69	-.09	-.23
1.385	3.518	.31	.79	-.14	-.36	.963	2.446	.22	.56	-.09	-.23
1.616	4.105	.23	.58	-.12	-.30	1.124	2.855	.16	.41	-.08	-.20
1.848	4.694	.16	.41	-.08	-.20	1.284	3.261	.12	.30	-.06	-.15
2.079	5.281	.09	.23	-.05	-.13	1.445	3.670	.07	.18	-.04	-.10
2.310	5.867	.04	.10	0	0	1.605	4.077	.04	.10	0	0

TABLE II.- AIRFOIL COORDINATES FOR WING, VANE, AND FLAP – Continued

(g) Vane coordinates, outboard vane

Inboard end						Outboard end					
x		y_{upper}		y_{lower}		x		y_{upper}		y_{lower}	
in.	cm	in.	cm	in.	cm	in.	cm	in.	cm	in.	cm
0	0	0	0	0	0	0	0	0	0	0	0
.080	.203	.19	.48	.14	.36	.064	.163	.16	.41	.08	.20
.160	.406	.26	.66	.15	.38	.128	.325	.19	.48	.09	.23
.240	.610	.30	.76	.12	.30	.190	.483	.22	.56	.07	.18
.322	.818	.31	.79	.08	.20	.254	.645	.24	.61	.01	.03
.402	1.021	.33	.84	.04	.10	.318	.808	.26	.66	-.01	-.03
.482	1.224	.33	.84	-.01	-.03	.381	.968	.26	.66	-.05	-.13
.642	1.631	.31	.79	-.07	-.18	.508	1.290	.23	.58	-.07	-.18
.803	2.040	.26	.66	-.09	-.23	.635	1.613	.20	.51	-.08	-.20
.963	2.446	.22	.56	-.11	-.28	.763	1.938	.18	.46	-.08	-.20
1.124	2.855	.19	.48	-.09	-.23	.889	2.258	.12	.30	-.05	-.13
1.284	3.261	.14	.36	-.08	-.20	1.016	2.581	.09	.23	-.05	-.13
1.445	3.670	.08	.20	-.05	-.13	1.143	2.903	.08	.20	-.03	-.08
1.605	4.077	.04	.10	0	0	1.270	3.226	.05	.13	0	0

TABLE II.- AIRFOIL COORDINATES FOR WING, VANE, AND FLAP – Continued

(h) Flap coordinates, inboard flap

Inboard end						Outboard end					
x		y_{upper}		y_{lower}		x		y_{upper}		y_{lower}	
in.	cm	in.	cm	in.	cm	in.	cm	in.	cm	in.	cm
0	0	0	0	0	0	0	0	0	0	0	0
.330	.838	.65	1.65	.33	.84	.229	.582	.38	.97	.23	.58
.661	1.679	.92	2.34	.30	.76	.459	1.166	.56	1.42	.22	.56
.991	2.517	1.11	2.82	.27	.69	.688	1.748	.65	1.65	.22	.56
1.320	3.353	1.21	3.07	.26	.66	.917	2.329	.73	1.85	.22	.56
1.650	4.191	1.28	3.25	.24	.61	1.147	2.913	.75	1.91	.20	.51
1.981	5.032	1.29	3.28	.22	.56	1.376	3.495	.75	1.91	.19	.48
2.641	6.708	1.19	3.02	.19	.48	1.835	4.661	.72	1.83	.16	.41
3.302	8.387	1.04	2.64	.15	.38	2.293	5.824	.64	1.63	.15	.38
3.961	10.061	.87	2.21	.11	.28	2.752	6.990	.53	1.35	.12	.30
4.622	11.740	.66	1.68	.08	.20	3.211	8.156	.41	1.04	.09	.23
5.281	13.414	.47	1.19	.05	.13	3.669	9.319	.28	.71	.08	.20
5.942	15.093	.24	.61	.04	.10	4.128	10.485	.15	.38	.05	.13
6.602	16.769	.04	.10	.04	.10	4.587	11.651	0	0	.04	.10

TABLE II.- AIRFOIL COORDINATES FOR WING, VANE, AND FLAP – Concluded

(i) Flap coordinates, outboard flap

Inboard end						Outboard end					
x		y_{upper}		y_{lower}		x		y_{upper}		y_{lower}	
in.	cm	in.	cm	in.	cm	in.	cm	in.	cm	in.	cm
0	0	0	0	0	0	0	0	0	0	0	0
.229	.582	.39	.99	.26	.66	.182	.462	.26	.66	.22	.56
.459	1.166	.53	1.35	.24	.61	.362	.919	.37	.94	.20	.51
.688	1.748	.62	1.57	.23	.58	.544	1.382	.46	1.17	.19	.48
.917	2.329	.71	1.80	.22	.56	.726	1.844	.50	1.27	.19	.48
1.147	2.913	.75	1.91	.22	.56	.906	2.301	.53	1.35	.18	.46
1.376	3.495	.76	1.93	.20	.51	1.088	2.764	.53	1.35	.16	.41
1.835	4.661	.73	1.85	.19	.48	1.451	3.686	.50	1.27	.15	.38
2.293	5.824	.62	1.57	.16	.41	1.814	4.608	.45	1.14	.12	.30
2.752	6.990	.52	1.32	.15	.38	2.177	5.530	.37	.94	.11	.28
3.211	8.156	.39	.99	.12	.30	2.539	6.449	.28	.71	.08	.20
3.669	9.319	.27	.69	.09	.23	2.901	7.369	.19	.48	.07	.18
4.128	10.485	.14	.36	.08	.20	3.265	8.293	.09	.23	.05	.13
4.587	11.651	0	0	.05	.13	3.627	9.213	0	0	.04	.10

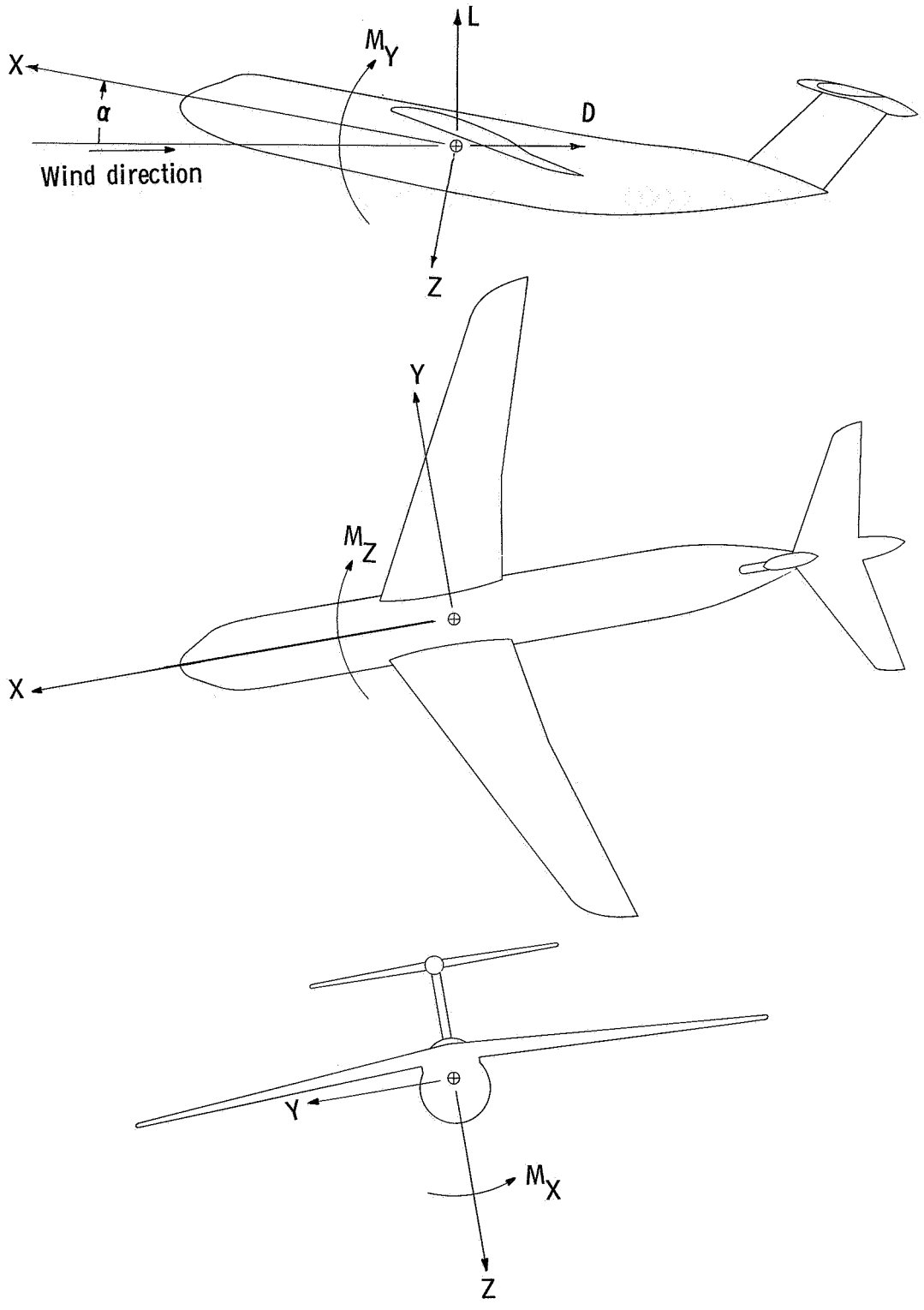

Figure 1.- Axis system used in presentation of data. Arrows indicate direction of moments, forces, and angles.

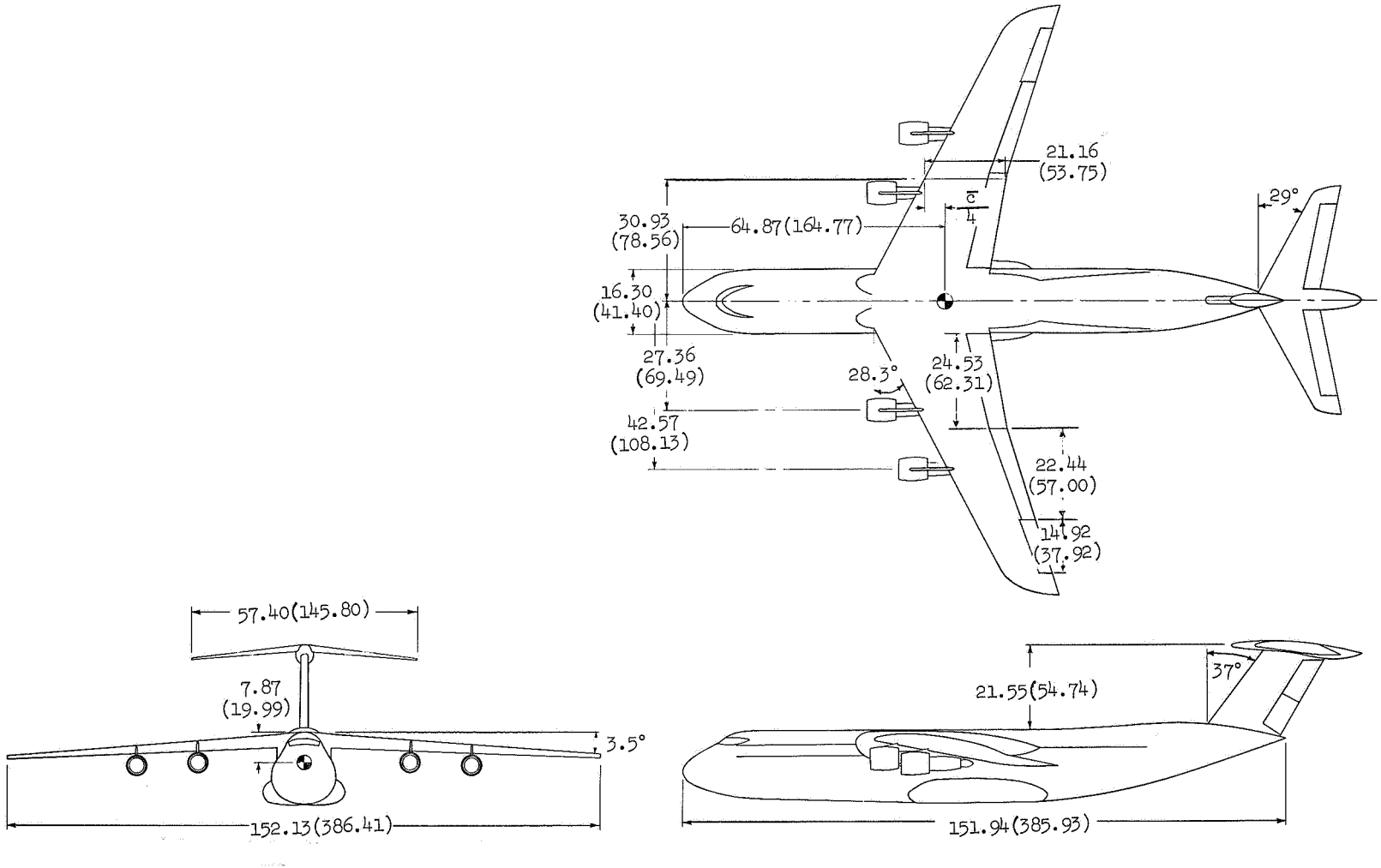

(a) Three-view drawing of complete model.

Figure 2.- Drawing of model used in investigation. Dimensions are in inches (centimeters).

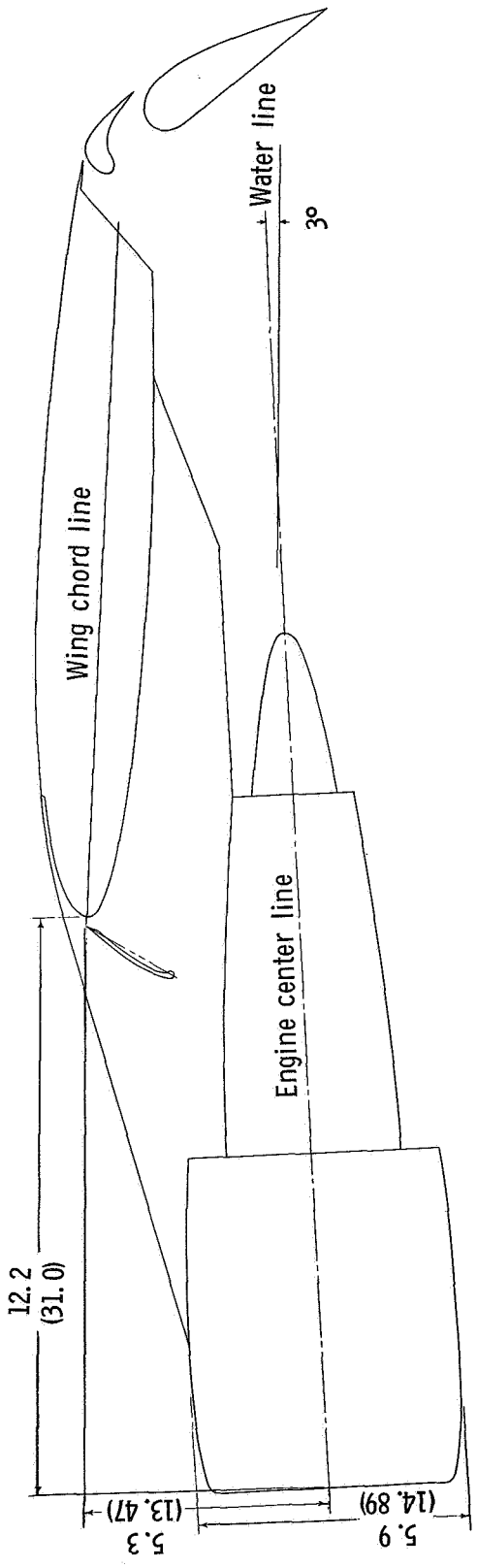

(b) Wing-pylon-nacelle assembly detail.

Figure 2.- Continued.

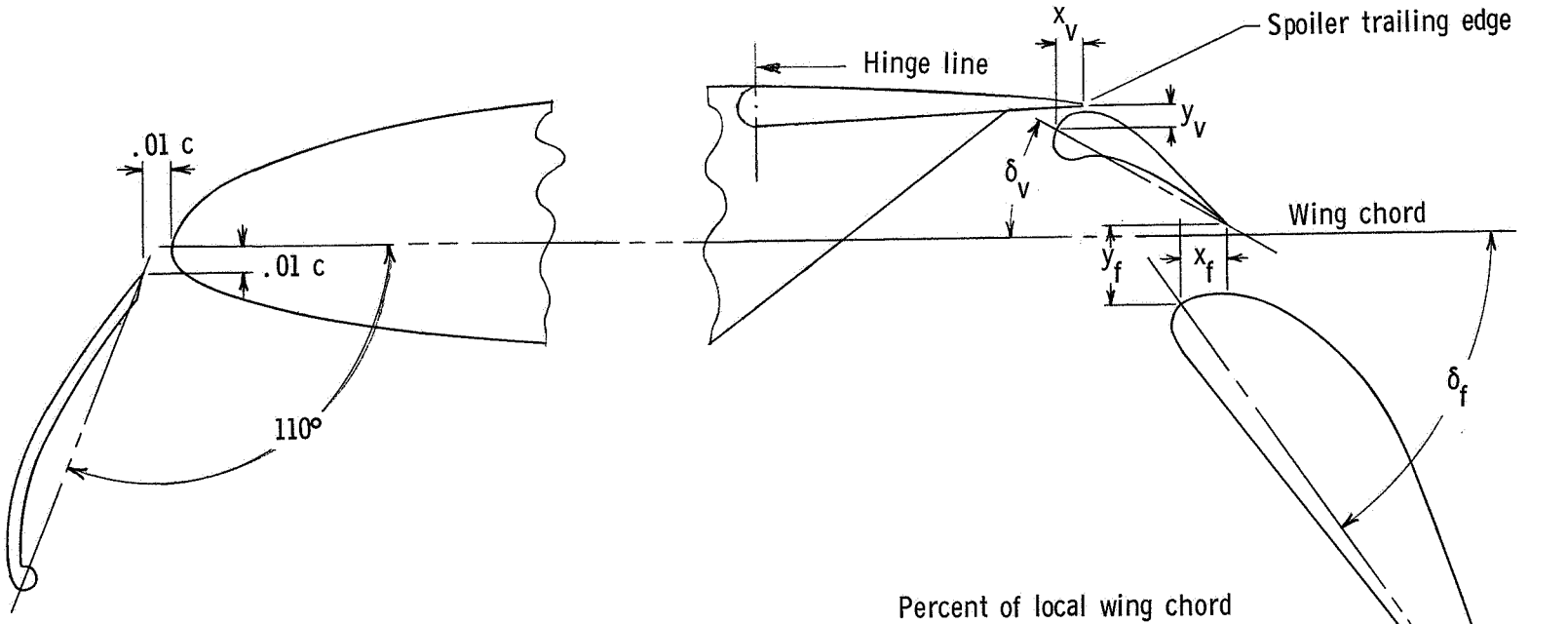

Percent of local wing chord

δ_f	δ_{vane}	x_v	y_v	x_f	y_f
25	15	1.0	2.5	3.0	5.0
35	15	1.0	2.5	3.0	5.0
55	30	1.0	1.0	2.0	3.0
70	45	1.0	1.0	2.0	3.0

(c) Flap detail showing slot dimensions.

Figure 2.- Concluded.

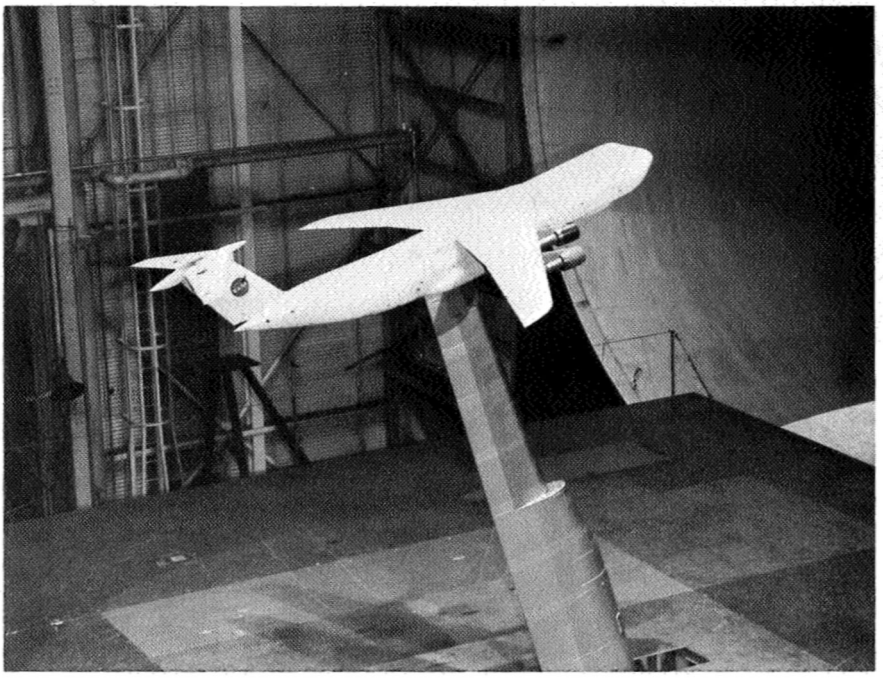

(a) Clean configuration. L-67-9567

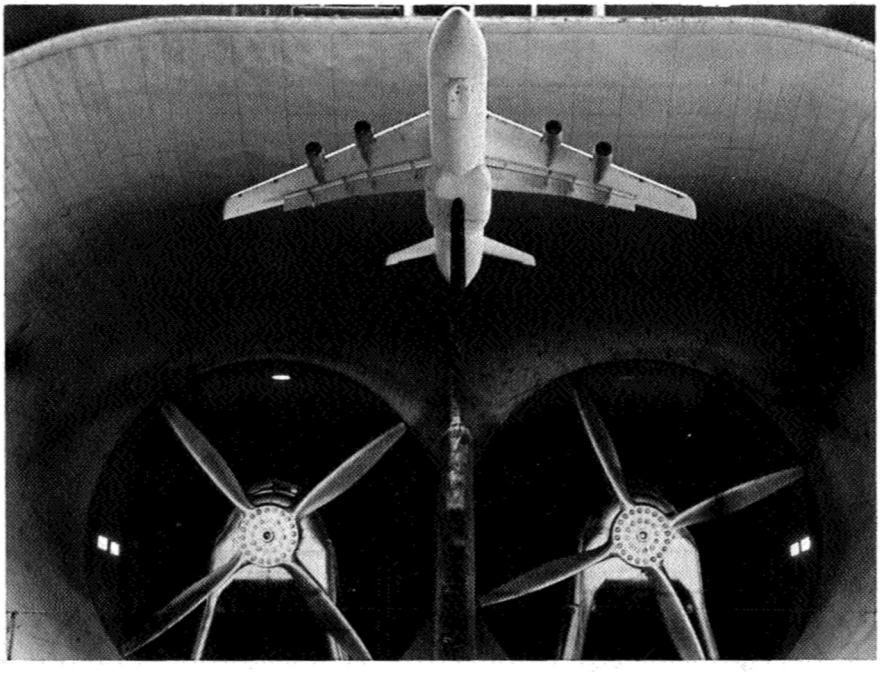

(b) Landing configuration. L-66-3111

Figure 3.- Photographs of model mounted in Langley full-scale-tunnel test section.

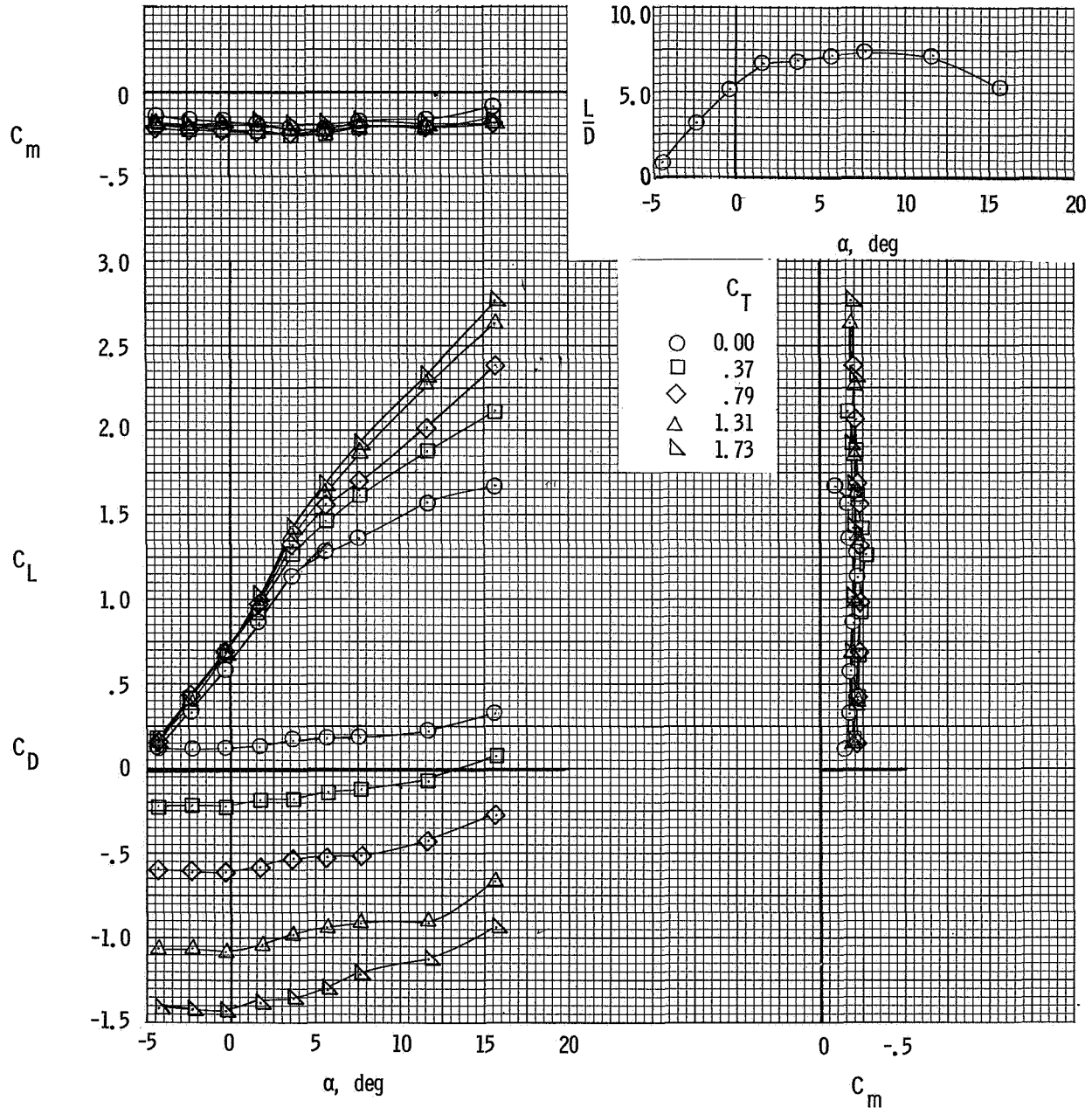

(a) $\delta_f = 25^0$.

Figure 4.- Basic longitudinal data, tail off.

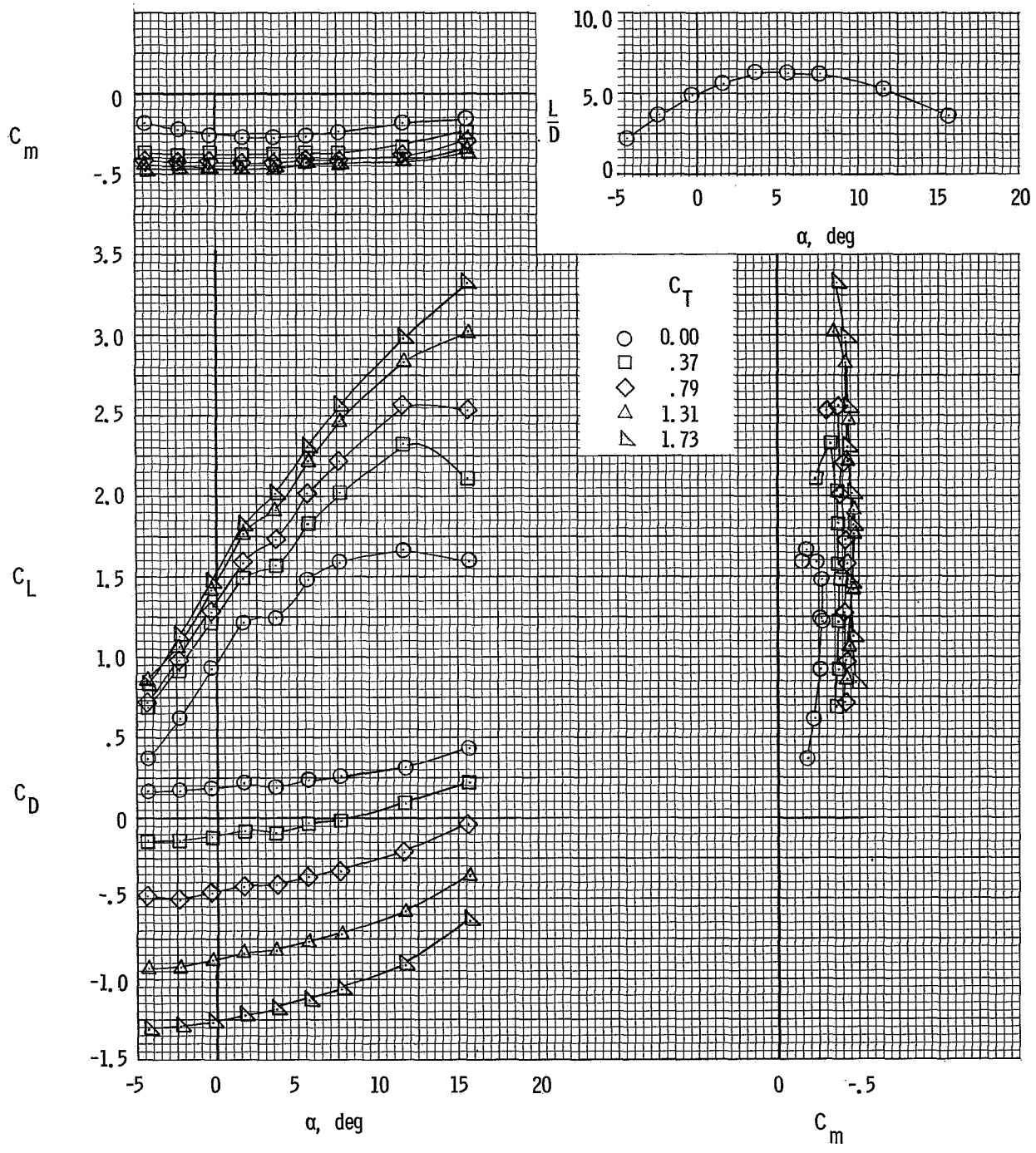

(b) $\delta_f = 35^0$.

Figure 4.- Continued.

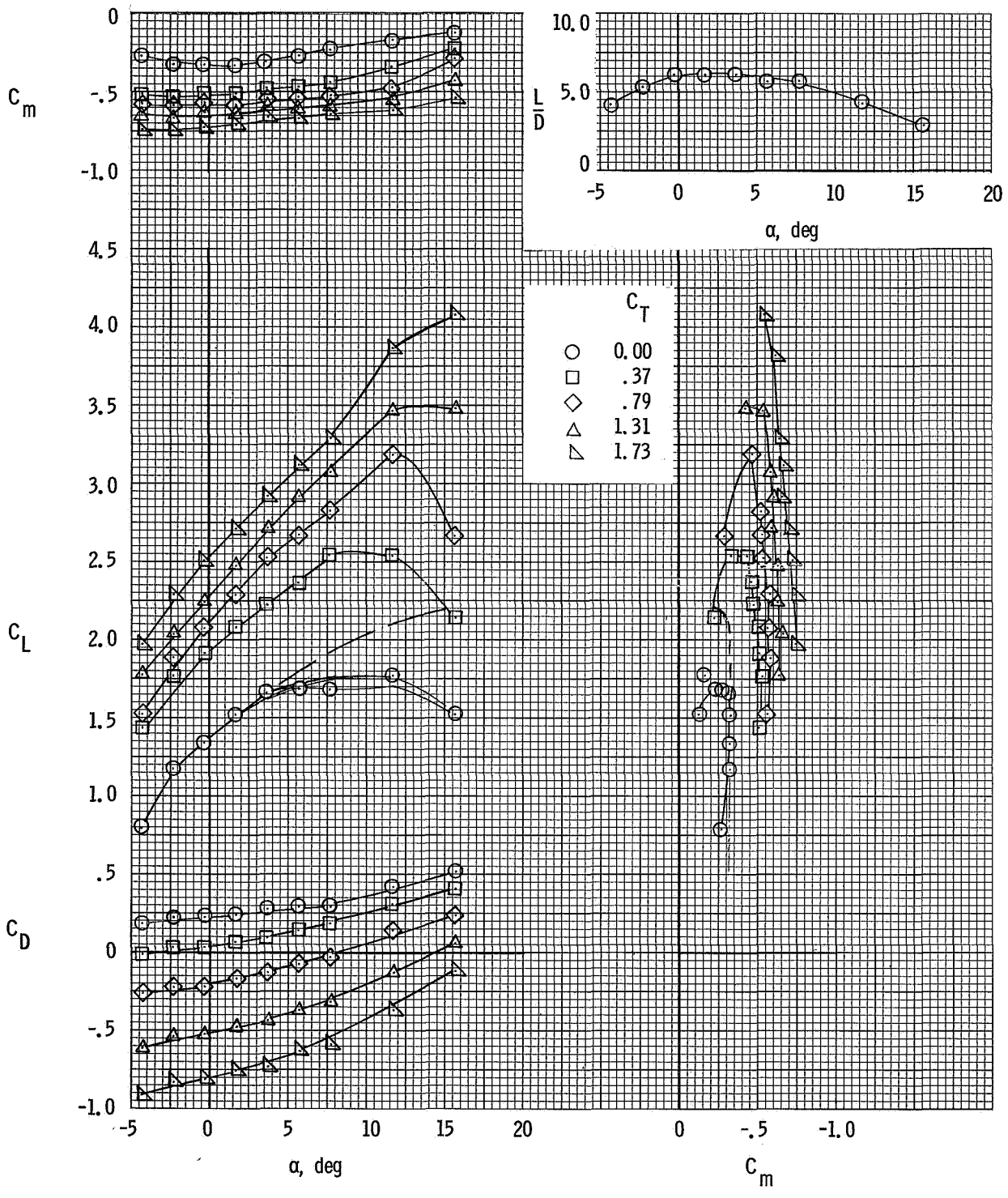

(c) $\delta_f = 55^0$.

Figure 4.- Continued.

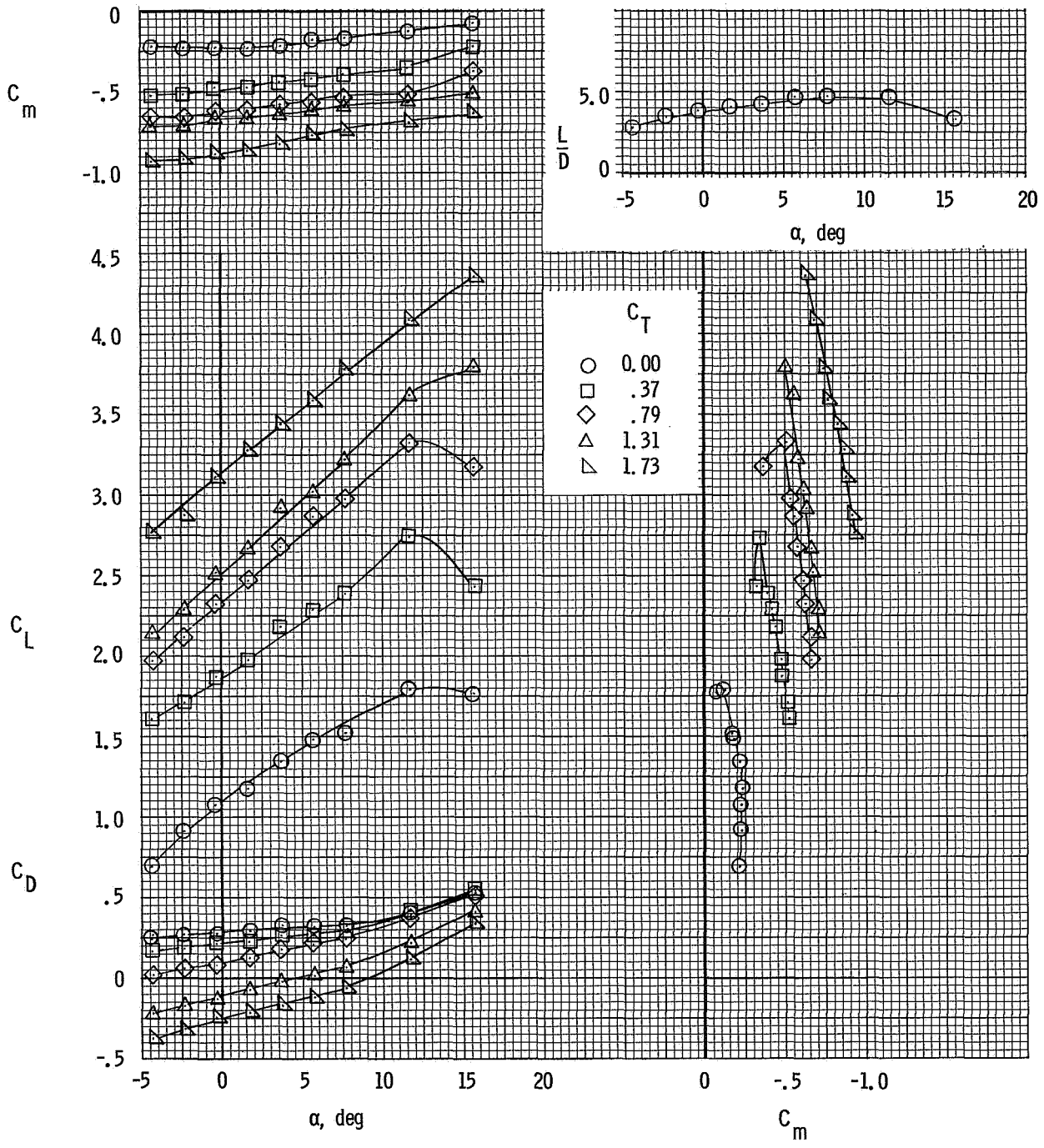

(d) $\delta_f = 70^0$.

Figure 4.- Concluded.

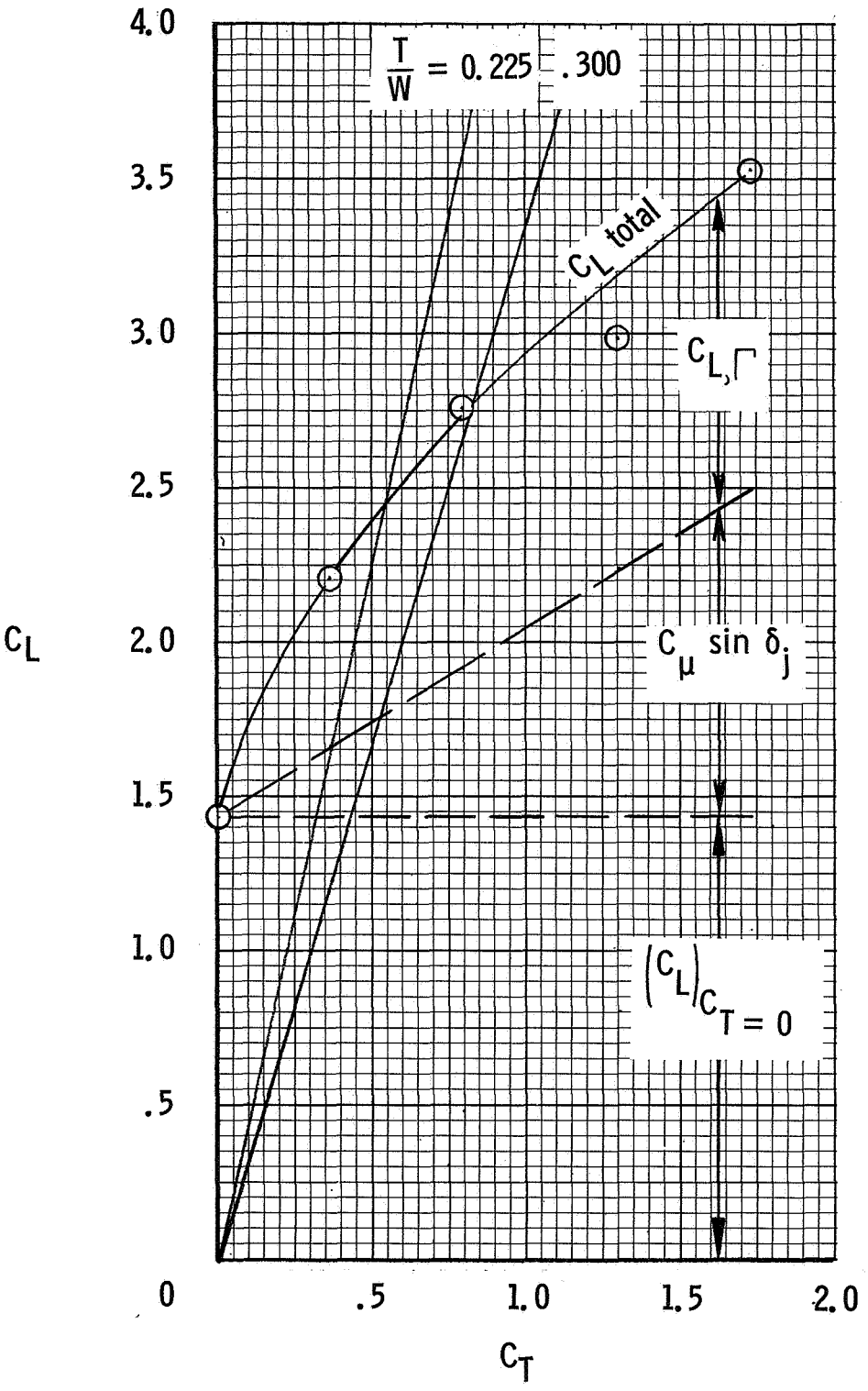

Figure 5.- Resolution of jet-flap lift into components.

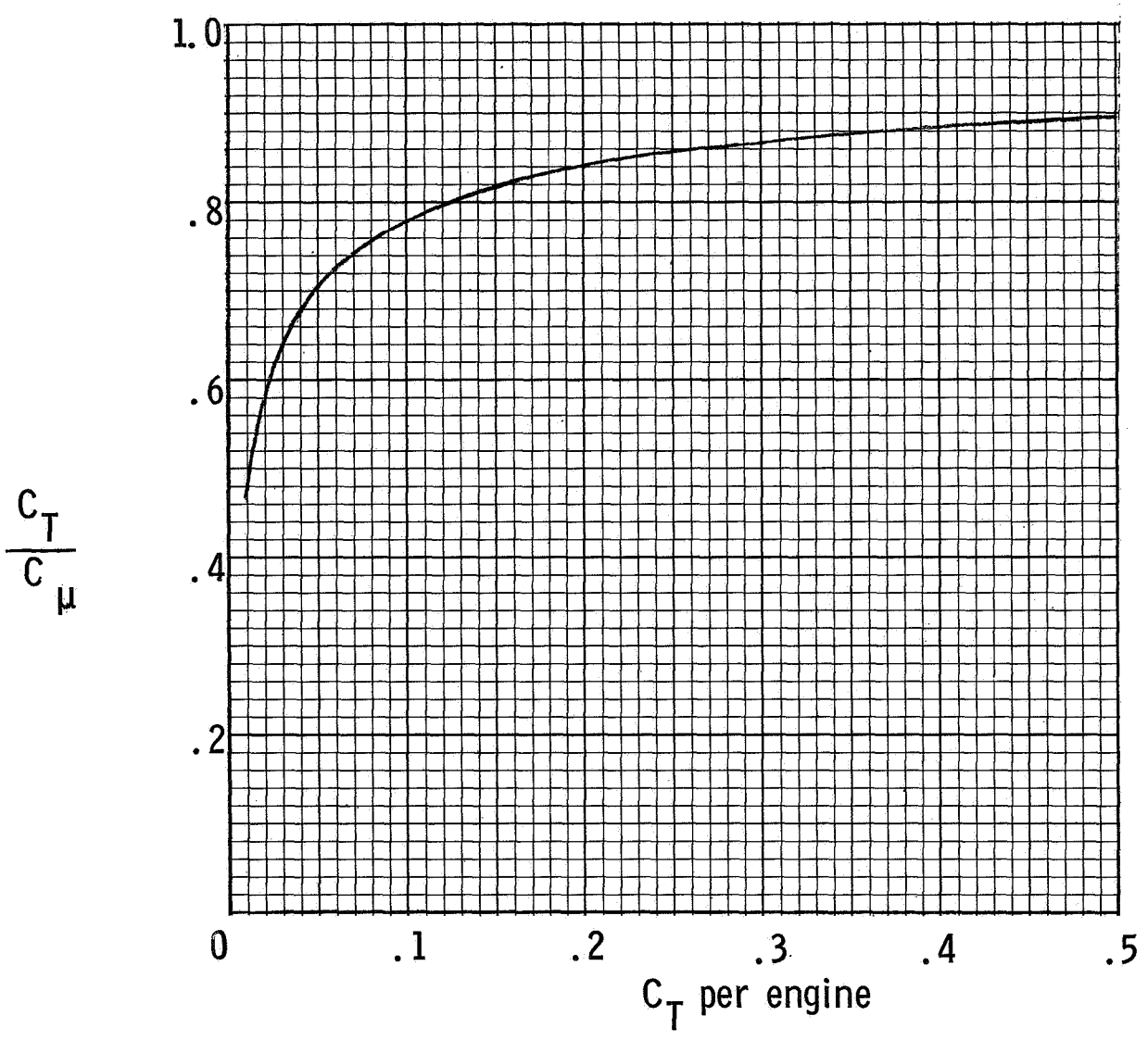

Figure 6.- Relationship between C_μ and C_T for engines of present model.

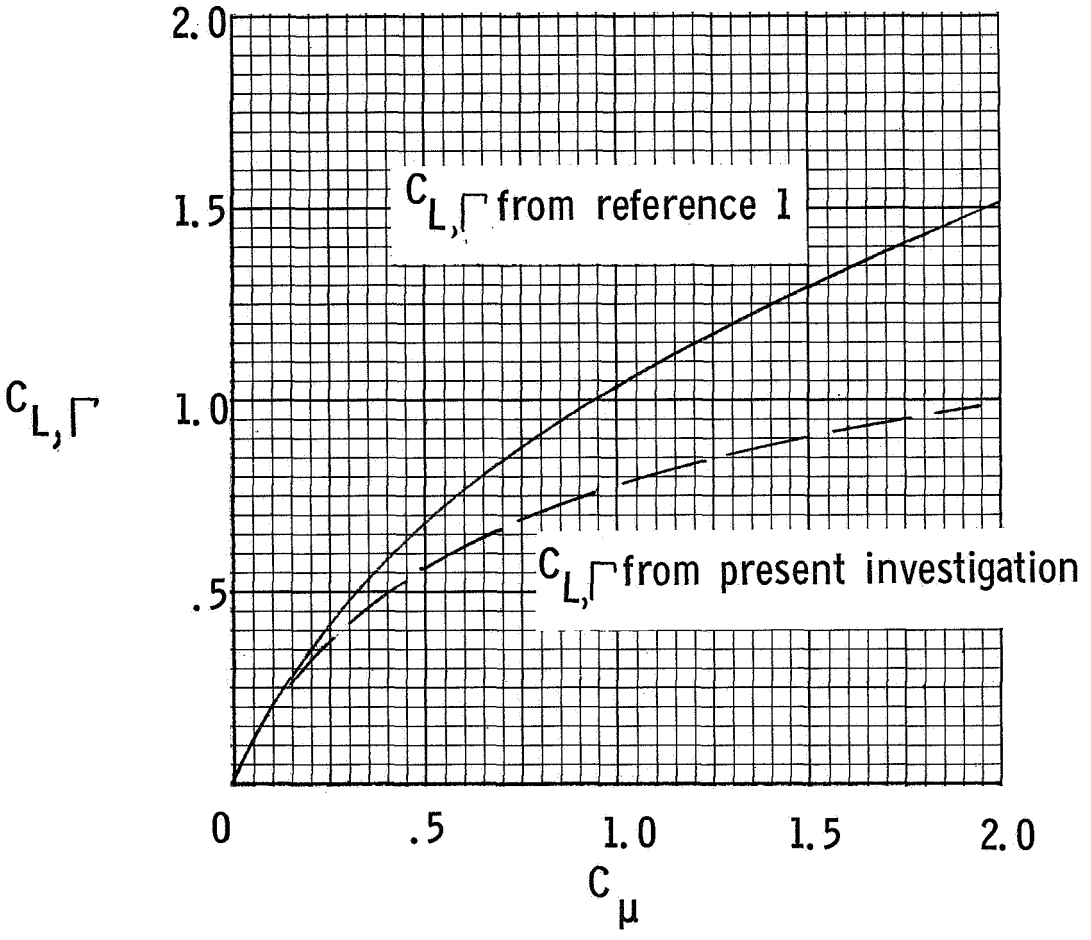

Figure 7.- Comparison of jet circulation lift produced by model of present investigation with that of reference 1. $\delta_f = 70^0$.

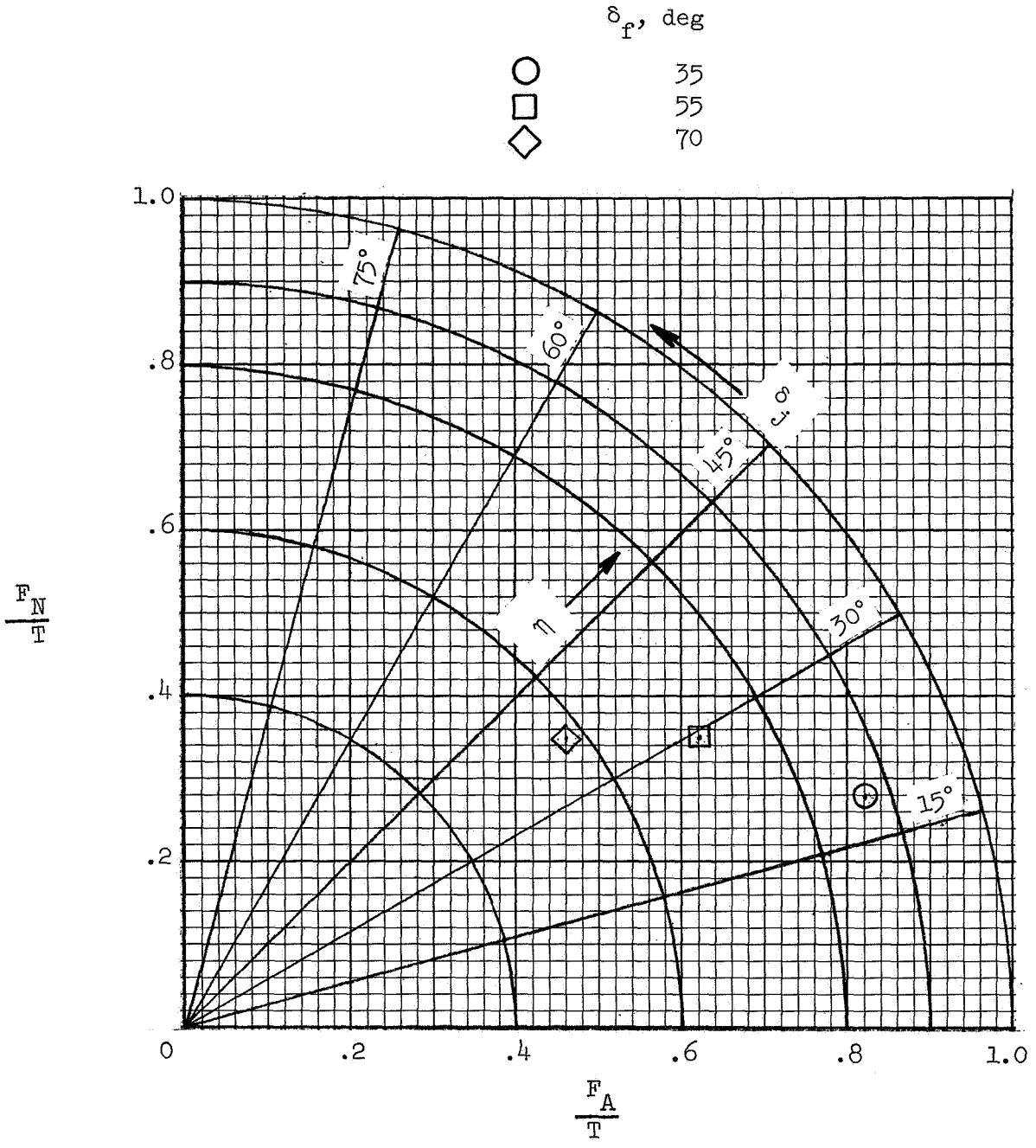

Figure 8.- Summary of turning efficiency and turning angle.

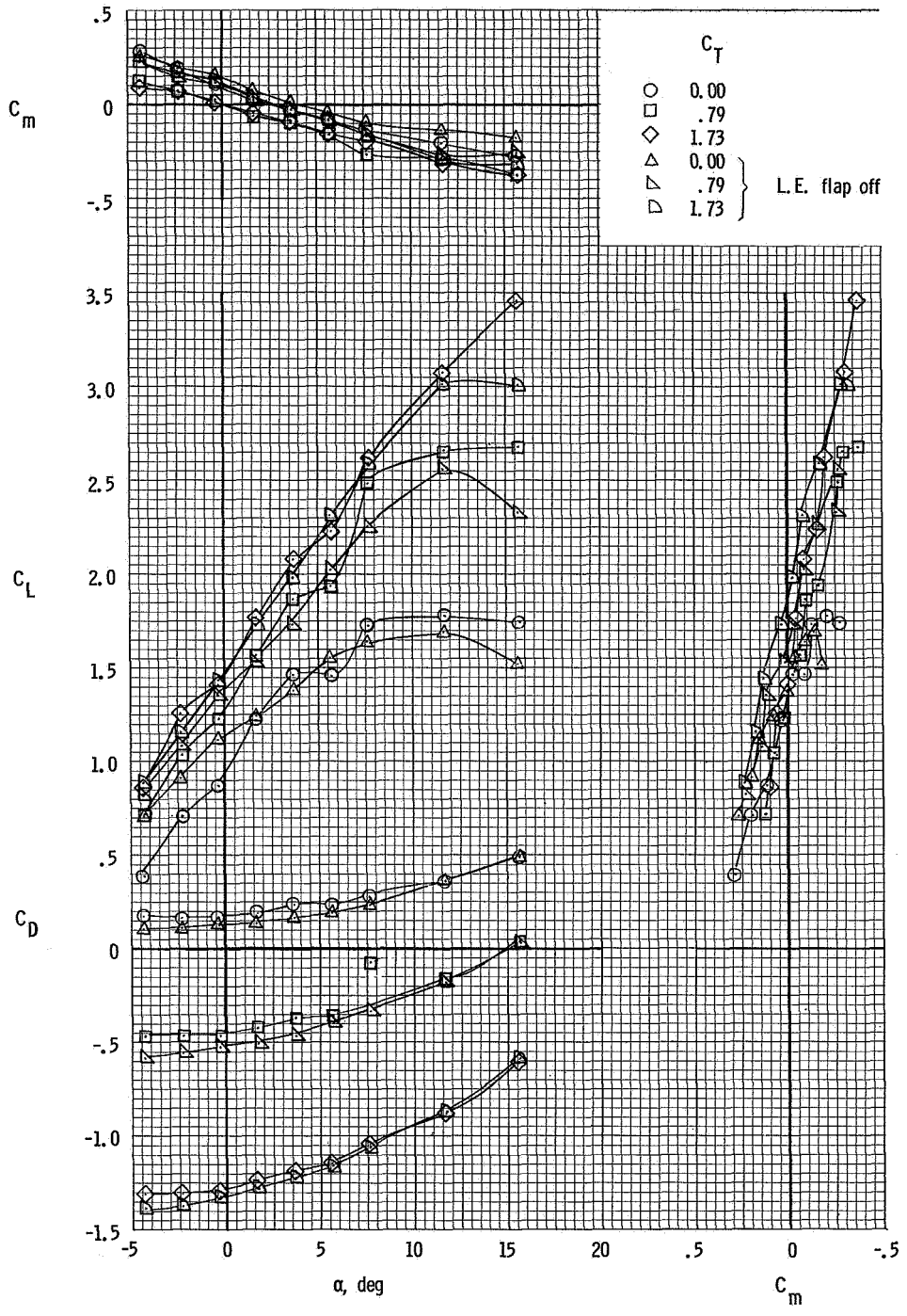

(a) Effect of leading-edge flap, gap open.

Figure 9.- Longitudinal characteristics of the model. $\delta_f = 35^0$; tail on; $\delta_e = 0^0$; $i_t = -5^0$.

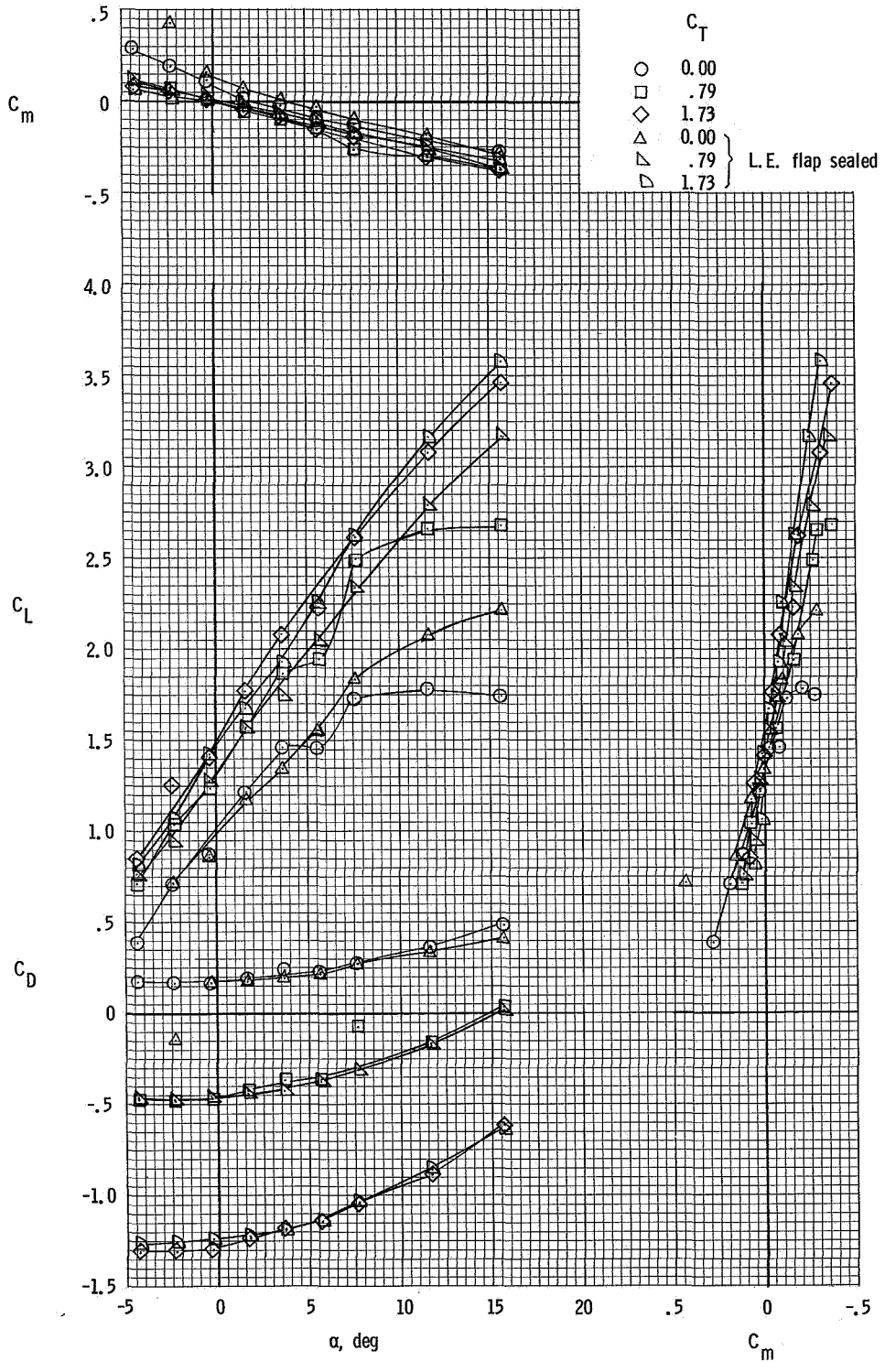

(b) Effect of sealing leading-edge gap.

Figure 9.- Concluded.

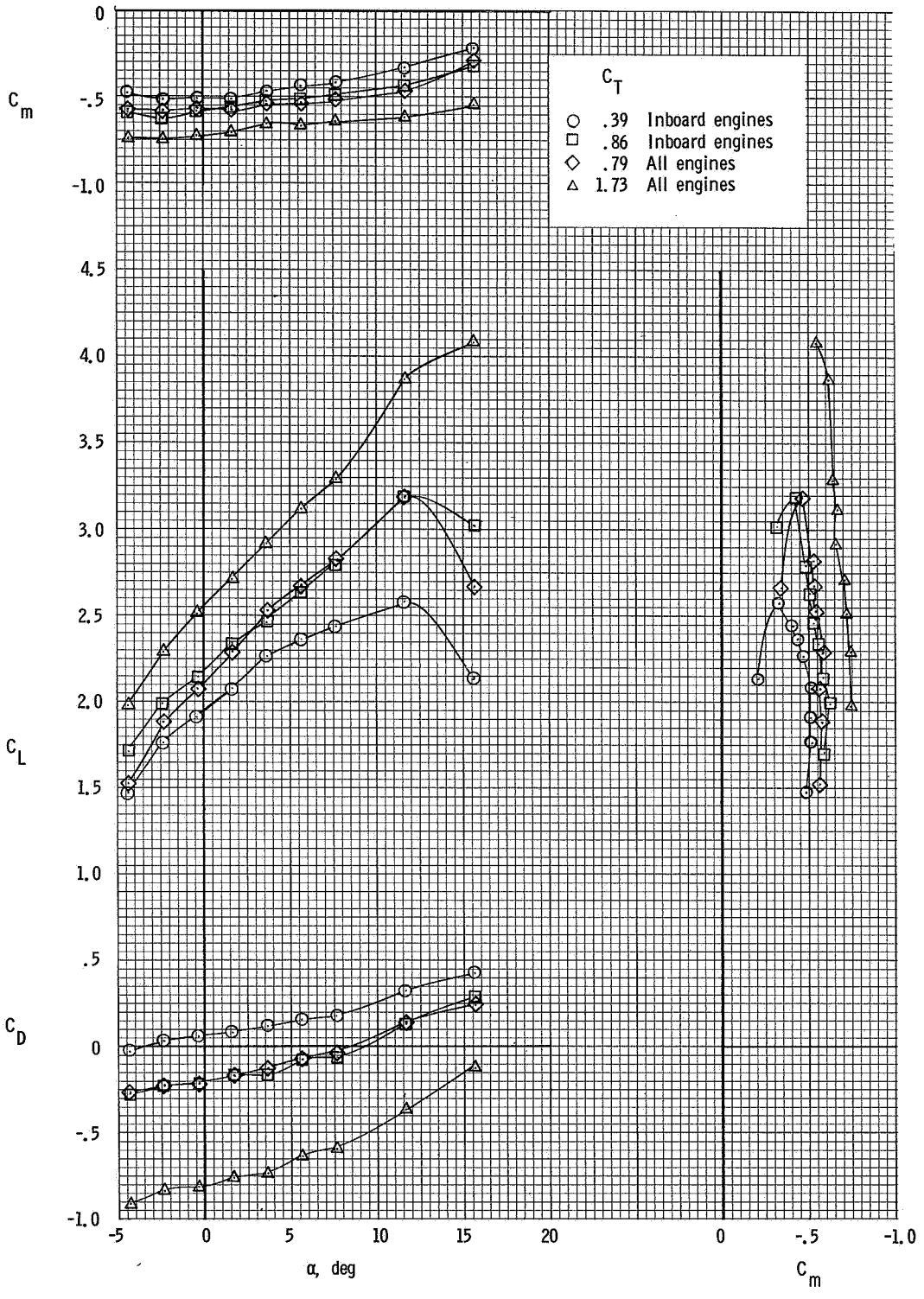

(a) Longitudinal characteristics.

Figure 10.- Effect of thrust distribution on characteristics of the model. $\delta_f = 55^o$; tail off.

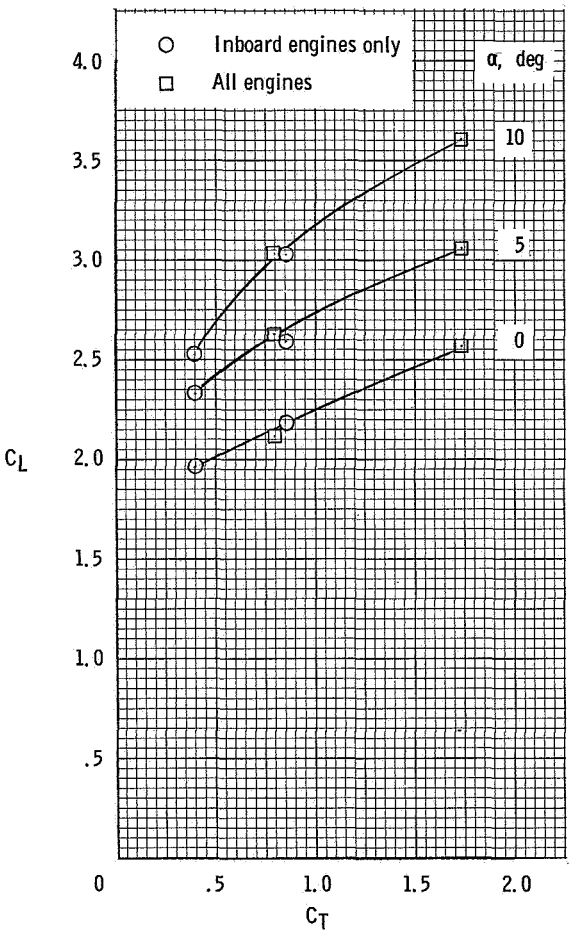

(b) Lift characteristics.

Figure 10.- Concluded.

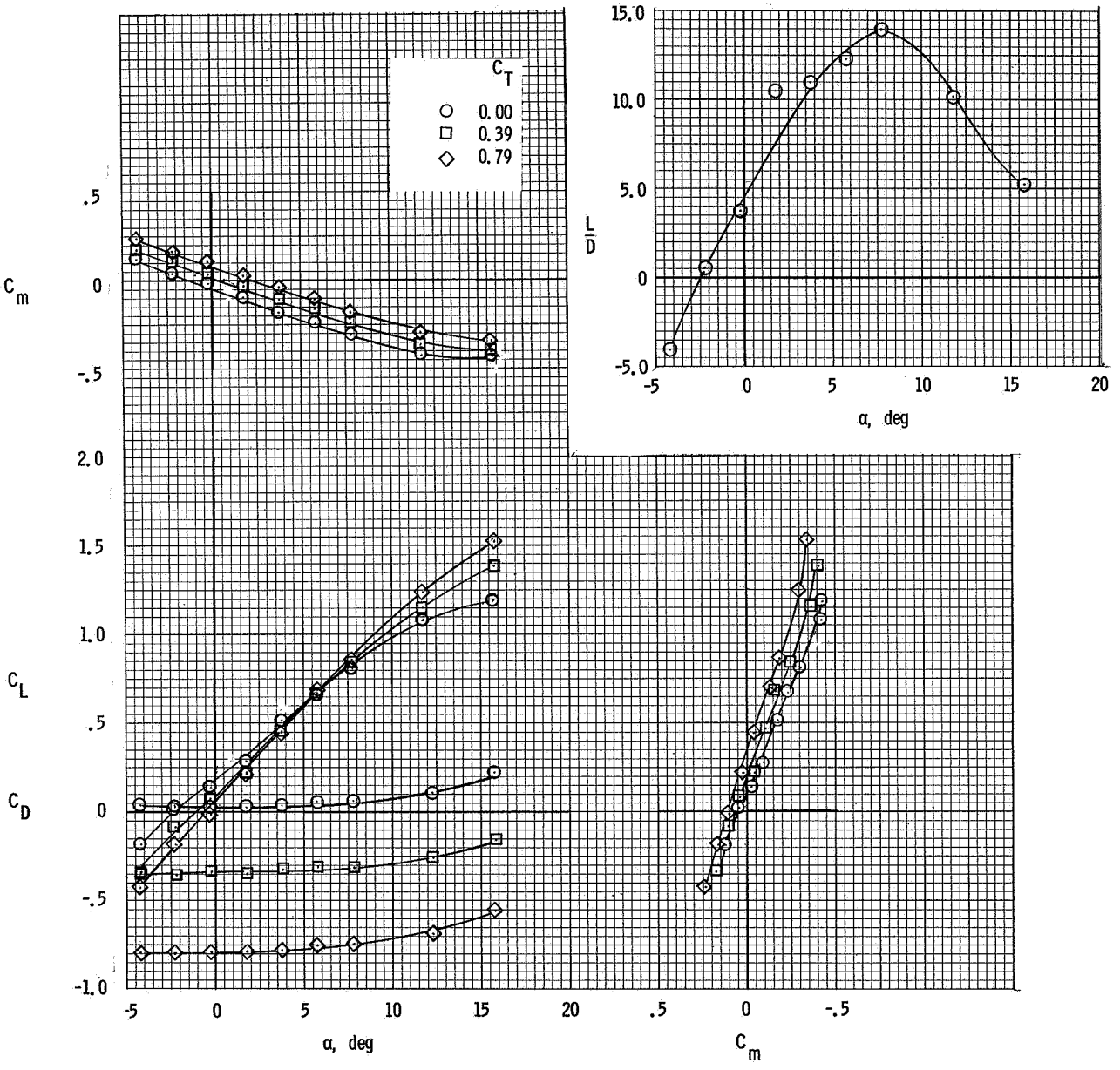

Figure 11.- Effect of thrust on longitudinal characteristics for the clean condition. $\delta_f = 0^0$; $i_t = 0^0$; $\delta_e = 0^0$.

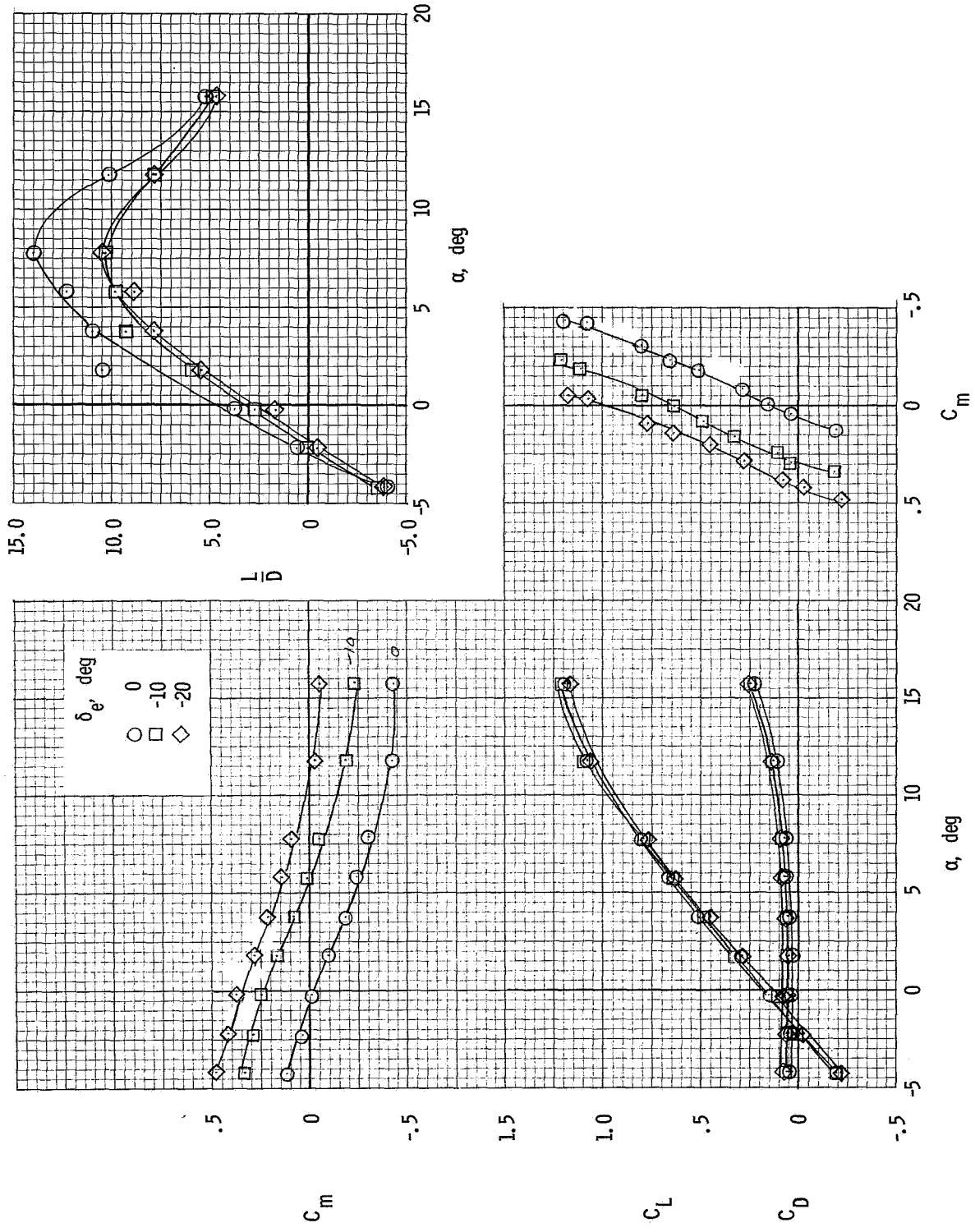

Figure 12.- Elevator effectiveness for clean condition. $\delta_f = 0^o$; $i_t = 0^o$; $C_T = 0$.

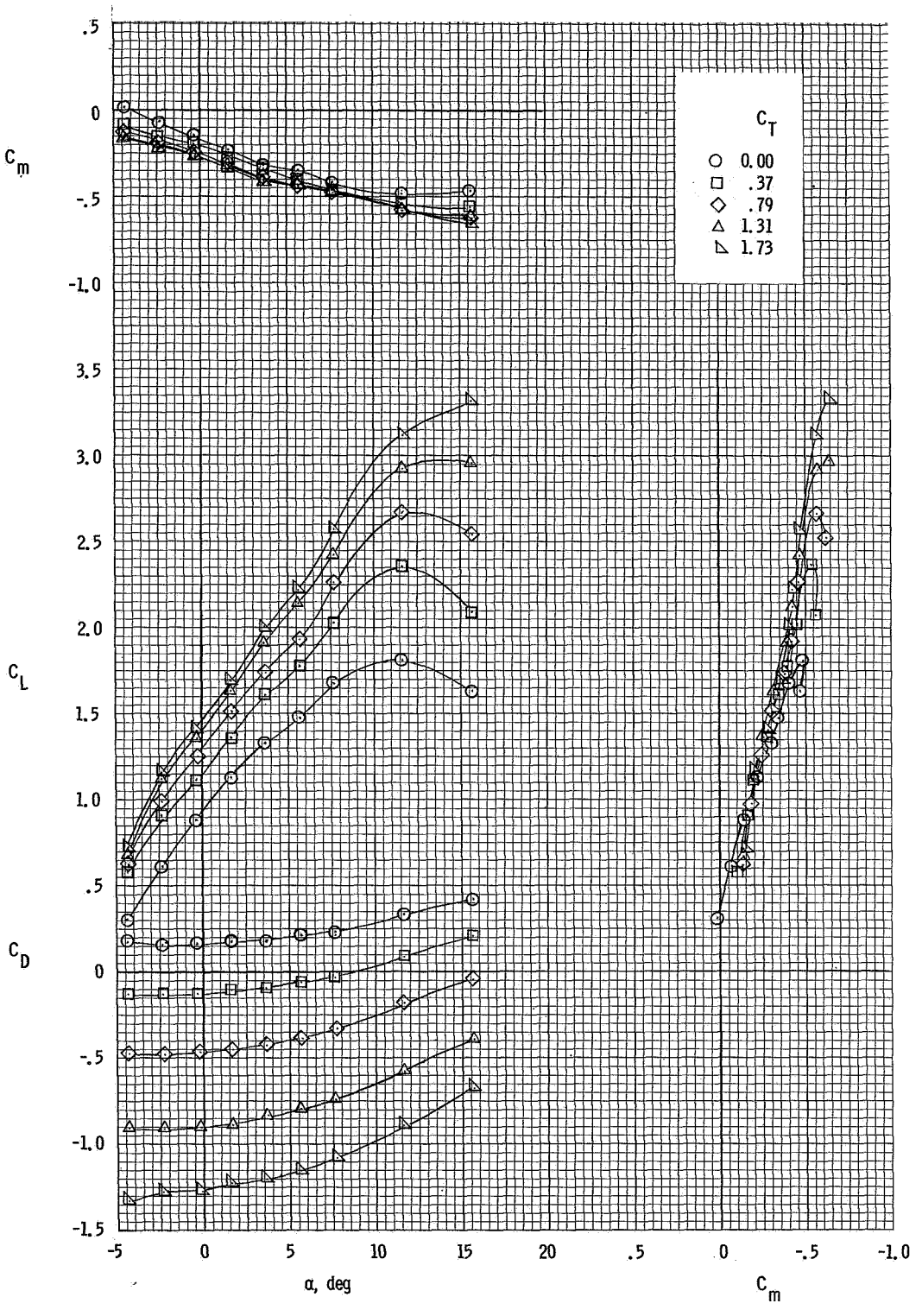

(a) $\delta_f = 35^0$.

Figure 13.- Effect of thrust on longitudinal characteristics of the model with flaps down. $i_t = 0^0$.

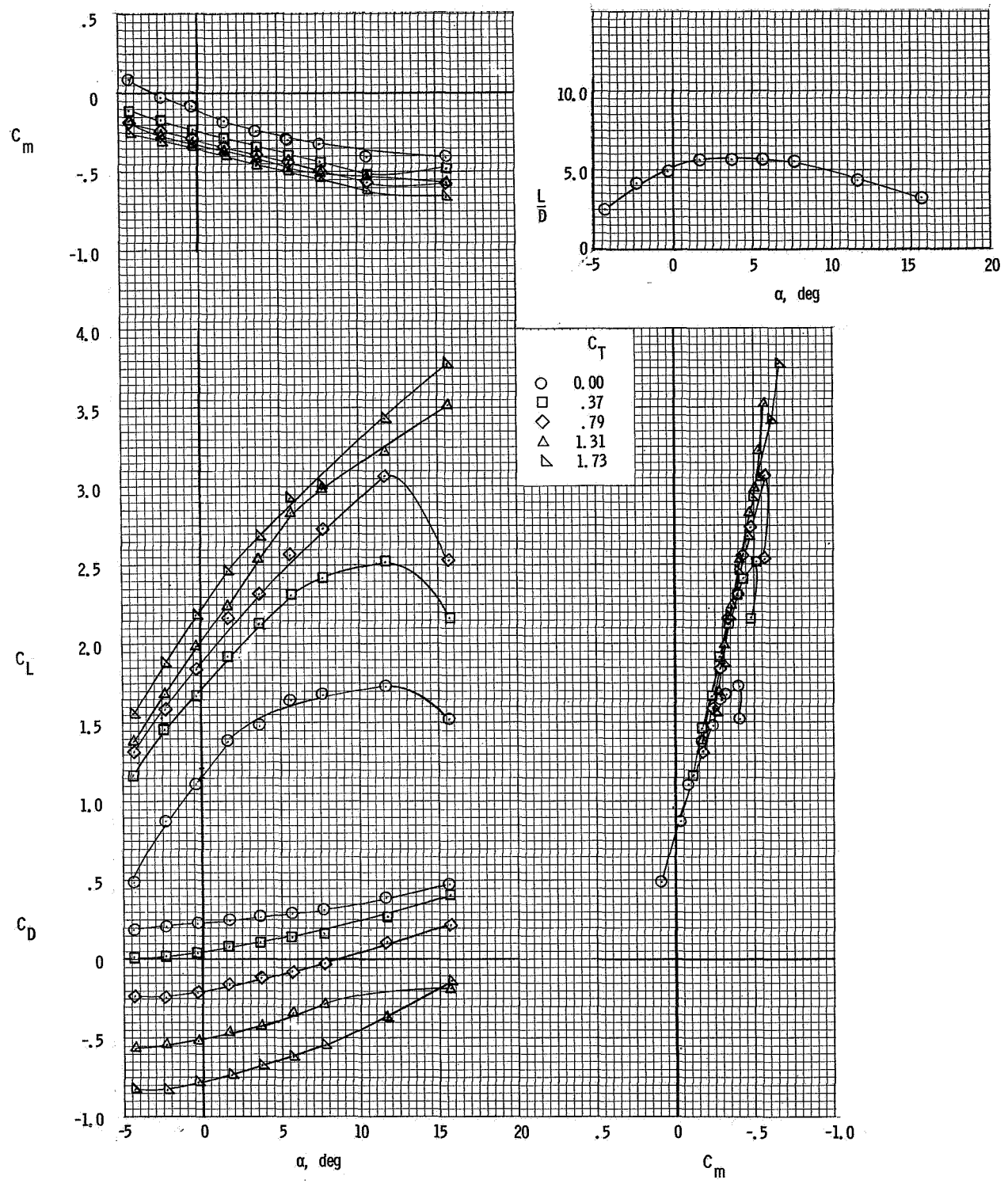

(b) $\delta_f = 55^0$.

Figure 13.- Concluded.

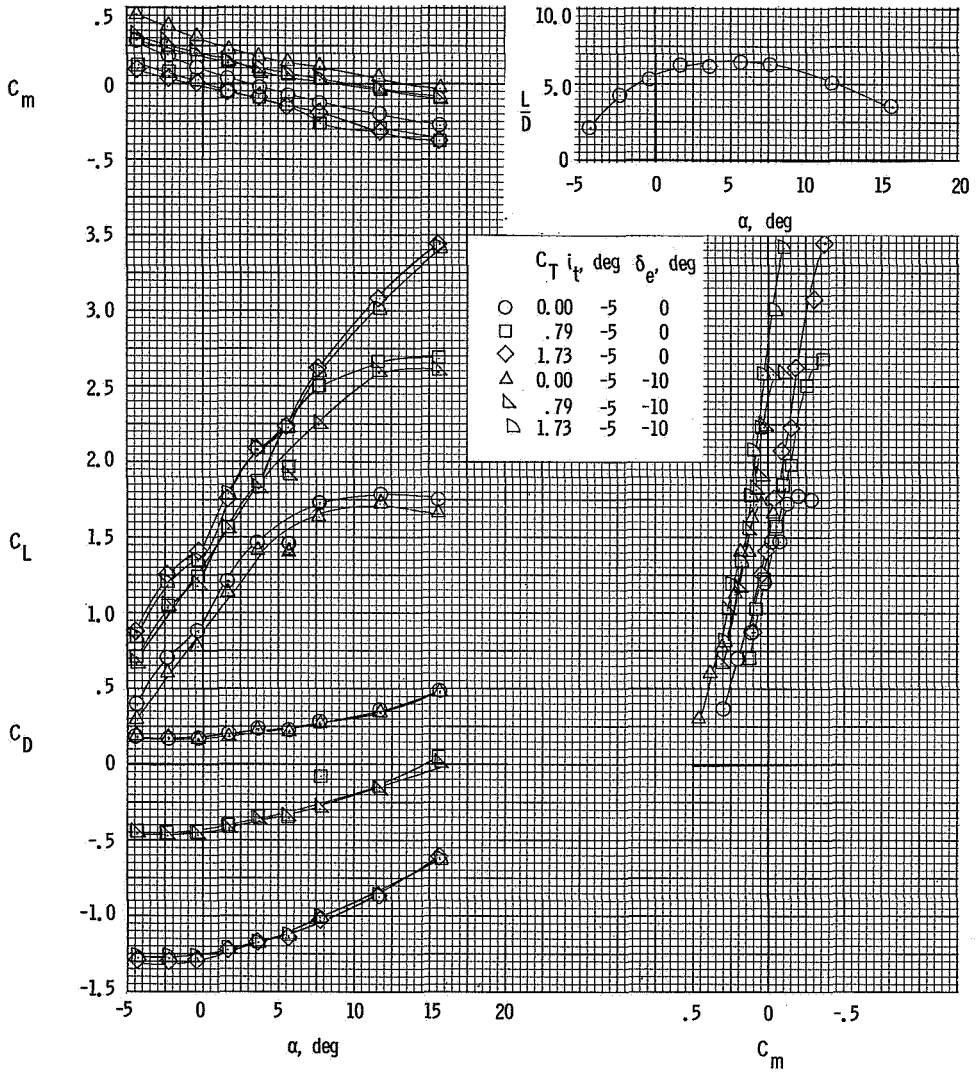

(a) $\delta_f = 35^0$.

Figure 14.- Longitudinal control effectiveness of the model with flaps down.

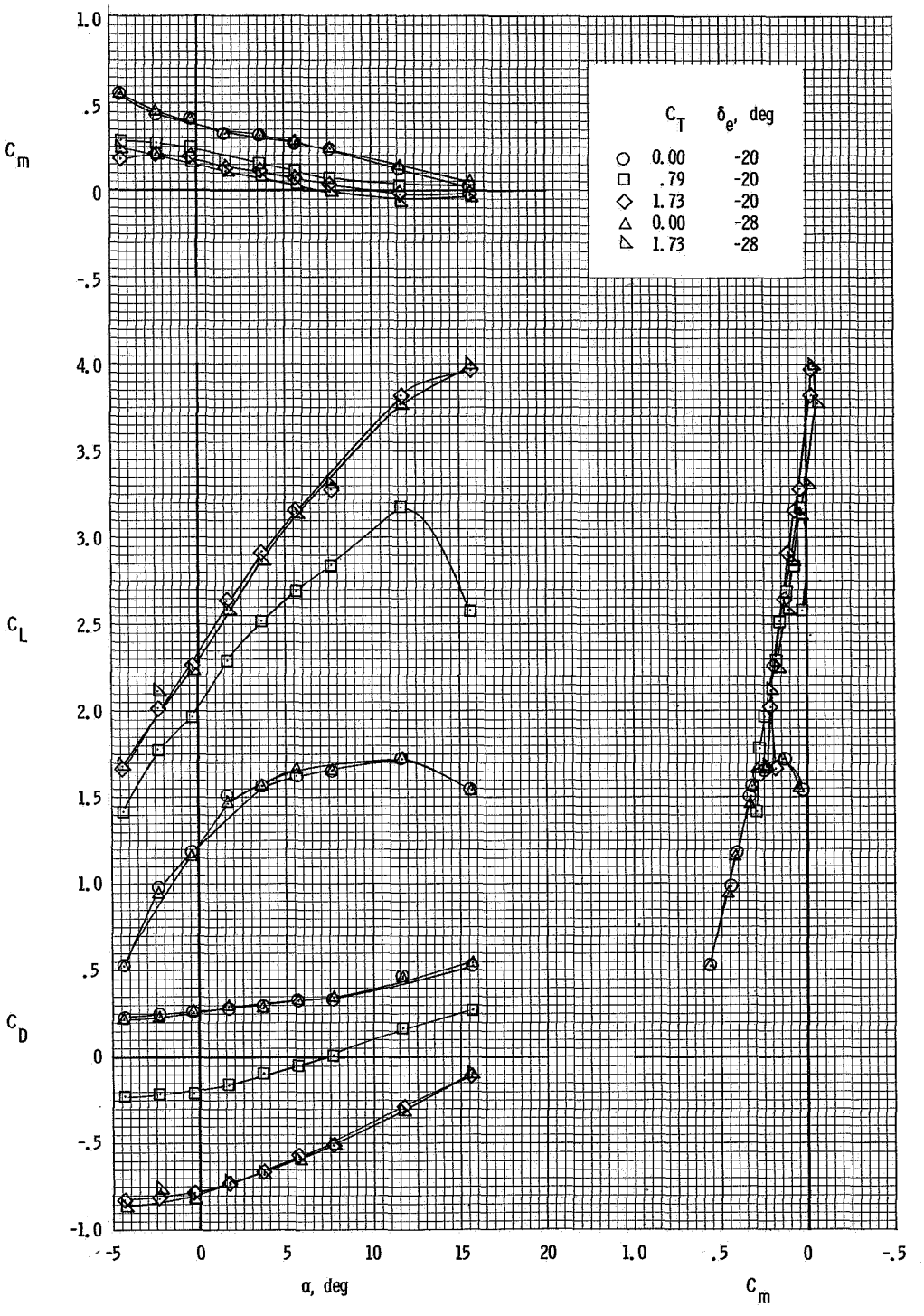

(b) $\delta_f = 55^0$.

Figure 14.- Concluded.

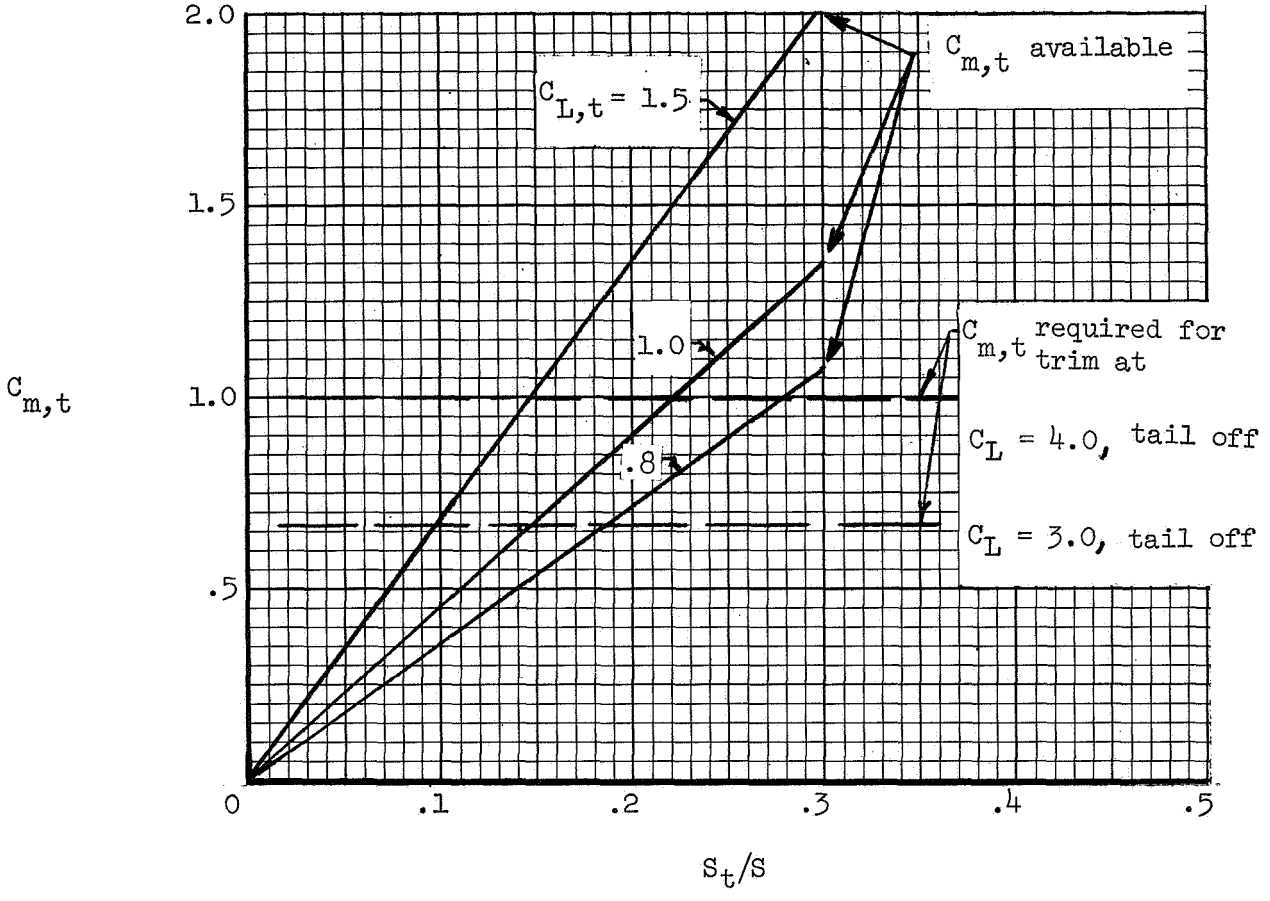

Figure 15.- Variation of pitching moment of the tail with horizontal-tail area. $\delta_f = 55^o$; $\alpha = 5^o$.

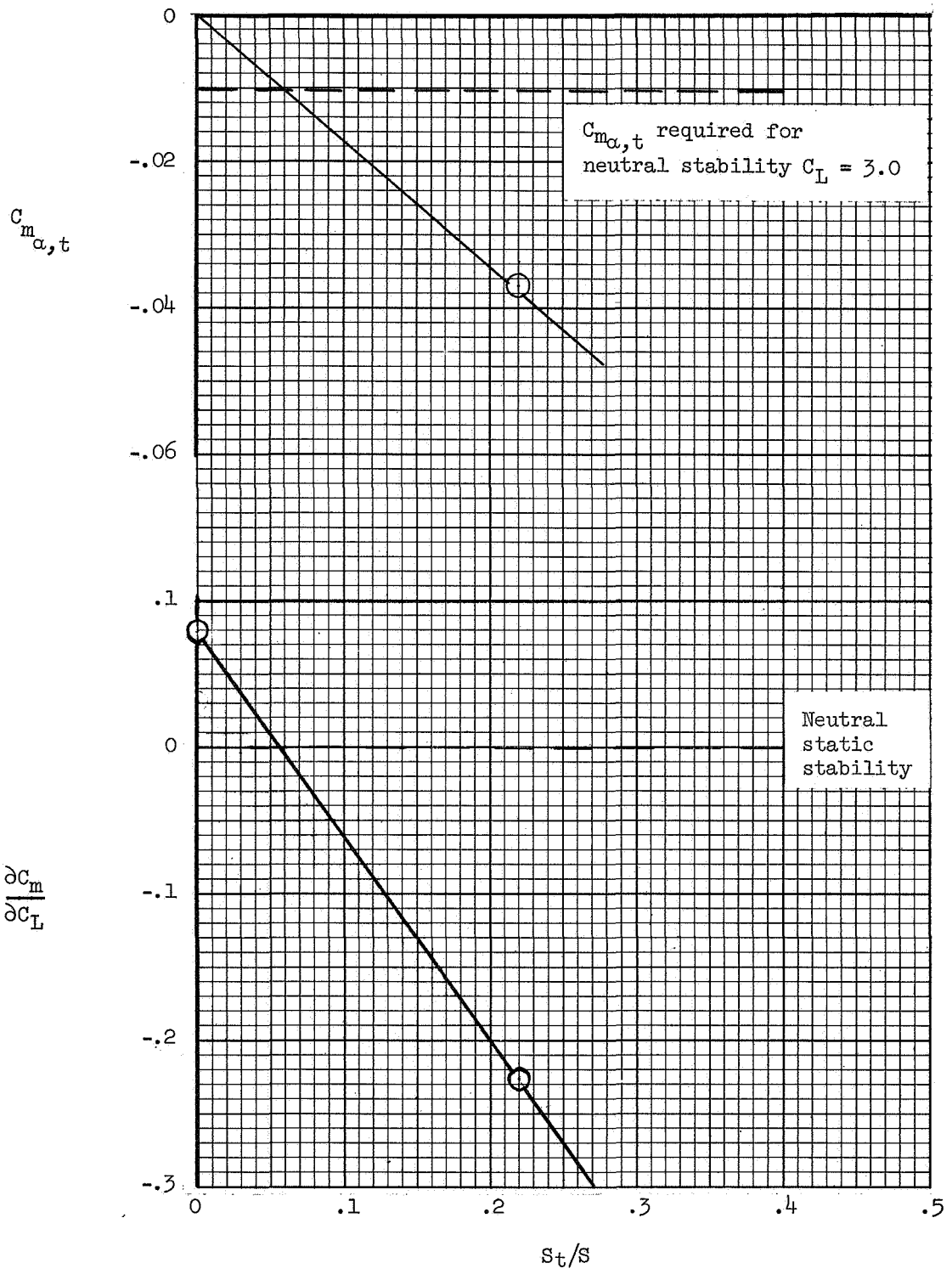

Figure 16.- Variation of longitudinal stability parameters with horizontal-tail area. $\delta_f = 55^0$; $\alpha = 5^0$.

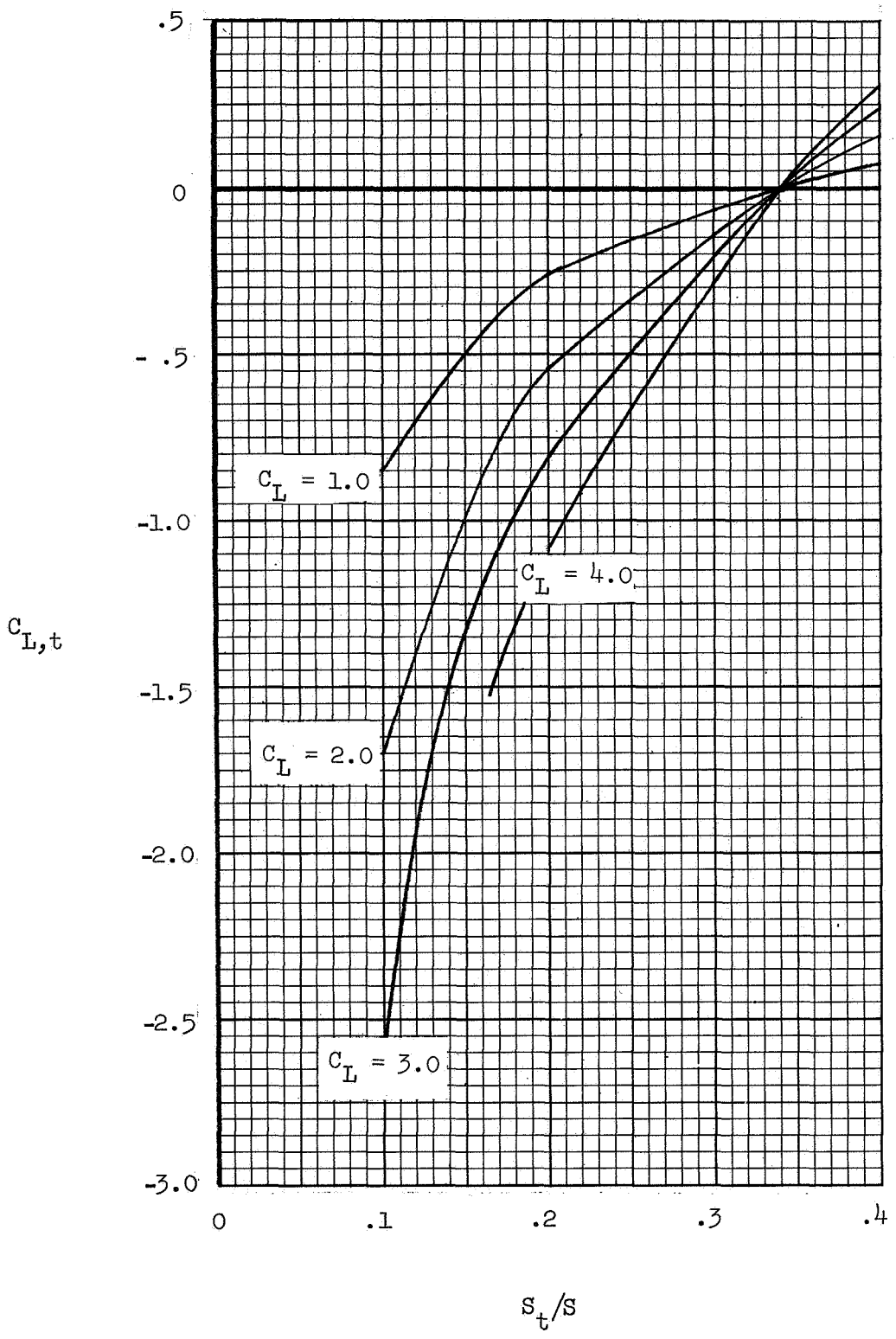

Figure 17.- Variation of tail lift coefficient required for trim and 10-percent static margin with horizontal-tail area. $\delta_f = 55^0$; $\alpha = 5^0$.

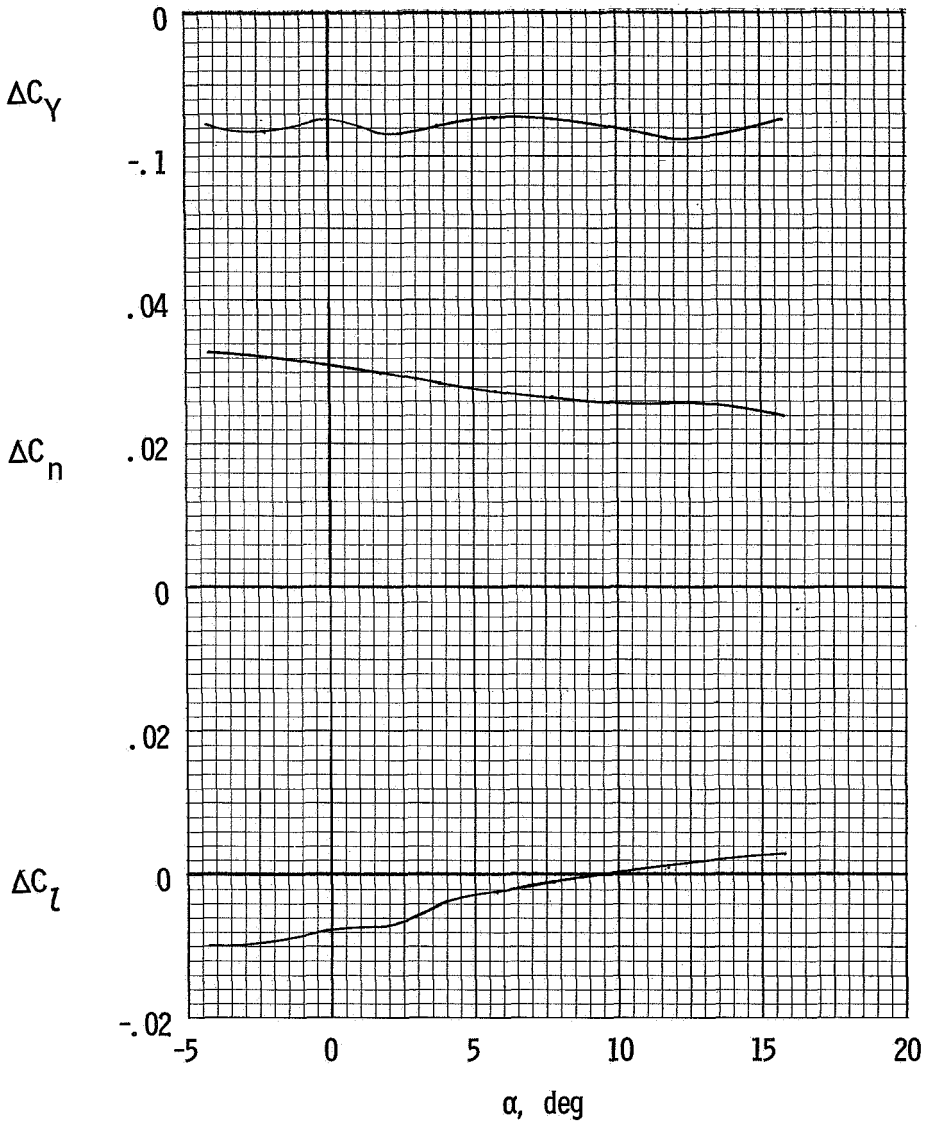

(a) $\delta_f = 0^0$.

Figure 18.- Incremental lateral forces and moments produced by rudder deflection. $\delta_r = -35^0$; $C_T = 0$; $\delta_e = 0^0$; $i_t = 0^0$.

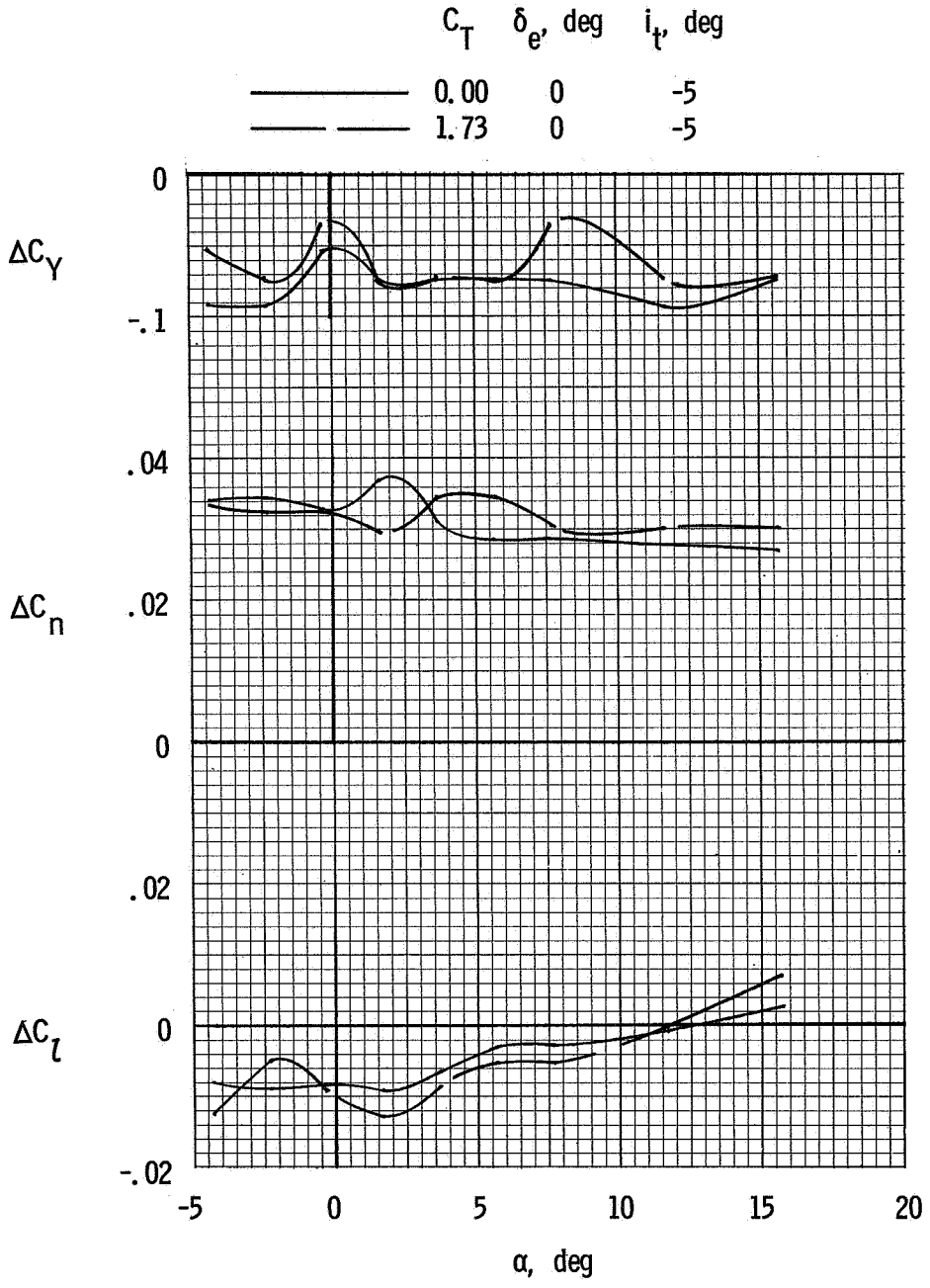

(b) $\delta_f = 35^0$.

Figure 18.- Continued.

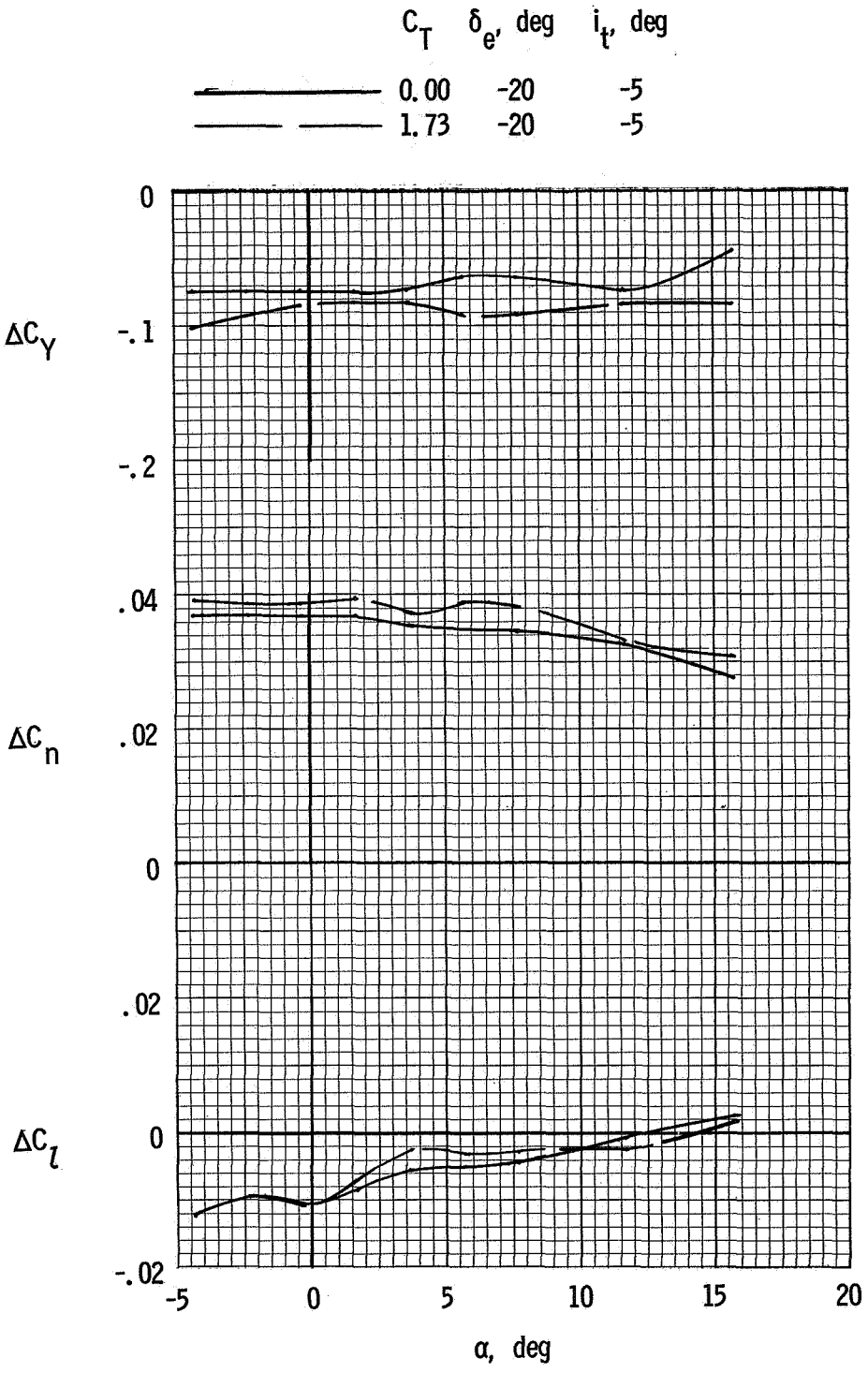

(c) $\delta_f = 55^0$.

Figure 18.- Concluded.

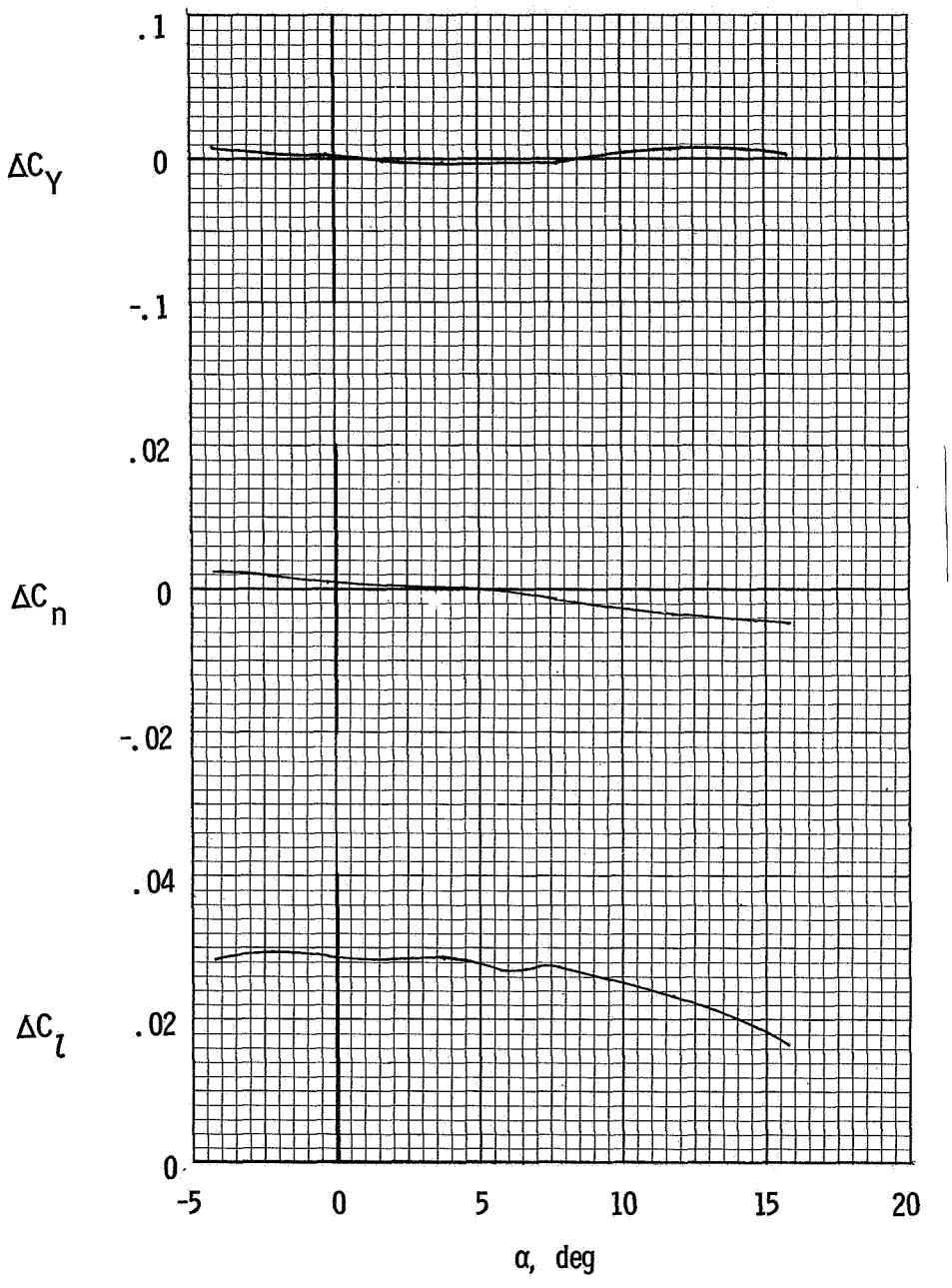

(a) $\delta_f = 0^0$.

Figure 19.- Incremental lateral forces and moments produced by aileron deflection. $C_T = 0$; $\delta_e = 0^0$; $i_t = 0^0$; $\delta_{a,R} = -25^0$; $\delta_{a,L} = 15^0$.

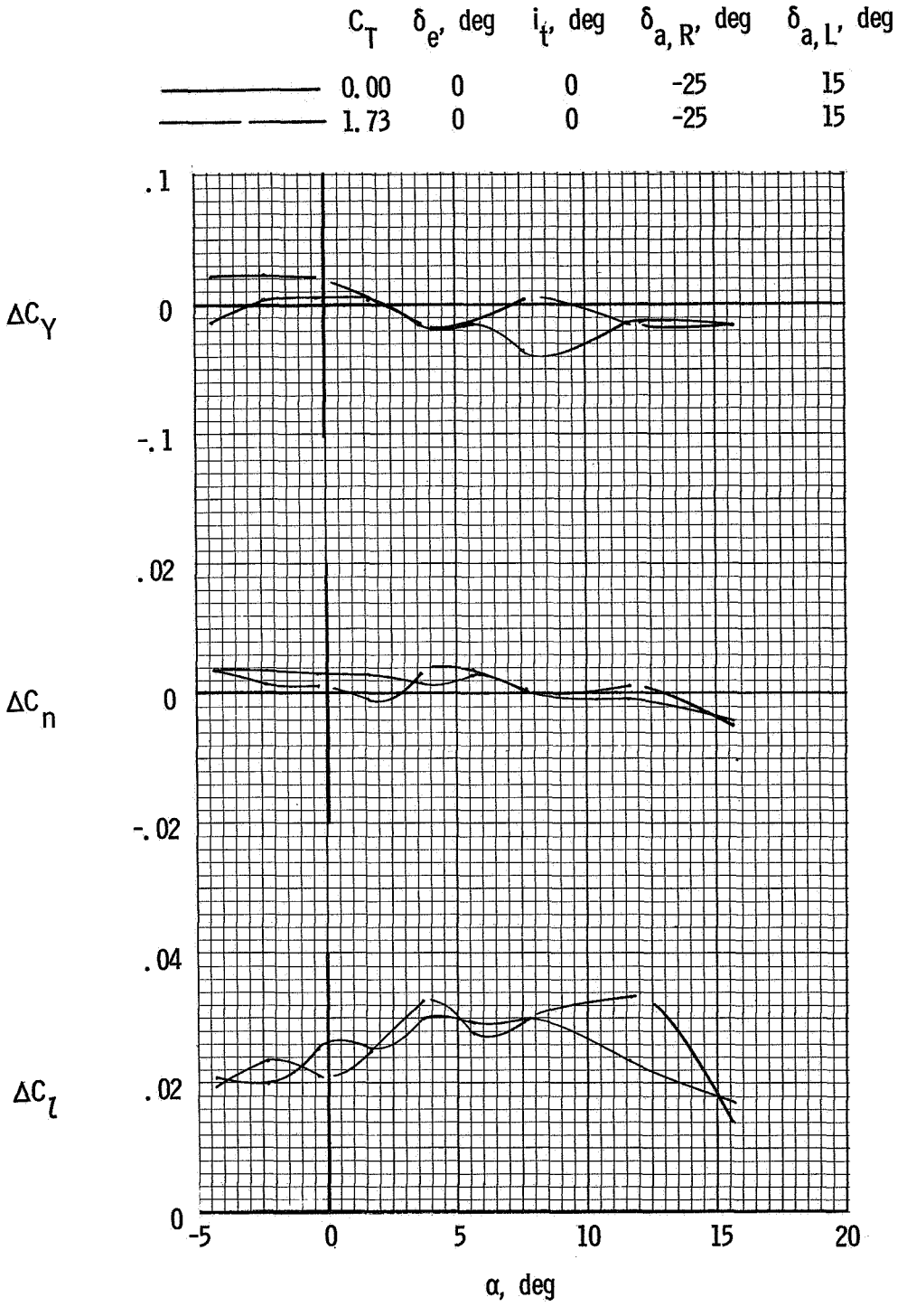

(b) $\delta_f = 35^o$.

Figure 19.- Continued.

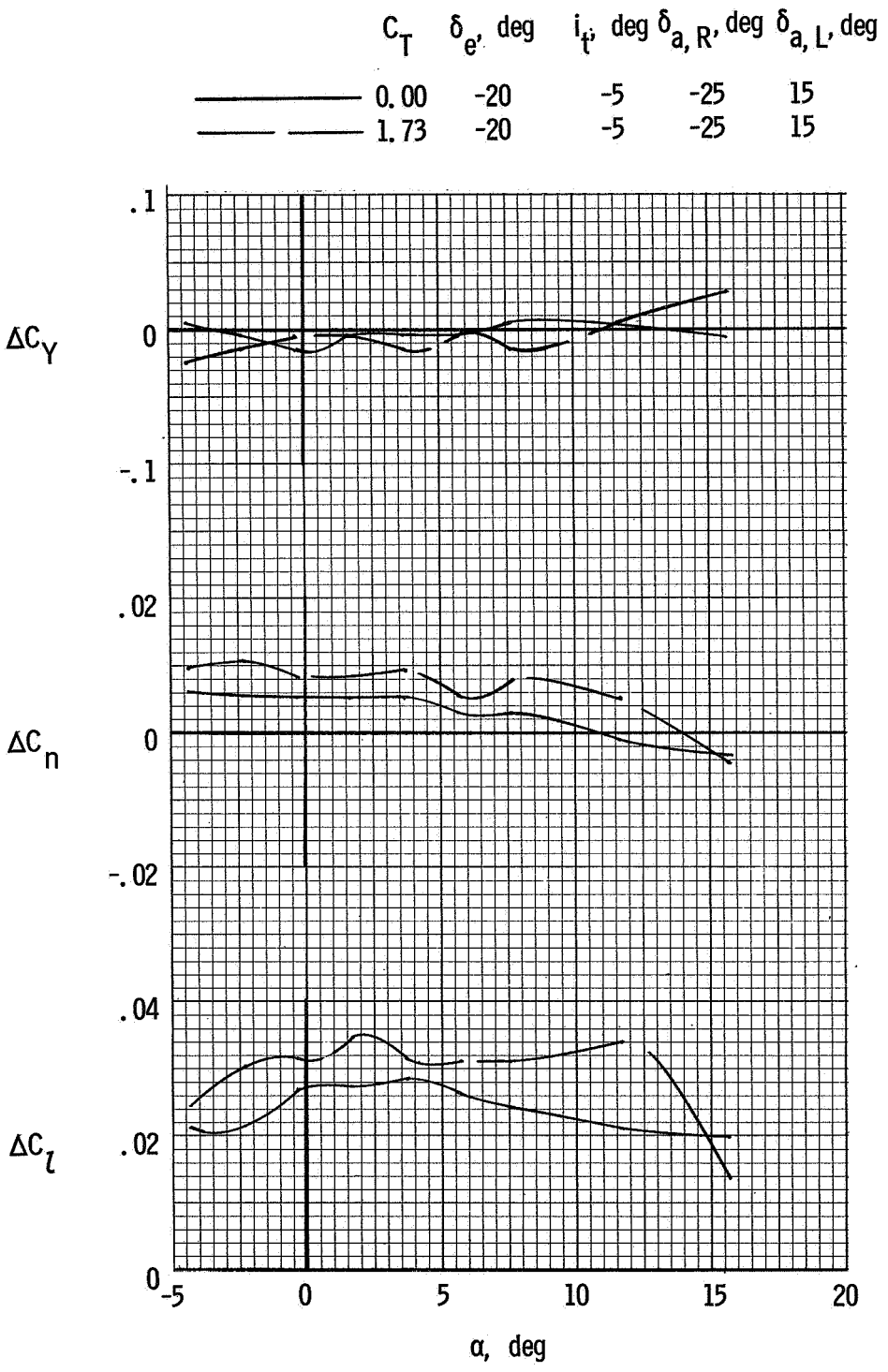

(c) $\delta_f = 55^0$.

Figure 19.- Concluded.

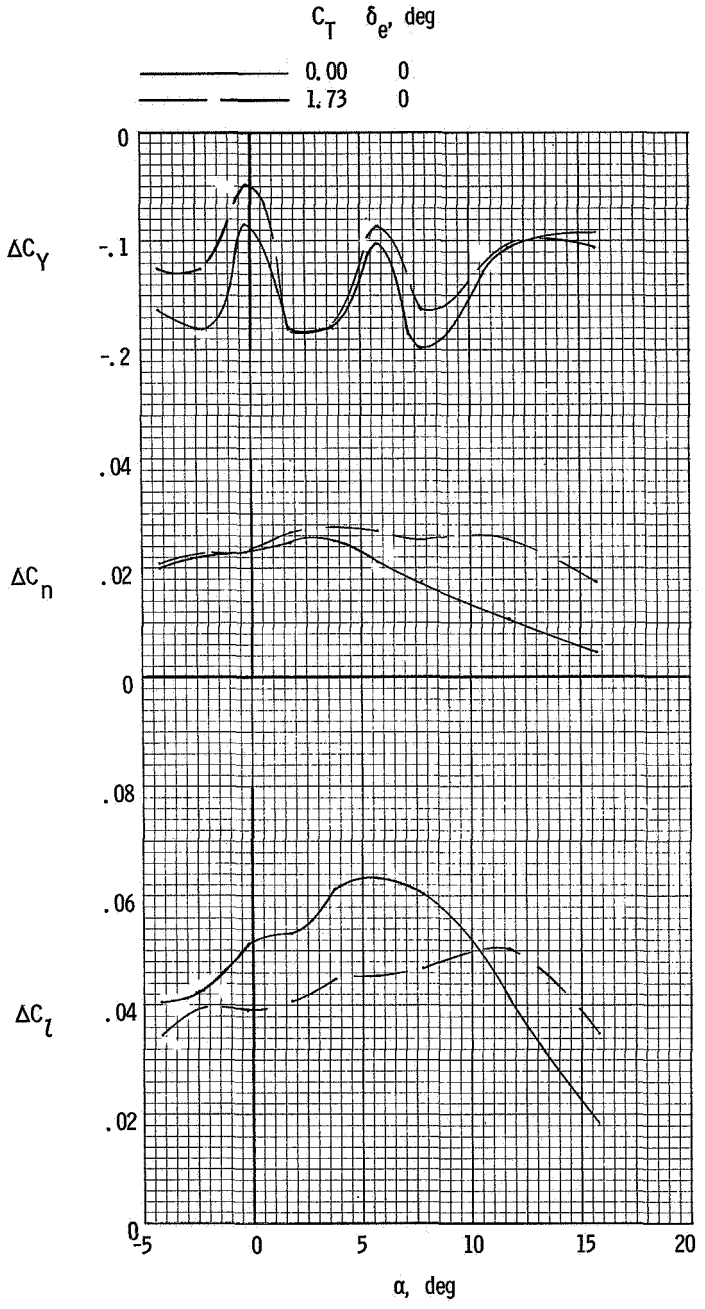

(a) $\delta_f = 35^0$.

Figure 20.- Incremental lateral forces and moments produced by spoiler deflection. $\delta_{s,R} = 30^0$; $i_t = -5^0$.

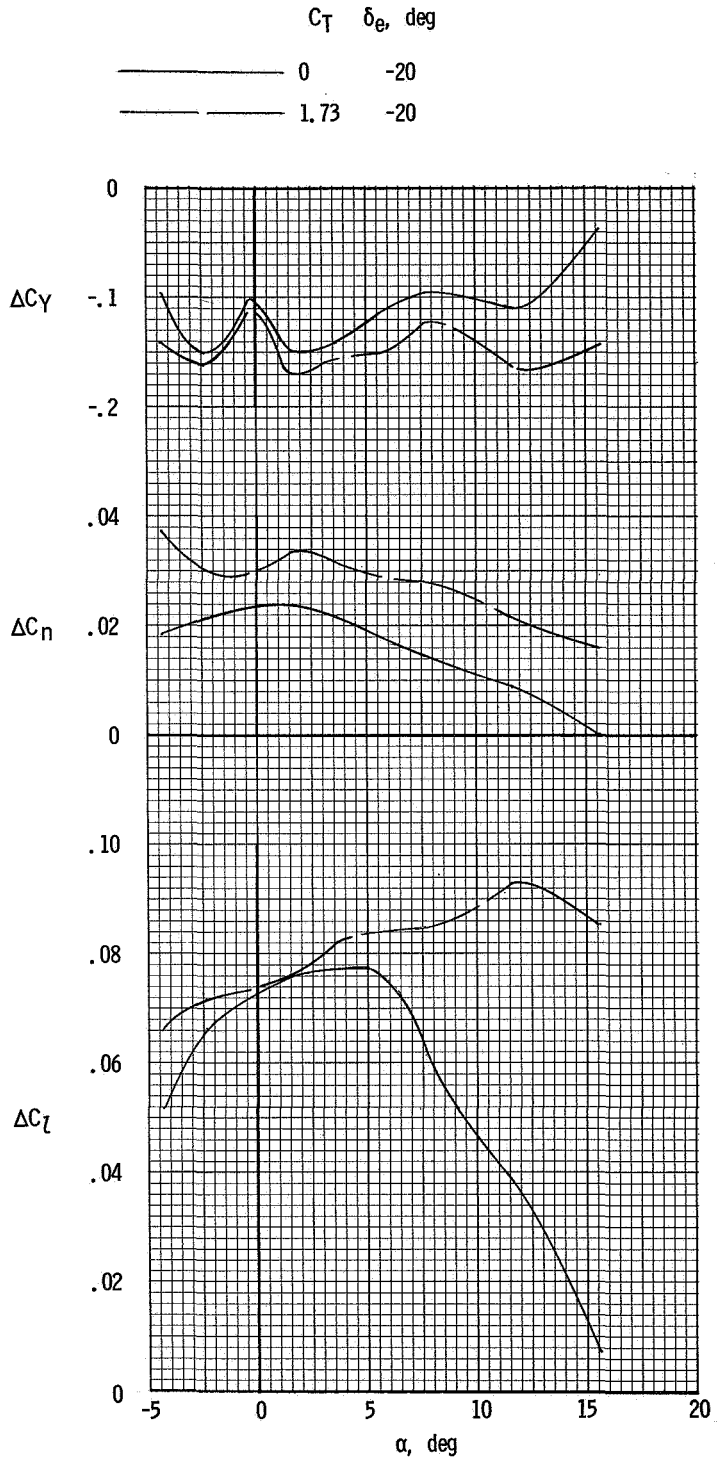

(b) $\delta_f = 55^0$.

Figure 20.- Concluded.

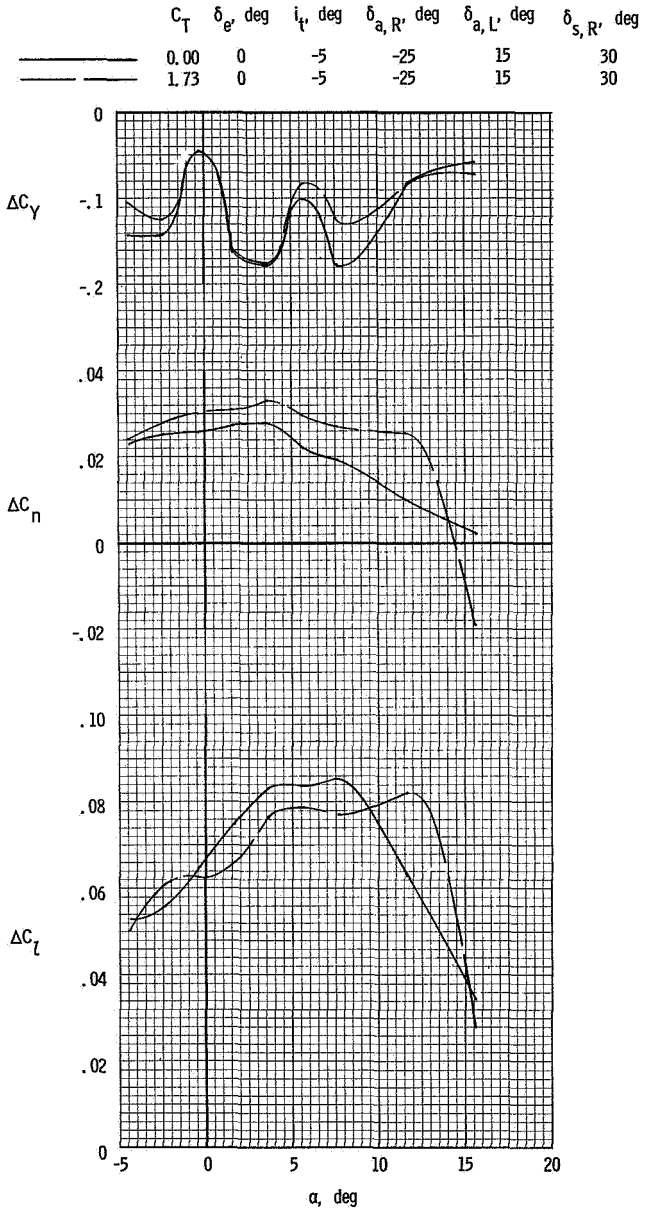

(a) $\delta_f = 35^0$.

Figure 21.- Incremental lateral forces and moments produced by simultaneous deflection of spoiler and aileron control. $\delta_e = 0^0$; $i_t = -5^0$; $\delta_{a,R} = -25^0$; $\delta_{a,L} = 15^0$; $\delta_{s,R} = 30^0$.

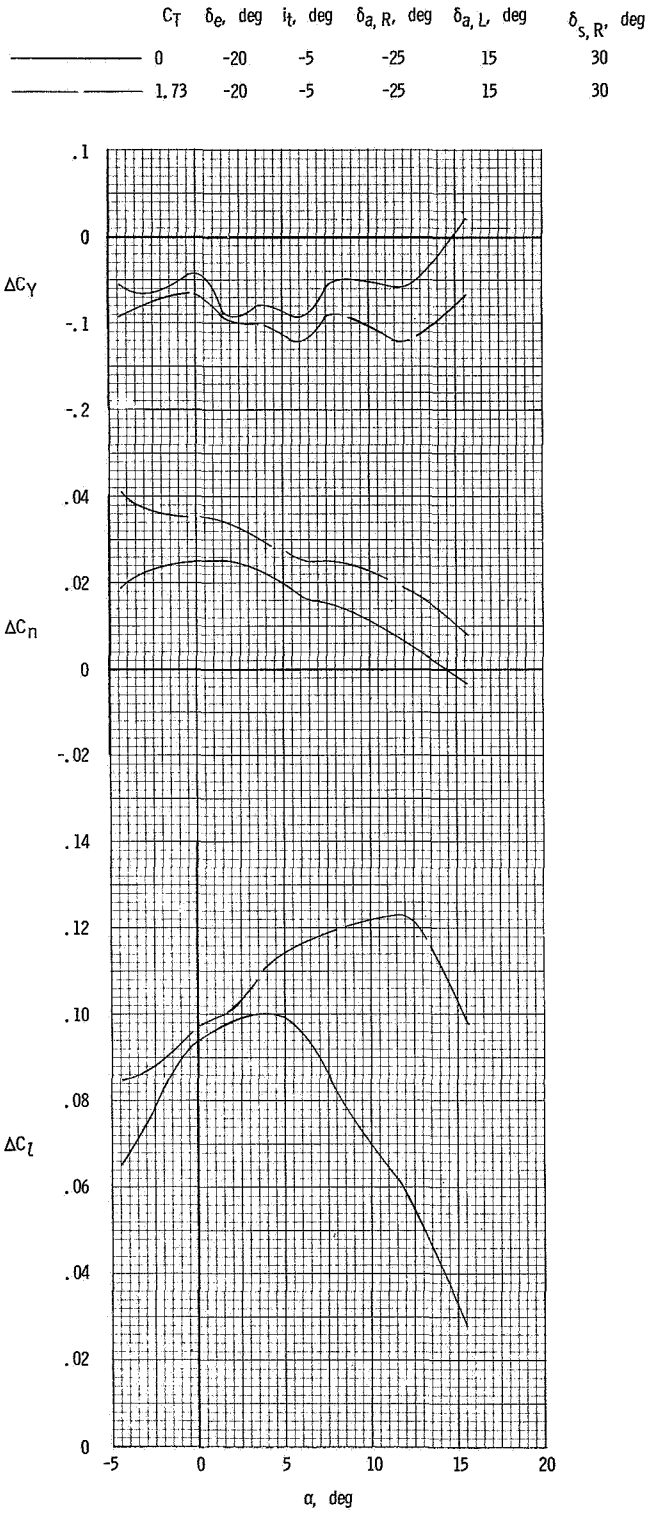

(b) $\delta_f = 55^0$.

Figure 21.- Concluded.

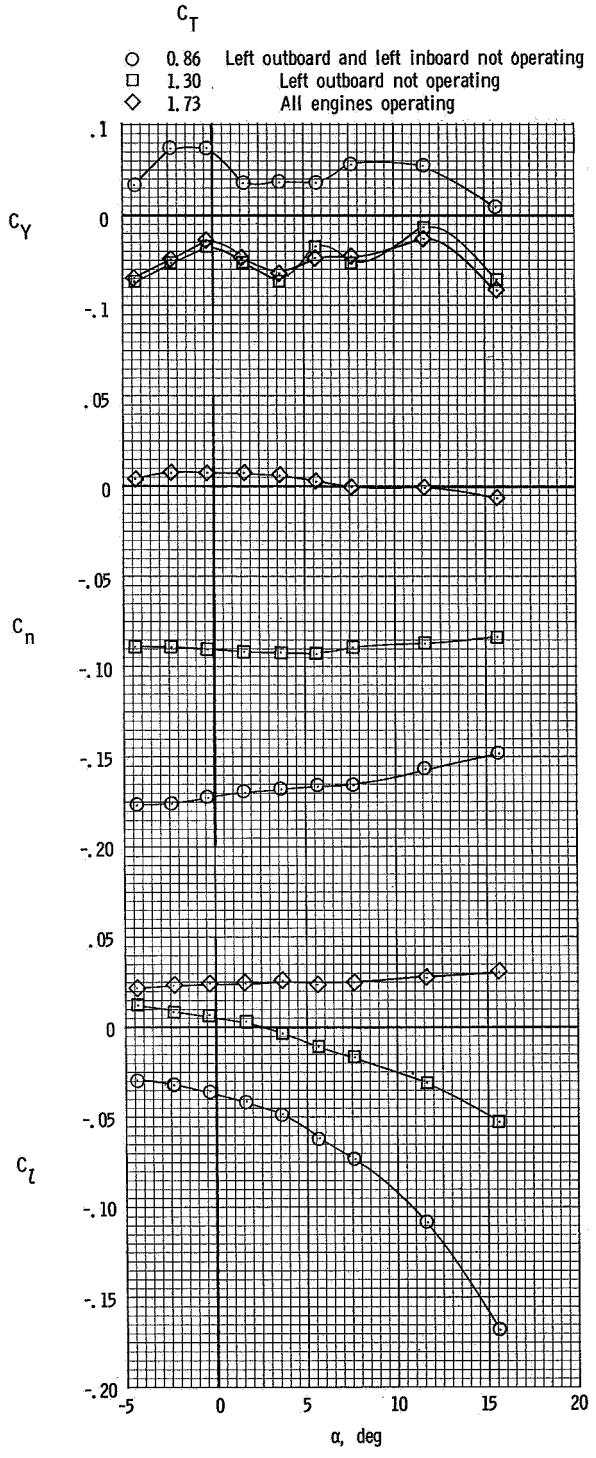

(a) $\delta_f = 35^0$.

Figure 22.- Lateral forces and moments produced by asymmetrical thrust conditions. $i_t = 0^0$; $\delta_e = 0^0$.

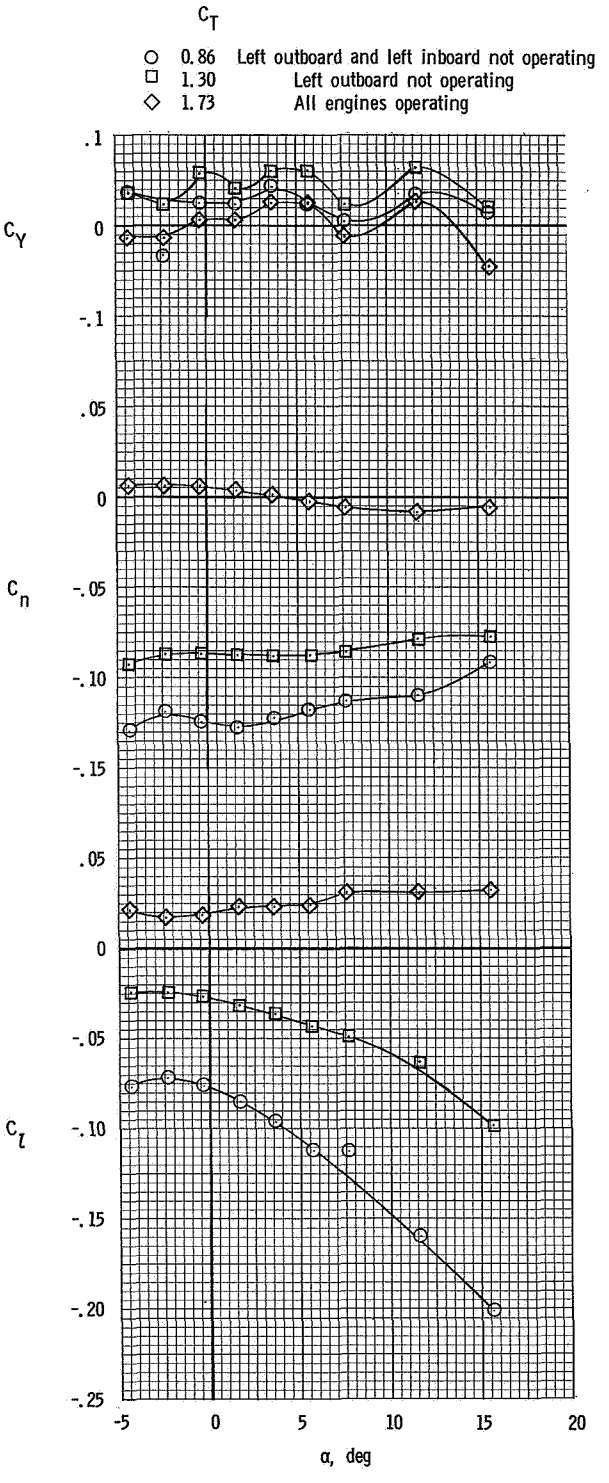

(b) $\delta_f = 55^o$.

Figure 22.- Concluded.

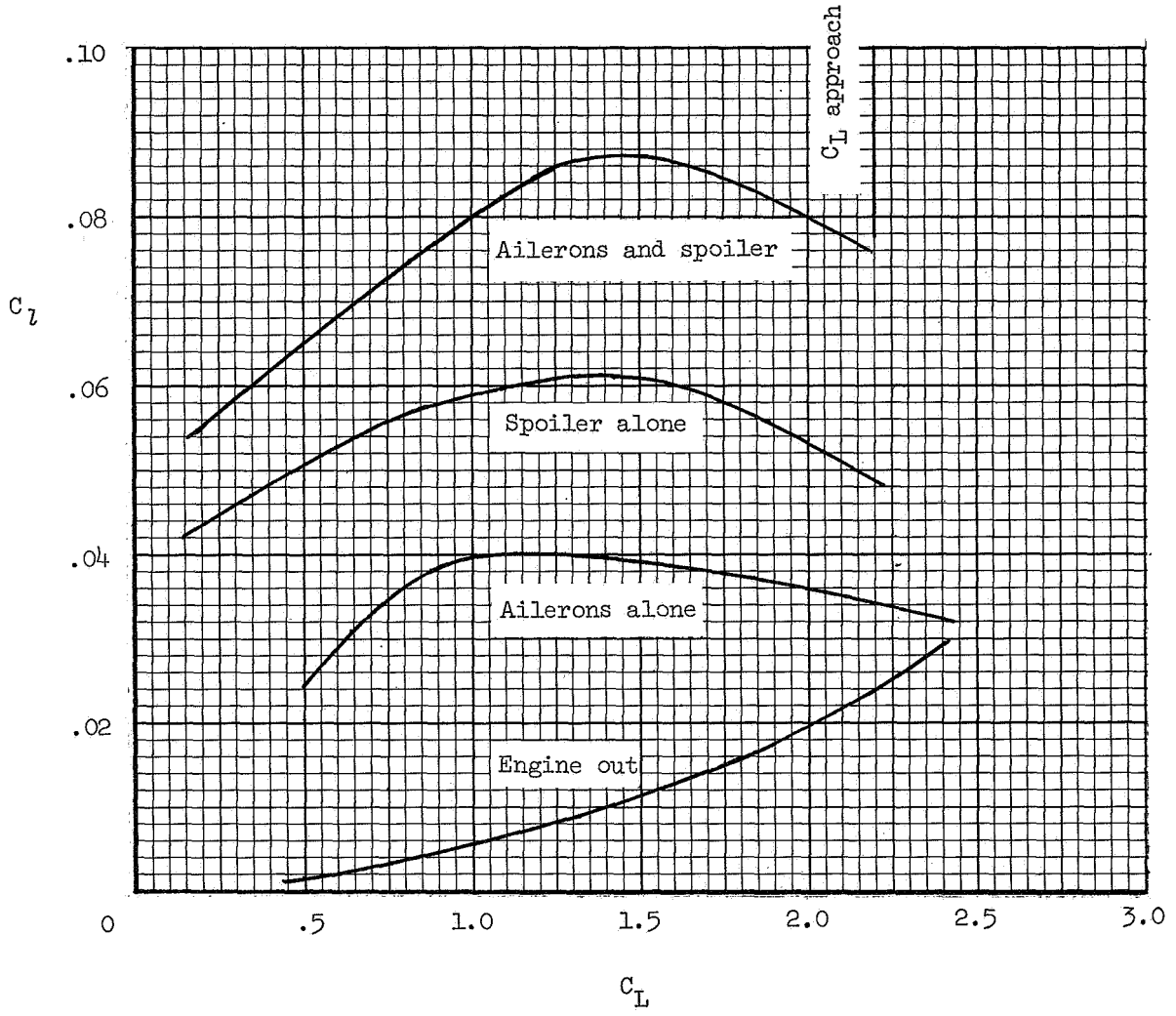

(a) $\delta_f = 35^0$.

Figure 23.- Rolling-moment trim capability of the model with one outboard engine out. T/W = 0.225.

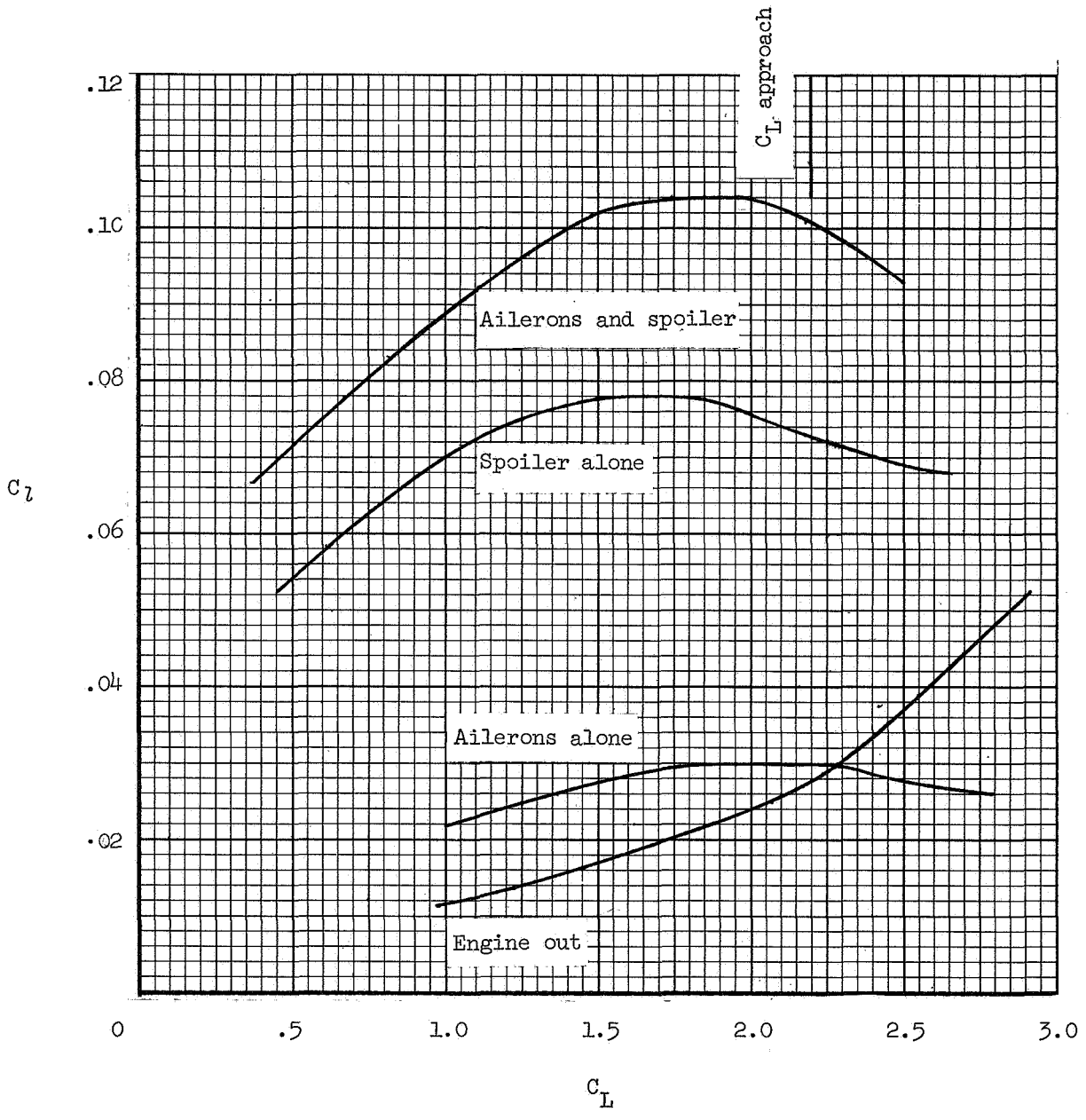

(b) $\delta_f = 55^0$.

Figure 23.- Concluded.

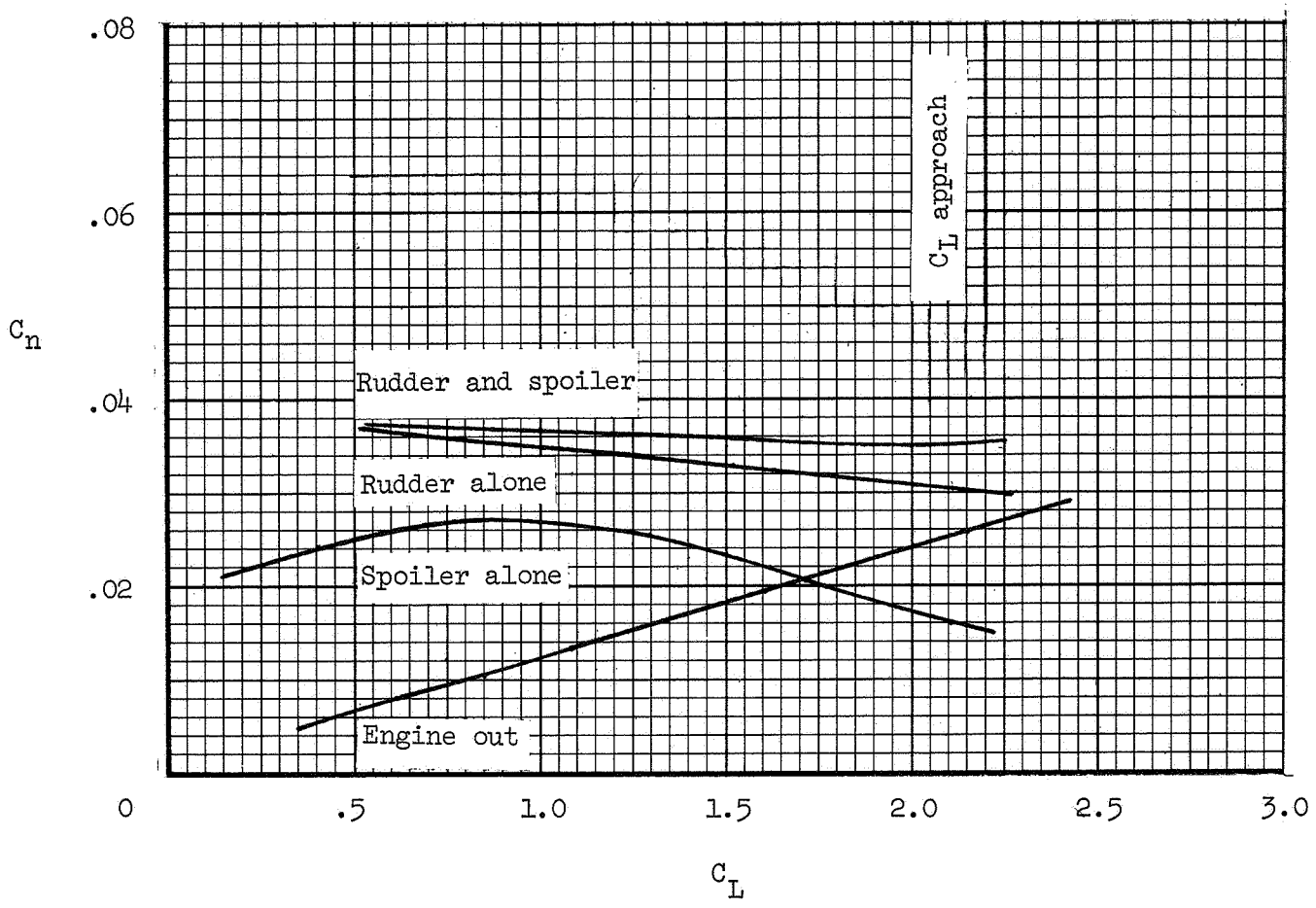

(a) $\delta_f = 35^0$.

Figure 24.- Yawing-moment trim capability of the model with one outboard engine out. T/W = 0.225.

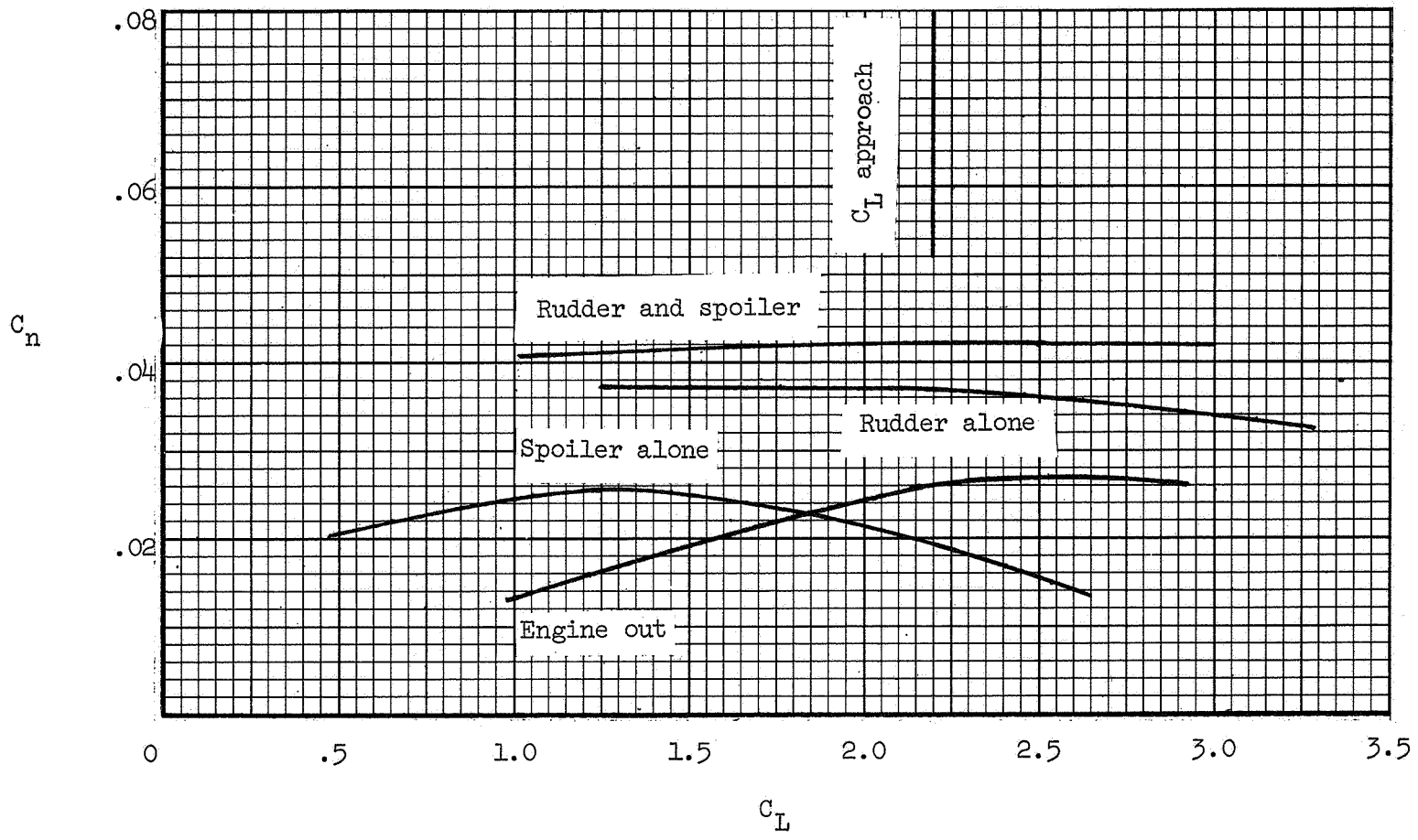

(b) $\delta_f = 55^0$.

Figure 24.- Concluded.

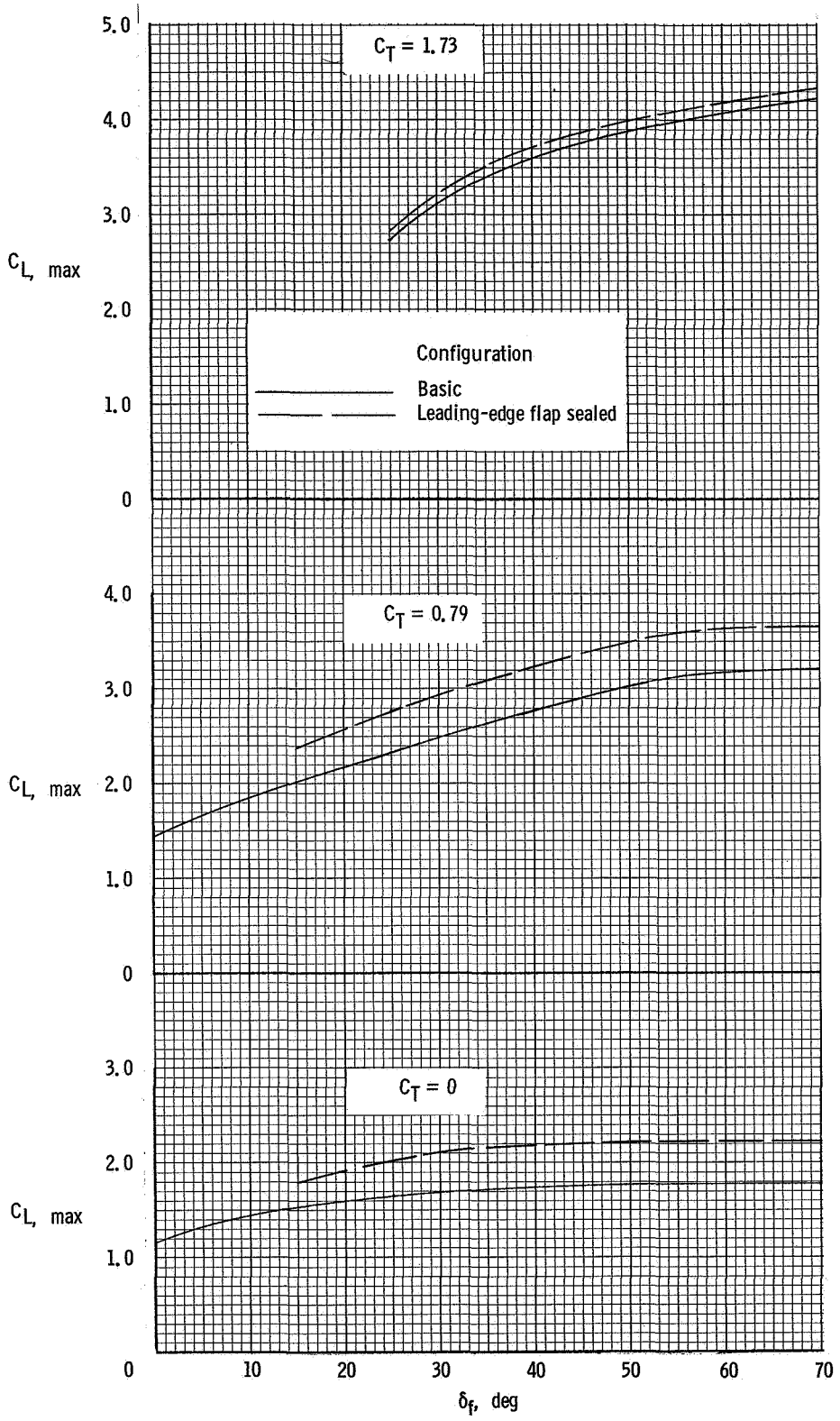

Figure 25.- Effect of sealing leading-edge gap on lift coefficient of model.

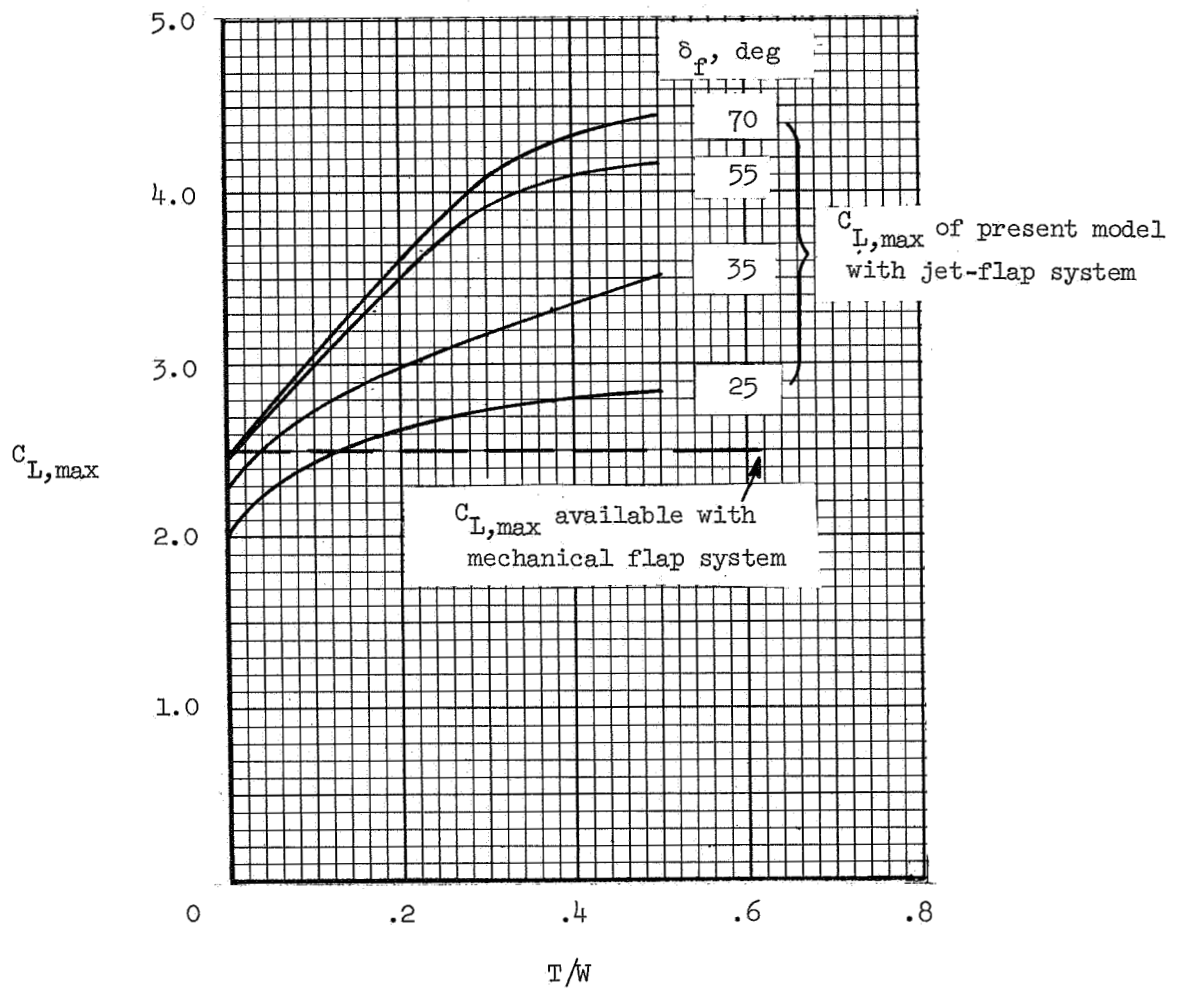

Figure 26.- Comparison of maximum lift coefficients from jet-flap system with that of mechanical flap system.

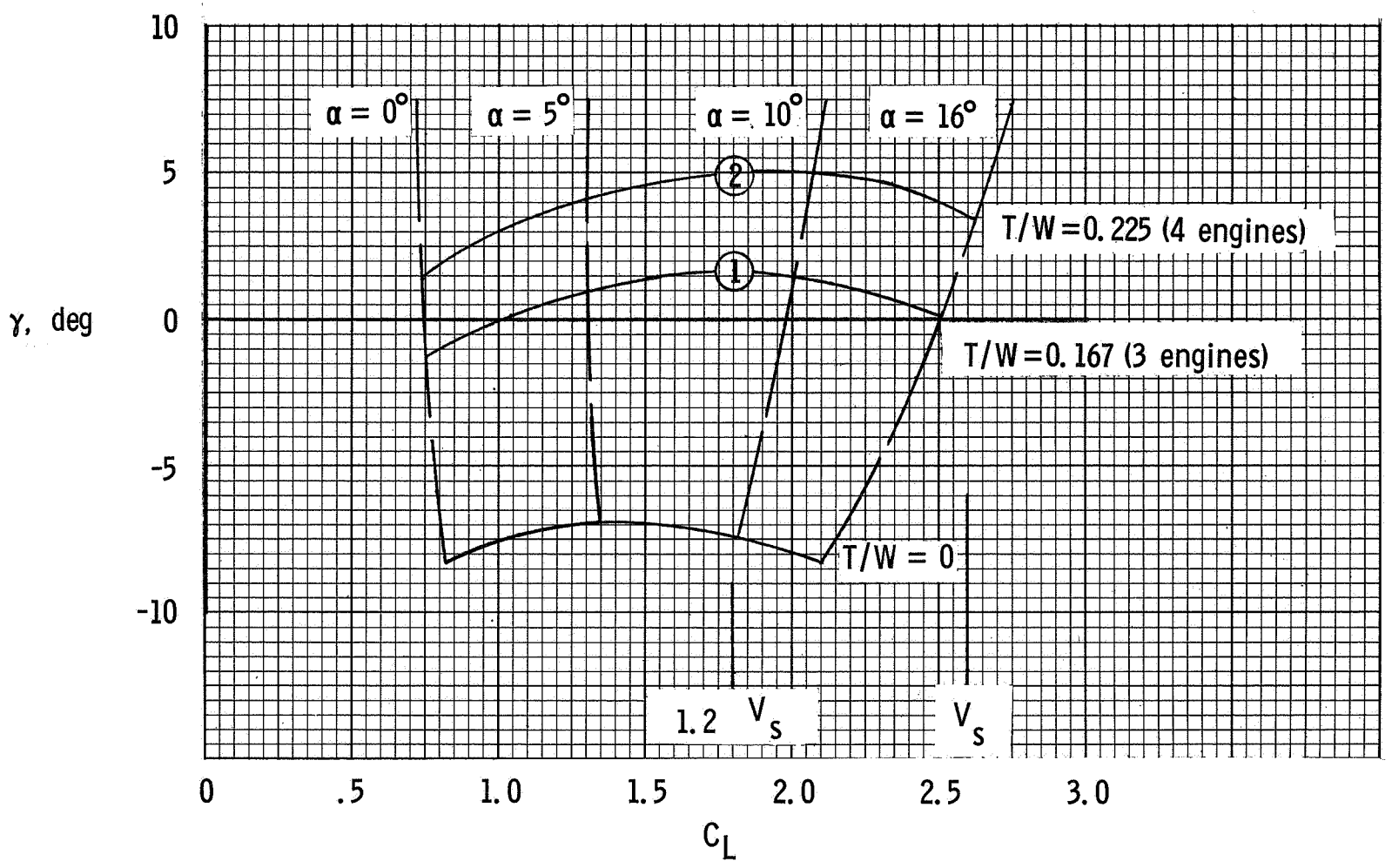

(a) $\delta_f = 20^0$.

Figure 27.- Take-off operation envelope numbers encircled indicate different power conditions.

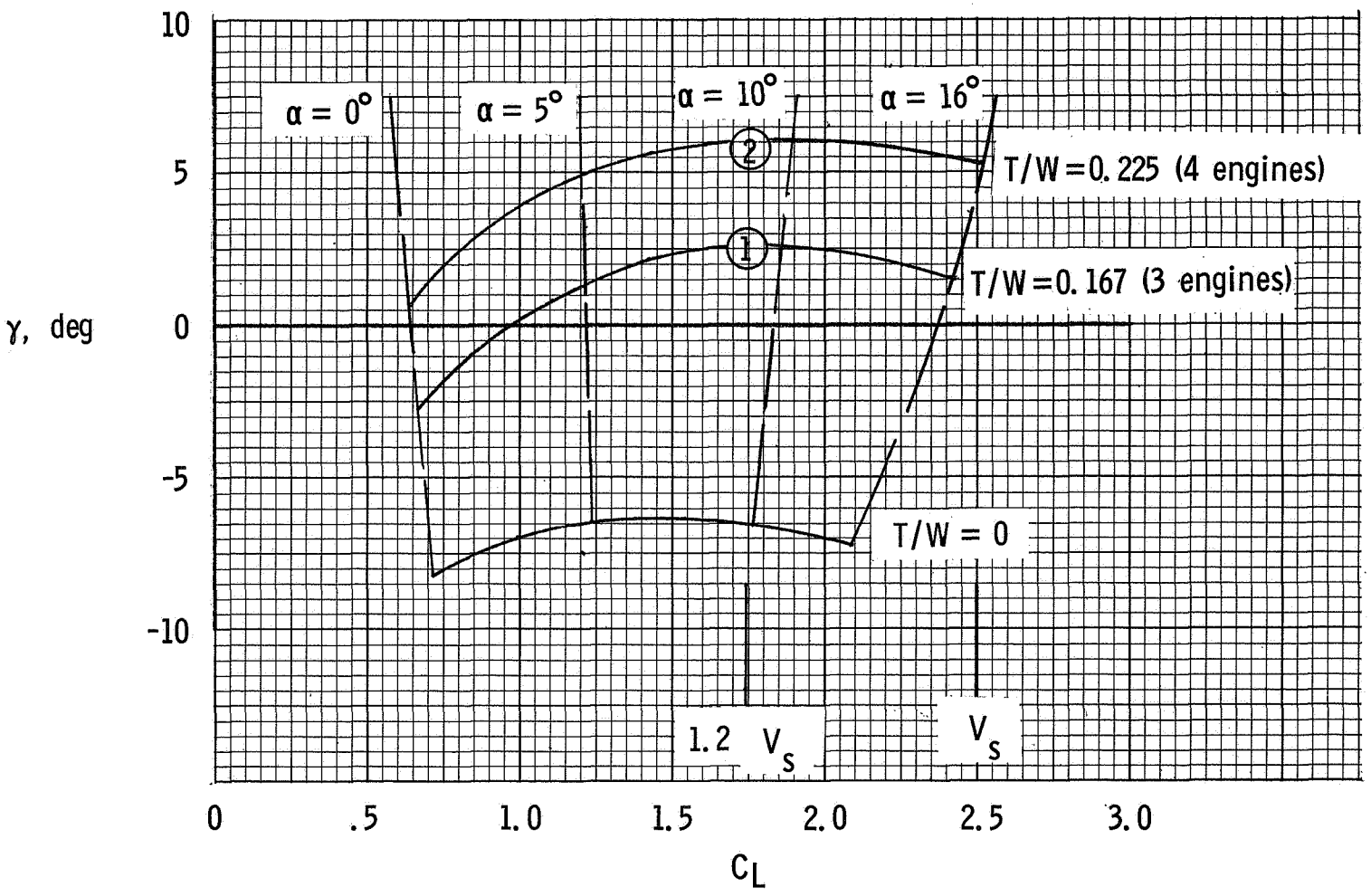

(b) $\delta_f = 15^0$.

Figure 27.- Concluded.

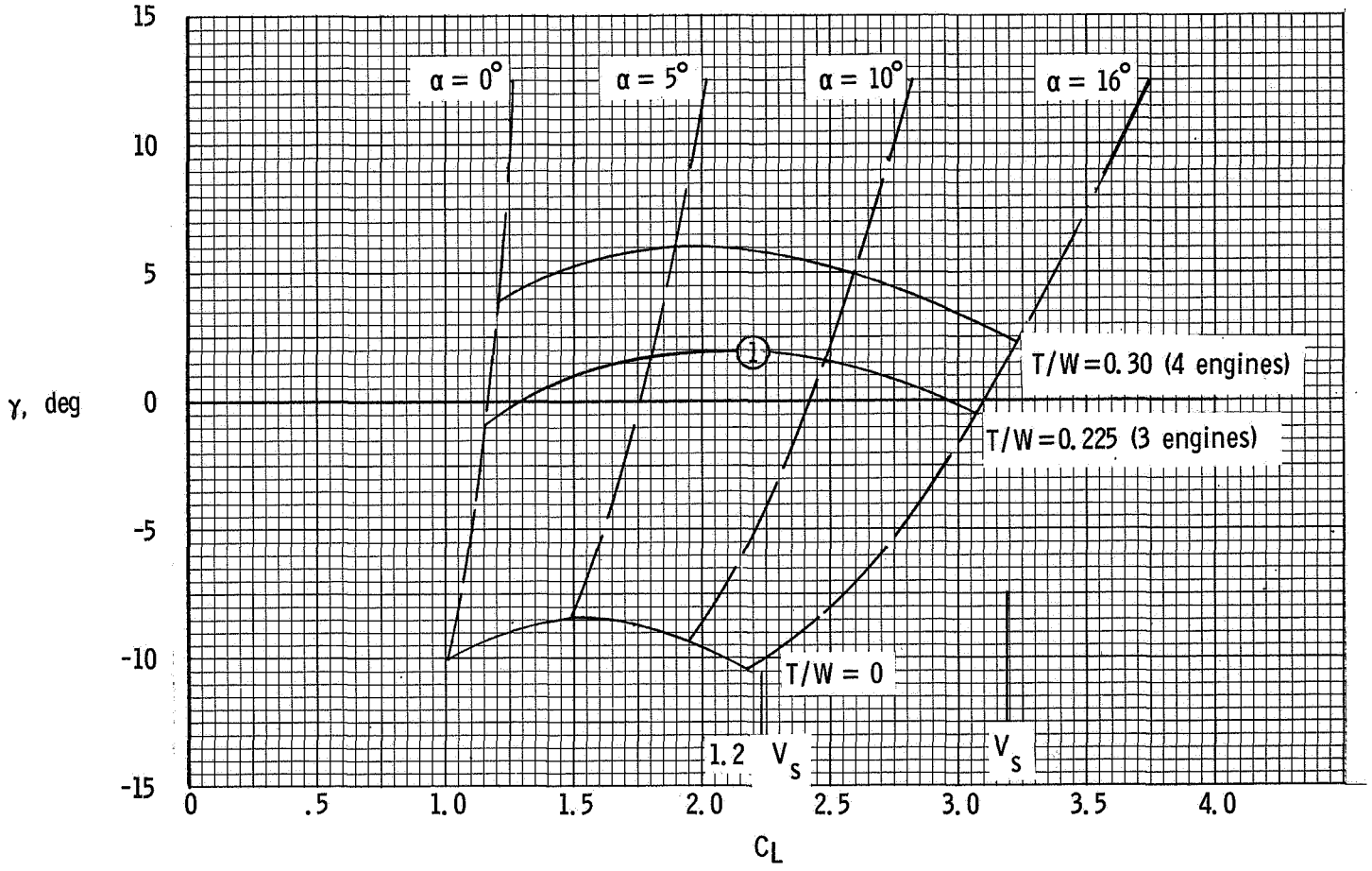

(a) $\delta_f = 35^0$.

Figure 28.- Landing operation envelope. Numbers encircled indicate different power conditions.

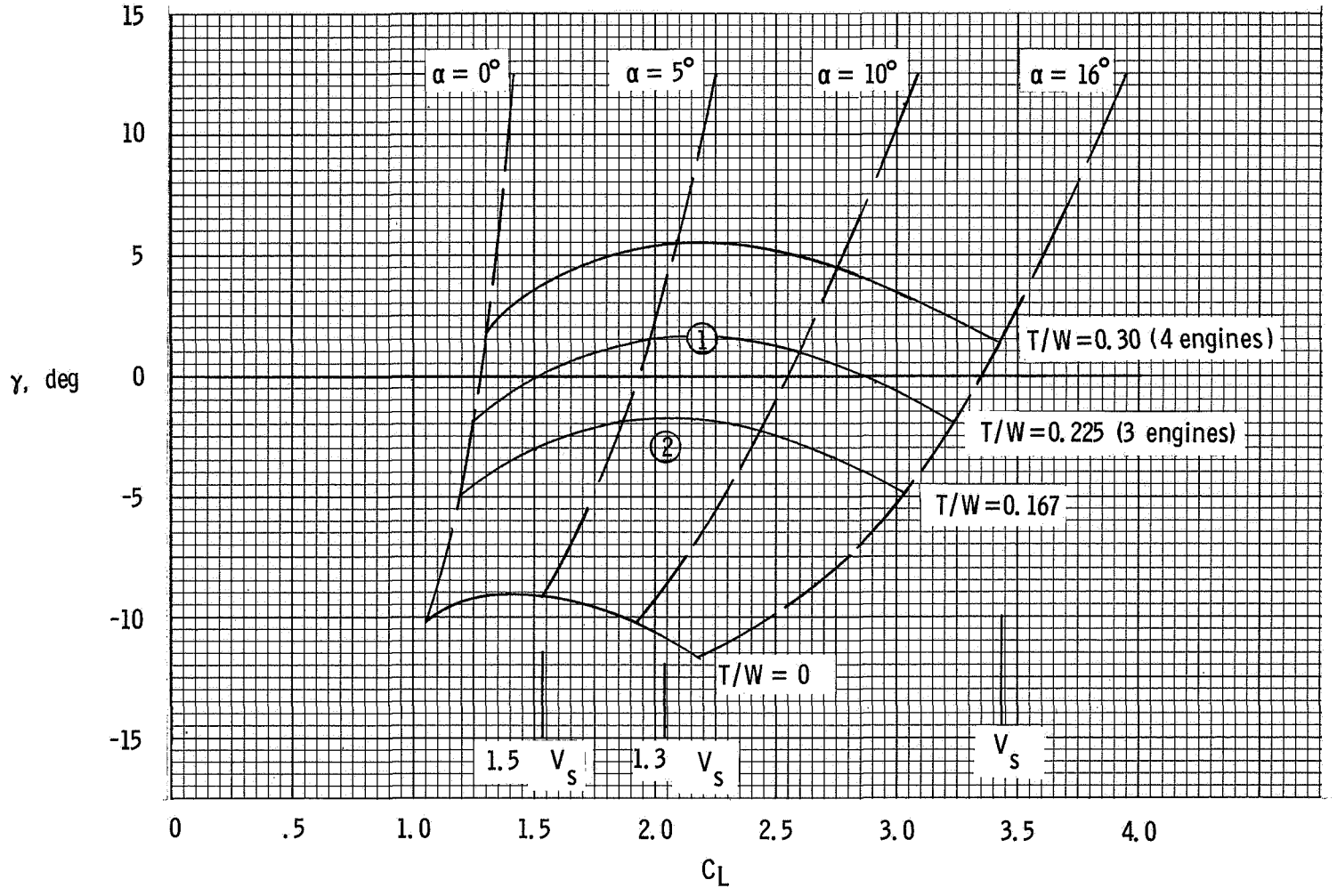

(b) $\delta_f = 40^o$.

Figure 28.- Continued.

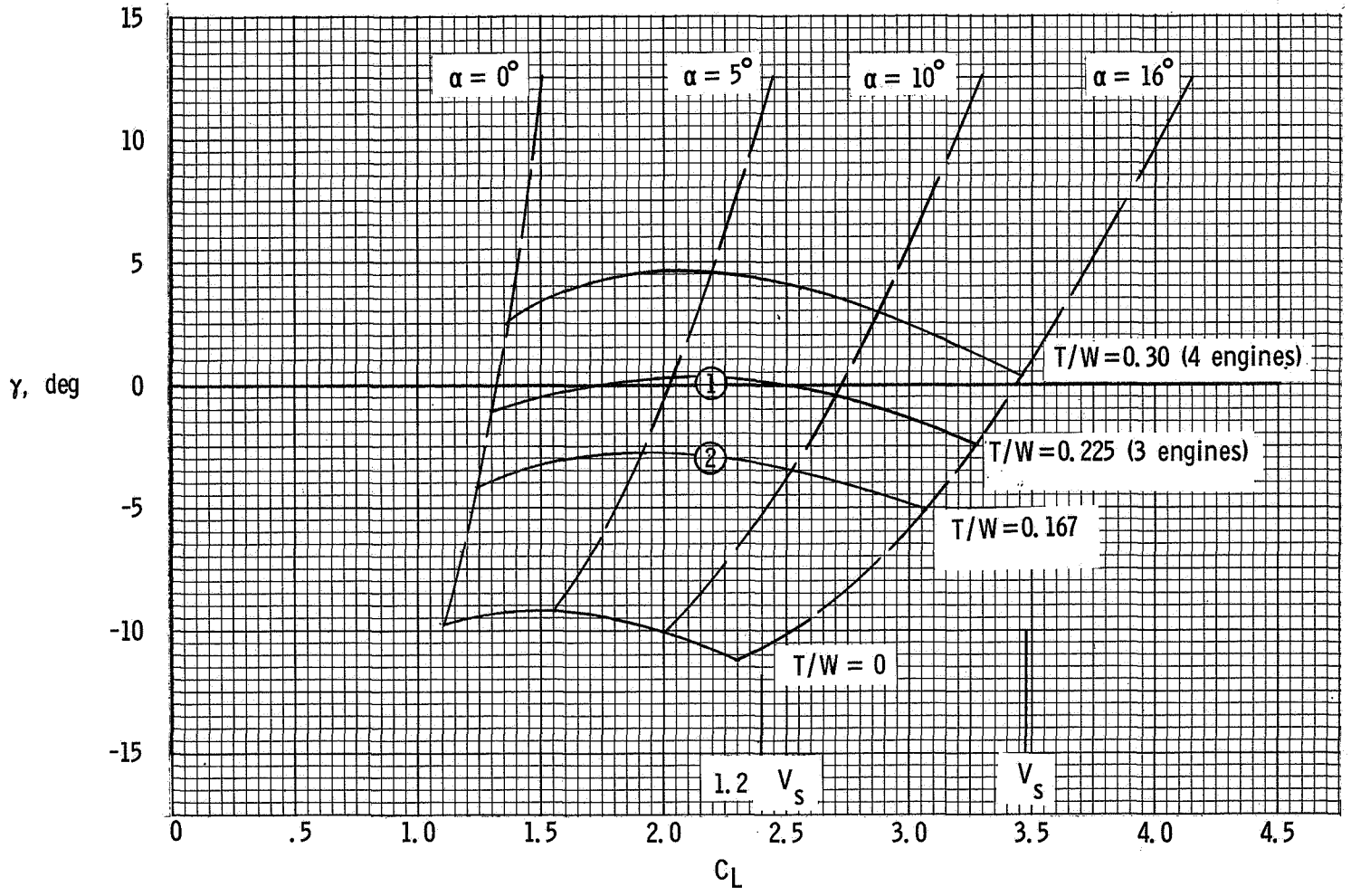

(c) $\delta_f = 45^0$.

Figure 28.- Continued.

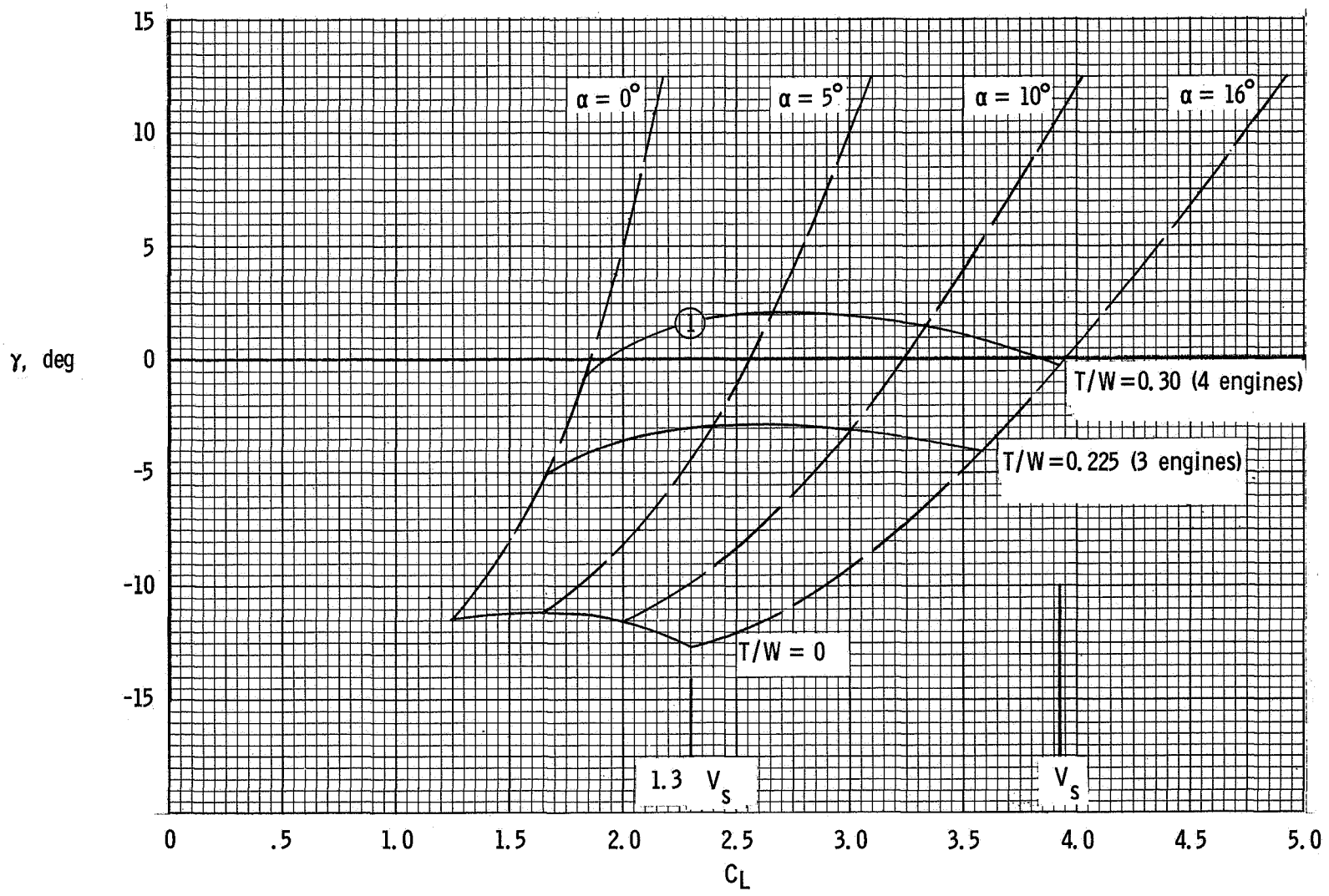

(d) $\delta_f = 55^o$.

Figure 28.- Concluded.

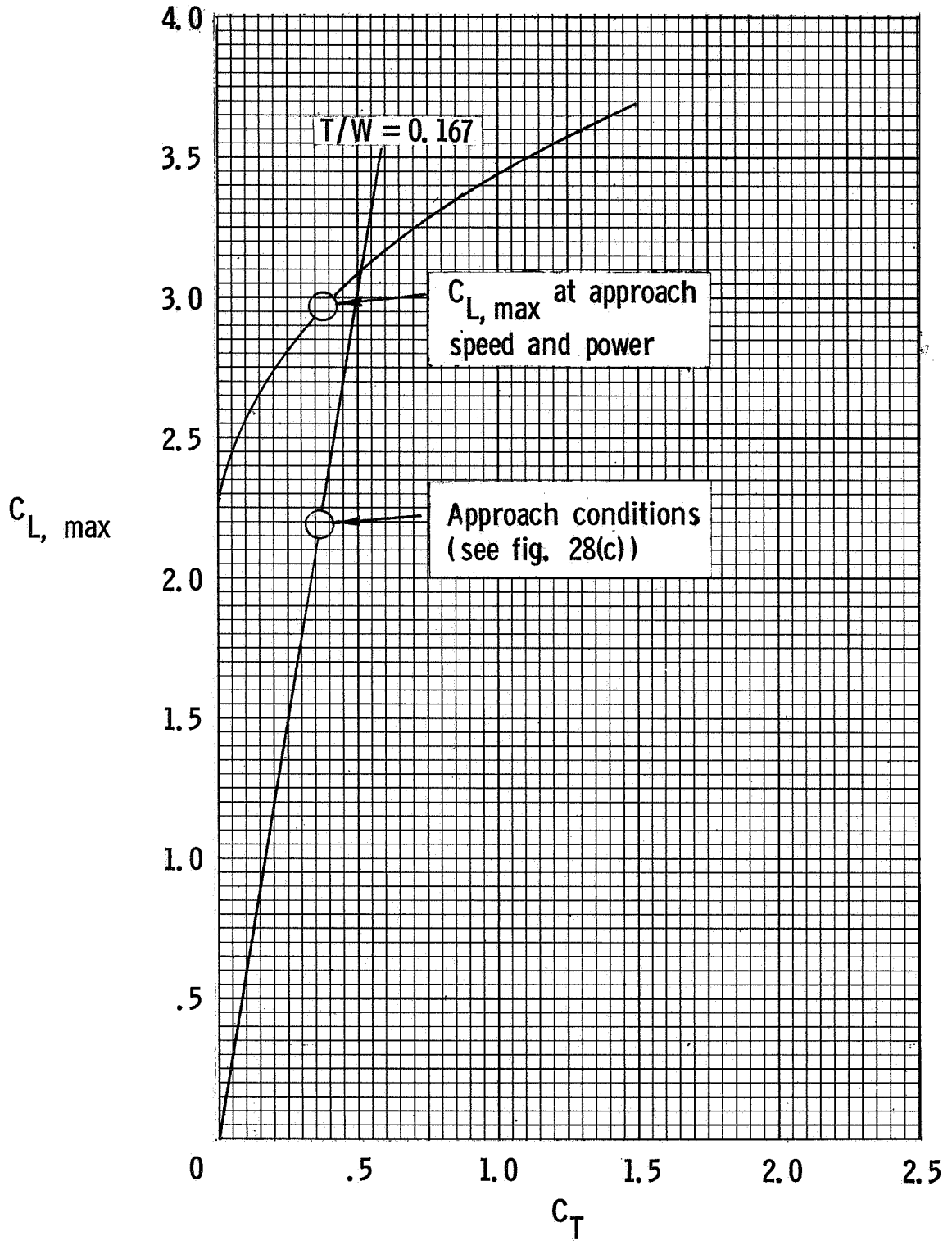

Figure 29.- Maneuver margin for the approach condition. $\delta_f = 45^o$.

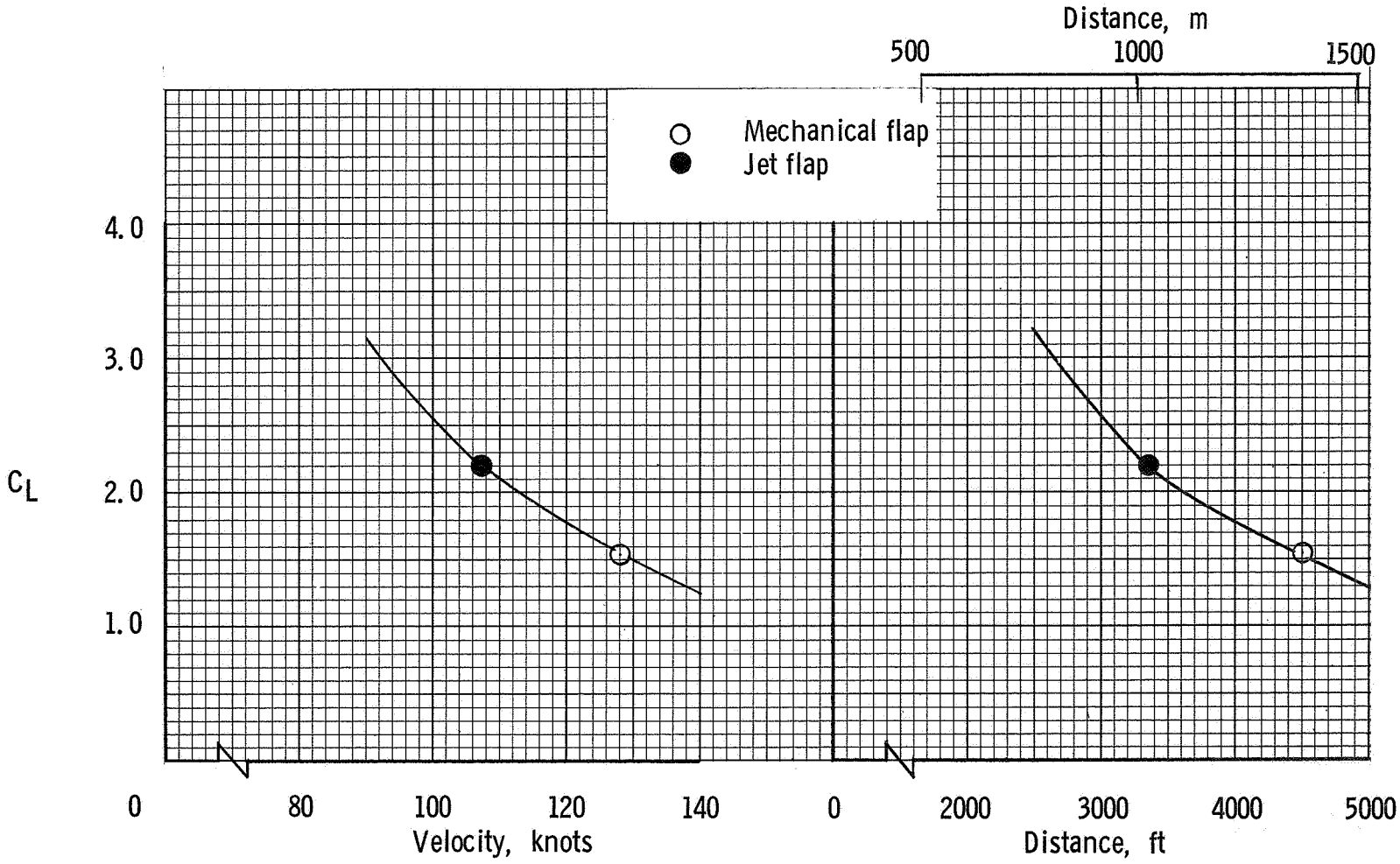

(a) Landing performance.

Figure 30.- Comparison of take-off and landing characteristics with jet flap and mechanical flap systems.

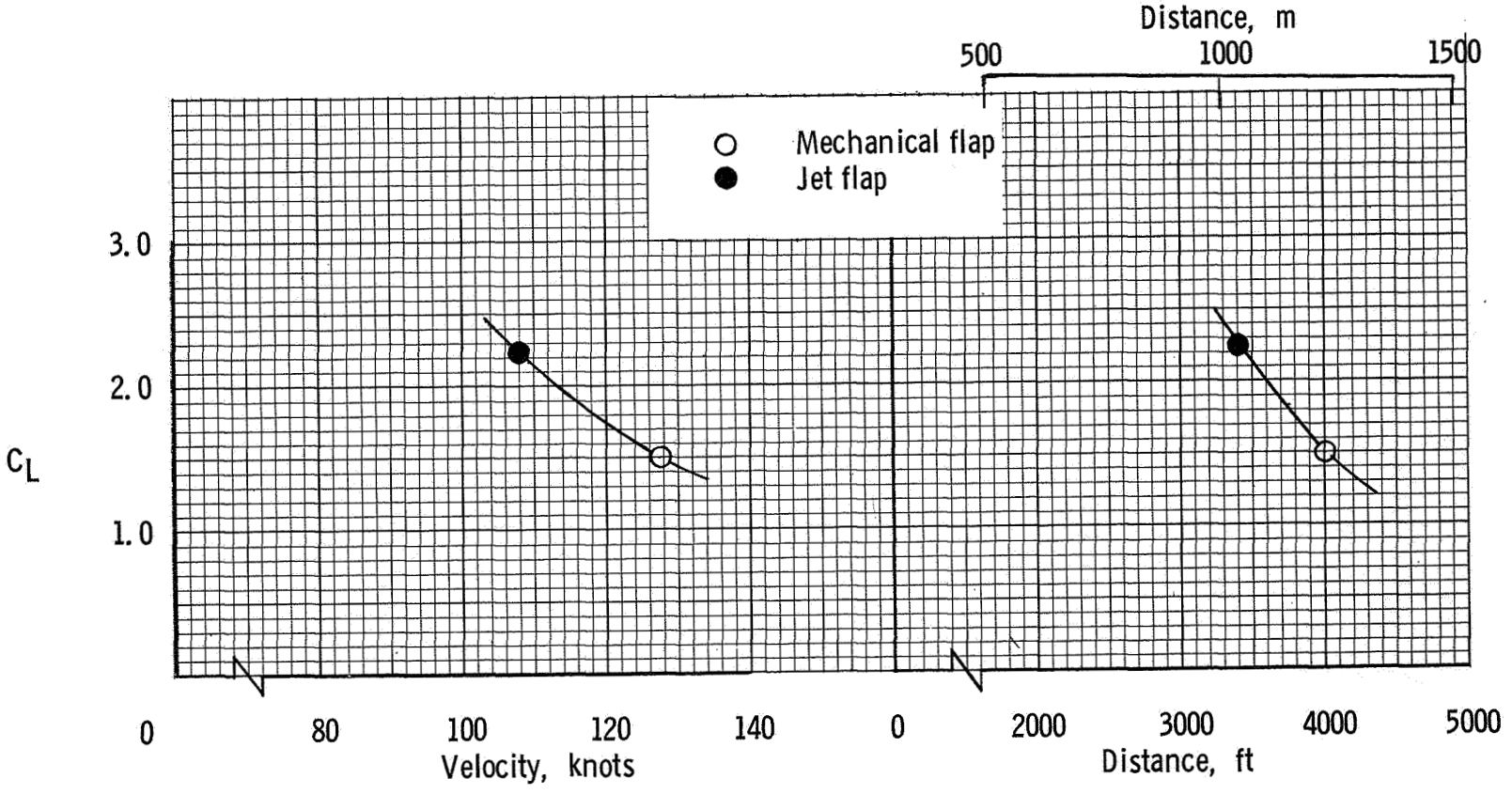

(b) Take-off performance.

Figure 30.- Concluded.

NATIONAL AERONAUTICS AND SPACE ADMINISTRATION
WASHINGTON, D. C. 20546
OFFICIAL BUSINESS

FIRST CLASS MAIL

POSTAGE AND FEES PAI
NATIONAL AERONAUTICS
SPACE ADMINISTRATIOI

POSTMASTER: If Undeliverable (Section
Postal Manual) Do Not F

"The aeronautical and space activities of the United States shall be conducted so as to contribute . . . to the expansion of human knowledge of phenomena in the atmosphere and space. The Administration shall provide for the widest practicable and appropriate dissemination of information concerning its activities and the results thereof."

—NATIONAL AERONAUTICS AND SPACE ACT OF 1958

NASA SCIENTIFIC AND TECHNICAL PUBLICATIONS

TECHNICAL REPORTS: Scientific and technical information considered important, complete, and a lasting contribution to existing knowledge.

TECHNICAL NOTES: Information less broad in scope but nevertheless of importance as a contribution to existing knowledge.

TECHNICAL MEMORANDUMS: Information receiving limited distribution because of preliminary data, security classification, or other reasons.

CONTRACTOR REPORTS: Scientific and technical information generated under a NASA contract or grant and considered an important contribution to existing knowledge.

TECHNICAL TRANSLATIONS: Information published in a foreign language considered to merit NASA distribution in English.

SPECIAL PUBLICATIONS: Information derived from or of value to NASA activities. Publications include conference proceedings, monographs, data compilations, handbooks, sourcebooks, and special bibliographies.

TECHNOLOGY UTILIZATION PUBLICATIONS: Information on technology used by NASA that may be of particular interest in commercial and other non-aerospace applications. Publications include Tech Briefs, Technology Utilization Reports and Notes, and Technology Surveys.

Details on the availability of these publications may be obtained from:

SCIENTIFIC AND TECHNICAL INFORMATION DIVISION

NATIONAL AERONAUTICS AND SPACE ADMINISTRATION

Washington, D.C. 20546